Zarrabi, Hassan J.

TIME RESOLVED SPECTROSCOPY OF TERNARY SEMICONDUCTORS GALLIUM(X)-INDIUM(1-X) PHOSPHIDE AND GALLIUM ARSENIDE(1-X)-PHOSPHIDE(X) UNDER PICOSECOND LASER PULSE EXCITATION

City University of New York PH.D. 1985

PLEASE NOTE:

In all cases this material has been filmed in the best possible way from the available copy. Problems encountered with this document have been identified here with a check mark _√_.

1. Glossy photographs or pages _____
2. Colored illustrations, paper or print _____
3. Photographs with dark background _____
4. Illustrations are poor copy _____
5. Pages with black marks, not original copy _____
6. Print shows through as there is text on both sides of page _____
7. Indistinct, broken or small print on several pages _✓_
8. Print exceeds margin requirements _____
9. Tightly bound copy with print lost in spine _____
10. Computer printout pages with indistinct print _____
11. Page(s) _____ lacking when material received, and not available from school or author.
12. Page(s) _____ seem to be missing in numbering only as text follows.
13. Two pages numbered _____. Text follows.
14. Curling and wrinkled pages _____
15. Other _____

Time Resolved Spectroscopy of ternary Semiconductors $Ga_x In_{1-x} P$ and $GaAs_{1-x} P_x$ under Picosecond Laser Pulse Excitation

Hassan J . Zarrabi

A dissertation submitted to the graduate faculty in physics for partial fulfilment of the requirement for the deree of the Doctor of Philosophy , The City University of NewYork

1985

This manuscript has been read and accepted for the Graduate Faculty in Physics in satisfaction of the dissertation requirement for the degree of Doctor of Philosophy .

2/14/85
date

Robert R. Alfano
Chairman of the Examining Committee

2/14/85
date

Executive Officer

Prof. R . R . Alfano

Prof. Joseph L. Birman

Prof. M . Sarachik

Dr. W . Miniscalco

Prof. P . Ho

THE CITY UNIVERSITY OF NEW YORK

Time Resolved Spectroscopy of ternary semiconductors $Ga_x In_{1-x} P$ and $GaAs_{1-x} P_x$ under Picosecond Laser Pulse Excitation

Hassan . J . Zarrabi

Advisor : Professor R . R . Alfano

ABSTRACT

In the thesis ,the ultrafast physics of carriers in two ternary semiconductors $Ga_x In_{1-x} P$ and $GaAs_{1-x} P_x$ were studied under picosecond Laser Pulse Excitation .

The dynamics of hot carriers In $Ga_{.5}In_{.5}P$, were studied by means of time resolved spectroscopy . The effect of high pump intensity on the temporal behavior of the emission at different wavelengths were investigated. At high excitation power fluence, the temporal profile at short wavelengths (high energy portion of the photoluminescence spectra) were exponential similar to the low excitation power fluence . However the temporal profiles at long wavelengths (low energy portion of the photoluminescence spectra close to band edge) exhibited an unusual and complex profile . The time resolved profiles at long wavelength acquired a district tail as excitation power increased even to the point of developing a secondary peak. A model is proposed to explain the temporal behavior of

the emission at different wavelengths. The rate equations describing the time dependence of dynamical variables (n_e , T_c , $\phi(\nu)$) were solved numerically by computer to simulate the temporal behavior of the emission at different wavelengths under different excitation power fluence .

The time resolved photoluminescence spectra in $Ga_{.56}In_{.44}P$ was measured with 10 ps time resolution using the streak camera as a detection system . From the theoretical fitting of the photoluminescence spectra we have determined the time evolution of carrier density and carrier temperature. We found that the carrier energy loss rate to be slower than predicted from a simple model assuming a Maxwell Boltzmann distribution function. This is attributed to the screening of the hot carrier energy relaxation under high carrier densities. Integro-differential equations describing the time dependence of carrier temperature have been solved and the results are compared with the experimental data.

The time resolved photoluminescence kinetics in $GaAs_{.62}P_{.38}$, were measured by streak camera to determine the radiative, non radiative recombination rates. The photoluminescence decay profile was found to be intensity dependent. When excitation power fluence increased above 6×10^8 W/cm^2, the decay profile of emission deviated from an exponential form. This is attributed to bimolecular and Auger processes. The biomolecular and Auger rates were determined to be $B_R = 9\times10^{-10} cm^{-3}/s$ and $C_{NR} = 3\times10^{-29} cm^6/s$ by fitting the time resolved photoluminescence decay profiles to the solution of rate equations which describes the dynamical behavior of the photogenerated carriers.

DEDICATION

This thesis is dedicated to my mother who did her best at hardest times beyond motherhood .

Acknowledgements

I would like to thank my research advisor , Professor Robert R . Alfano for his advice and helpful discussions during the course of this work .

I am grateful to my brother Al for his encouragements in the past eight years . Many thanks to my wife , Robin for her unusual moral support . I also would like to extend may thanks to Karren Zarrabi for her help in typing this manuscript into my Mackintosh computer . I am grateful to my colleagues at Institute for Ultrafast Spectroscopy and Lasers particularly Dr. Doukas , Dr. Ockman , Dr. Dorsinville , Mr. W. Wang , Mr. Junnarkar , Mr. A. Katz , Mr. D. Rosen , Mr. Yury and Mrs. Gibbs . I also would like to thank Prof. M . Lax and Dr. S. Chitanvis for helping me to transfer my files from Mackintosh to VAX computer , Mr. C . L . Wang for helpful discussion in computations and Dr. Joe Eccles of the computer center of CCNY . I would like to thank Dr. G. Olsen of RCA , Dr. Nurmikko of Brown University , Dr. G . Duggan of Phillips Laboratories in London for providing the samples .

Finally I would like to thank Air Force Office of Scientific Research and Dr. Gerald Witt for providing the financial support .

TABLE OF CONTENTS

CHAPTER		PAGE
Chapter 1	Introduction	1
Chapter 2	Experimental Techniques	8
2.1	Steady state photoluminescence setup	8
2.2	Time Resolved Experimental setup	8
2.2.1	Laser Resonator	11
2.3	Single Pulse Selection , Amplifier	14
2.4	Second Harmonic Generation	19
2.5	Streak camera	19
	References	24
Chapter 3	Picosecond Carrier Dynamics in Optically Pumped GaInP	25
3.1	Experimental Results	25
3.2	Band structure of $Ga_x In_x P$	28

3.3	Carrier Dynamics in $Ga_{.5}In_{.5}P$	36
3.4	Energy Loss Mechanisms of photogenerated carriers	39
	Screening of hot carriers	45
	Intervalley Scattering	52
	Gain / Loss in semiconductors	54
	References	86
Chapter 4	Time Resolved Photoluminescence Spectra in $Ga_{.56}In_{.44}P$ measured by streak camera	89
4.1	Introduction	89
4.2	Experimental Methods	90
4.3	Experimental Results	91
4.4	Recombination Models	96
4.5	Theoretical Fitting	100
4.6	Discussion	105
4.7	Conclusion	110
	References	111
Chapter 5	Time Resolved Kinetics of e-h plasma in $GaAs_{1-x}P_x$	
	under Intense Picosecond Laser Pulse Excitation	113

5.1	Introduction	113
5.2	Band structure of GaAsP	114
5.3	Experimental Setup	118
5.4	Experimental Results	120
5.5	Recombination models for rate equations	124
	References	128
TABLE 1	The physical parameters used for calculations in $Ga_xIn_{1-x}P$	131
TABLE 2	The physical parameters used for calculations in $GaAs_{1-x}P_x$	132
Appendix 1	List of the program used to calculate the Fermi integral ie ; Eq. 3.3.5	133
Appendix 2	List of the program used to calculate the Fermi level ie : Eq. 3.3.8	134
Appendix 3	List of the program used for calculations of Fig. 3.3.5 and Fig. 3.3.6	135
Appendix 4	List of the program to calculate temperature evolution of carriers for the case of M.B. distribution	136
Appendix 5	List of the program used to calculate Eq. 3.3.22	137

Appendix 6	List of the program to calculate the temperature evolution of carriers in the presence of screening	139
Appendix 7	List of the program used to calculate Eq. 3.3.36	141
Appendix 8	List of the program used to calculate Eq. 3.3.40	142
Appendix 9	List of the program used to calculate Eq. 3.3.57 and Eq. 3.3.58	143
Appendix 10	List of the program used to calculate Eq. 3.3.60	145
Appendix 11	List of the program used to calculate Eq. 4.4.6	147
Appendix 12	List of the program used to calculate Eq. 4.4.8	149
Appendix 13	List of the program used to calculate the effective decay time in Eq. 5.4.2	150
Appendix 14	Derivation of Eq. 3.3.54	151

LIST OF ILLUSTRATIONS

Figure		Page
Fig. 2 . 1 . 1	Schematic diagram of the steady state luminescence setup .	9
Fig. 2 . 2 . 1	Schematic diagram of picosecond time resolved spectroscopy setup .	10
Fig. 2 . 2 . 2	Configuration of the optical cavity resonator .	12
Fig. 2 . 2 . 3	Energy level of Nd : glass laser .	13
Fig. 2 . 3 . 1	Nd : glass laser with second harmonic generation and amplifier .	15
Fig. 2 . 3 . 2	(a) - The picture of the picosecond laser pulse train with one pulse selected .	
	(b) - The picture of a selected laser pulse .	17
Fig. 2 . 3 . 3	Schematic diagram of the setup for two photon fluorescence measurements .	18
Fig. 2 . 5 . 1	Schematic diagram of a streak camera tube	21
Fig. 2 . 5 . 2	(a) - Schematic diagram of calibration technique for a streak camera .	

(b) - Graphic representation of the intensity profile for a 8 ps laser pulse passing through a 30 ps etalon. 22

Fig. 3 . 1 . 1 (a) - Time resolved photoluminescence profile of $Ga_{.5}In_{.5}P$ at short wavelengths ($\lambda < 620nm$) for excitation fluence of $10MW / cm^2$. 26

Fig. 3 . 1 . 1 (b) - Time resolved photoluminescence profile of $Ga_{.5}In_{.5}P$ at long wavelengths $\lambda > 620\ nm$ for excitation fluence of $10MW / cm^2$. 26

Fig. 3 . 1 . 2 (a) - Time resolved photoluminescence profile of $Ga_{.5}In_{.5}P$ at short wavelengths $\lambda < 620nm$ for excitation fluence of $50\ MW / cm^2$ 27

Fig. 3 . 1 . 2 (b) - Time resolved photoluminescence profile of $Ga_{.5}In_{.5}P$ at long wavelengths $\lambda > 620\ nm$ for excitation fluence of $50MW / cm^2$. 27

Fig. 3 . 2 . 1 - Absorption coefficient of $Ga_x In_{1-x} P$ (x=.69) at 77 and 300 K . The position of direct band edge (E_Γ) is shown by arrow . Also indicated are the photoluminescence peaks . 32

Fig. 3 . 2 . 2 - Dependence of absorption edge and photoluminescence peak energy on alloy composition in $Ga_x In_{1-x} P$ at T=77 K . The absorption band edges are indicated by squares and photoluminescence peak energies by circles . 33

Fig. 3 . 2 . 3 - Dependence of absorption edge and photoluminescence peak energy on alloy composition in $Ga_x In_{1-x} P$ at T=300 K . The absorption band edges are indicated by squares and photoluminescence peak energies by circles . 33

Fig. 3 . 2 . 4 Simplified band structure of $Ga_x In_{1-x} P$. 35

Fig. 3 . 3 . 1 Degenerate and non-degenerate electron distributions n (E) . The density of states , g (E) is also shown . For the non-degenerate case the Fermi function f (E) is shown . ϕ is the Fermi level . Note , in non-degenerate case the Fermi level is below the conduction band edge and in degenerate case the Fermi level in the conduction band . 38

Fig. 3 . 3 . 2 Fermi level (in mev) in $Ga_x In_{1-x} P(x=.5)$ calculated from Fermi integral Eq. 3 . 3 . 5 (solid line) and approximate value calculated from Eq. 3 . 3 . 8 (dashed line) . 40

Fig. 3 . 3 . 3 Electron energy loss rate in $Ga_x In_{1-x} P(x=.5)$ as a function of electron temperature calculated from Eq. 3 . 3 . 18 for 1×10^{18} (dot-dash) , 5×10^{18} (dashed) and $1\times10^{19} cm^{-1}$ (solid line) . The Maxwellian result is independent of electron density . 46

Fig. 3 . 3 . 4 Electron energy loss rate vs electron density in $Ga_x In_{1-x} P(x=.5)$ on semi-log scale for 500 , 1000 ,

	2000 K calculated from Eq. 3 . 3 . 22 . The lowest curve corresponds to 500 K and dashed lines are for Maxwell distribution case .	47
Fig. 3 . 3 . 5	Electron energy loss rate to lattice via optical phonon interaction as a function of temperature with screening effects included as calculated from Eq. 3 . 3 . 27 for $n=1\times10^{18}cm^{-3}$ (solid line) , $5\times10^{18}cm^{-3}$ (dashed line) ,$1\times10^{19}cm^{-3}$ (dot-dashed line)	50
Fig. 3 . 3 . 6	Electron energy loss loss rate to lattice via optical phonon interaction , with screening effect included on a logarithmic scale . The three curves are for T=500 , 1000 , 2000 K , respectively . The upper curve is for T=2000 K and the lower curve is for T=500 K .	51
Fig. 3 . 3 .7	Intervalley scattering time in $Ga_{.5}In_{.5}P$ as a function of electron temperature .	55
Fig. 3 . 3 . 8	Schematic diagram for many valley effect	62
Fig. 3 . 3 . 9	The time dependence of a 8-ps laser pulse as calculated from Eq. 3.3.62 for 10 μj energy . The area under the curve is the number of photons in the pulse .	63
Fig. 3 . 3 .10	a - The electron density in Γ valley as a function of time for excitation fluence of $10MW/cm^2$ and $D_{\Gamma X} = 5\times10^8$ ev / cm .	65

	b - The electron density in X valley as a function of time for excitation power of $10MW/cm^2$ and $D_{\Gamma X} = 5\times10^8$ ev / cm .	65
Fig. 3 . 3 .11	Electron temperature as a function of time as calculated from Eq. 3 . 3 . 59 for excitation power of $10MW/cm^2$.	66
Fig. 3 . 3 . 12	(a) - The computed normalized output photon density at different wavelengths as a function of time for excitation of $P = 10MW/cm^2$, $D_{\Gamma X} = 5\times10^8$ ev / cm and confinement factor of $C_F = 3\times10^{-3}$.	67
Fig. 3 . 3 . 13	a - The time dependence of electron density in Γ valley as a function of time for excitation power of $25MW/cm^2$, $D_{\Gamma X} = 5\times10^8$ ev / cm .	68
	b - The time dependence of electron density in X valley as a function of time for excitation power of $25MW/cm^2$ and $D_{\Gamma X} = 5\times10^8$ ev / cm .	68
Fig. 3 . 3 . 14	The time dependence of electron temperature at excitation power of $25MW/cm^2$ and $D_{\Gamma X} = 5\times10^8$ ev / cm .	69
Fig. 3 . 3 . 15	The computed normalized output photon density at different wavelengths for excitation power of $25MW/cm^2$, $D_{\Gamma X} = 5\times10^8$ ev / cm and confinement factor of $C_F = 3\times10^{-3}$.	70

Fig. 3 . 3 . 16	a - The time dependence of electron density in Γ valley for excitation power of $50MW/cm^2$, $D_{\Gamma X} = 5\times10^8$ ev / cm .	72
	b - The time dependence of electron density in X valley for excitation power of $50MW/cm^2$, $D_{\Gamma X} = 5\times10^8$ ev / cm .	72
Fig. 3 . 3 . 17	Electron temperature as a function of time for excitation fluence of 50 MW/cm^2 , $D_{\Gamma X} = 5\times10^8$ ev / cm .	73
Fig. 3 . 3 . 18	The computed normalized output photon density at different wavelengths for excitation fluence of 50 MW/cm^2 , $D_{\Gamma X} = 5\times10^8$ ev / cm and confinement factor of $C_F = 3\times10^{-3}$.	74
Fig. 3 . 3 . 19	The superposition of the experimental output photon density at $\lambda > 620nm$ (solid line) and the computed result at $\lambda = 640nm$ (dashed line) for excitation power of $50MW/cm^2$, $D_{\Gamma X} = 5\times10^8$ ev / cm and confinement factor of $C_F = 3\times10^{-3}$.	75
Fig. 3 . 3 . 20	The computed normalized output photon density at different wavelengths for excitation power fluence of $50MW/cm^2$, $D_{\Gamma X} = 5\times10^8$ ev / cm and confinement factor of $C_F = 1.5\times10^{-3}$.	77
Fig. 3 . 3 .21	The computed normalized output photon density at different wavelengths for excitation power fluence of	

	$50MW/cm^2$, $D_{\Gamma X} = 5\times10^8$ ev / cm and confinement $C_F = 6\times10^{-3}$.	78
Fig. 3 . 3 . 22	a - The time dependence of electron density in Γ valley at excitation power of $50MW/cm^2$, $D_{\Gamma X} = 1\times10^9$ ev / cm .	79
	b- The time dependence of electron density in X valley at excitation power of $50MW/cm^2$, $D_{\Gamma X} = 1\times10^9$ ev / cm .	79
Fig. 3 . 3 . 23	The time dependence of electron temperature for excitation power of $50MW/cm$ and $D_{\Gamma X} = 1\times10^9$ ev / cm .	80
Fig. 3 . 3 . 24	The computed normalized output photon density at different wavelengths for excitation power of $50MW/cm^2$, $D_{\Gamma X} = 1\times10^9$ ev / cm and confinement factor of $C_F = 3\times10^{-3}$.	81
Fig. 3 . 3 . 25	a - The time dependence of electron density in Γ valley at excitation power of $50MW/cm^2$, $D_{\Gamma X} = 2.5\times10^8$ ev / cm .	82
	b - The time dependence of electron density in X valley at excitation power of $50MW/cm^2$, $D_{\Gamma X} = 2.5\times10^8$ ev / cm .	82
Fig. 3 . 3. 26	The time dependence of electron temperature for excitation power of $50MW/cm^2$,$D_{\Gamma X} = 2.5\times10^8$ ev /	

	cm .	83
Fig. 3 . 3 . 27	The time dependence of Fermi level of electrons in Γ valley as a function of time for excitation power fluence of 5 and 50 MW / cm^2 .	84
Fig. 4.3.1 (a)-(f)	Time resolved photoluminescence profile of $Ga_{.56}In_{.44}P$ at energies of 2.107 , 2.081 , 2.046 , 1.981 ,1.945 and 1.919 ev , respectively .	92
Fig. 4. 3 . 2	Plot of the rise time of the time resolved photo-luminescence profiles as a function of the energy .	93
Fig. 4 . 3 . 3	Plot of the decay time of the time resolved photo-luminescence profiles as a function of the energy .	94
Fig . 4 . 3 . 4	The photoluminescence spectra of $Ga_{.56}In_{.44}P$ at t = 0 , 25 , 50 , 100 , 150 and 200 ps following the exciting laser pulse .	96
Fig. 4 . 4 . 1	(a) - The calculated photoluminescence spectra in $Ga_{.56}In_{.44}P$ at RT for carrier density of $1\times10^{18}cm^{-3}$ for the case of direct transition (k-selection rule) .	
	(b) - The calculated photoluminescence spectra in $Ga_{.56}In_{.44}P$ at RT for carrier density of $1\times10^{18}cm^{-3}$ for the case of indirect transition (non-k-selection rule)	100
Fig. 4 . 4 . 2	(a) - The calculated photoluminescence spectra in $Ga_{.56}In_{.5}P$ at RT for carrier density of $5\times10^{18}cm^{-3}$ for	

the case of direct transition (k selection rule).

(b) - The calculated photoluminescence spectra in $Ga_{.56}In_{.44}P$ at RT for carrier density of $5\times10^{18}cm^{-3}$ in the case of indirect transition (non-k-selection rule) 101

Fig. 4 . 5 . 1 The time dependence of photogenerated carrier density . The circles are experimental points and dashed line is the fit assuming exponential . 104

Fig.4 . 5 . 2 The time evolution of electron temperature in $Ga_{.56}In_{.44}P$. The circles are the experimental data , dash-dot curve is calculated for M.B. distribution function , broken curve is calculated for F.D. distribution and the solid curve is calculated in the presence of screening . 107

Fig. 5 . 2 . 1 Schematic diagram for the band structure of $GaAs_{1-x}P_x$. 116

Fig. 5 . 2 . 2 The variation of the direct and indirect band gap in $GaAs_{1-x}P$ with composition . 117

Fig. 5 . 2 . 3 The schematic diagram for three possible Auger precesses in semiconductors . 119

Fig. 5.4.1 (a)-(d) The time resolved photoluminescence profile of $GaAs_{1-x}P_x$ at room temperature for excitation power fluence of 3×10^8 , 6×10^8 , 1.2×10^9 and 2.8×10^9 W/cm^2 121

, respectively .

Fig. 5 . 4 . 2 The effective decay time $\tau_{eff}(n)$ vs. excitation power fluence . The circles are the experimental points , solid line is calculated from model (1) for $A=3.4\times10^{9}/s$, $B_R=9\times10^{-10}cm^3/s$ and dots , dashs , dot-dashs curves are calculated from model (2) for $C_{NR}=1.3.5\times10^{-29}cm^6/s$, respectively . 122

Fig. 5 . 4 . 3 The peak intensity of the time resolved photoluminescence profile in $GaAs_{.62}P_{.38}$ versus the excitation power fluence . 123

CHAPTER 1

INTRODUCTION

Over the past two decades a great deal of effort has been devoted to the research for the study of large band gap III-V ternary alloy semiconductor system of the type $A_{1-x}B_xM$ and $AM_{1-x}N_x$. The interest is easily traced to the need for wide band gap semiconductor lasers especially materials with direct optical transitions for the generation of efficient visible p - n junction luminescence . The realization of efficient conversion of electrical energy to optical energy in GaAs has led to partial substitution of P for As or Al for Ga in order to widen the the forbiden gap while retaining the direct optical transitions of GaAs . This substitution provides $GaAs_{1-x}P_x$ and $Ga_{1-x}Al_xP$ ternary semiconductors . Recent developments in the growth techniques of the compound semiconductors (Molecular Beam Epitaxy , Vapor Phase Epitaxy) has led to the opening of a new era in the fabrication of multilayer heterostructures , thin layer superlattices and semiconductor lasers .

Alloy semiconductors are beset by three sets of problems . First the problem of preparing the material . It is difficult and sometimes impossible to prepare large single - crystal samples of uniform composition by any method . The second set of problems comes in defining the composition of such less than perfect samples . Finally , the third set of problems consists of measuring the optical properties of these samples and relating them to alloy composition .

The study of hot - electron effect in III-V compound semiconductors has been the subject of a large number of papers[1,2] . Considerable effort has been devoted to the investigation of momentum and energy loss mechanisms of the hot carriers to the

lattice . The comparison between the experimental results and the theoretical expressions has to overcome the difficulty that energy distribution function of carriers can not be determined directly from transport experiments . Therefore , one has to solve the Boltzmann equation for various type of scattering mechanisms . An alternative method is to assume a certain type of distribution function and to obtain a calculated mobility - field characteristic from momentum and energy balance considerations . If the assumed distribution function is a Maxwellian or a Fermi Dirac distribution with the only adjustable parameter being the carrier temperature T_c , this model is called " electron - temperature model " . However it was pointed out by Straton[3] that it is applicable only for semiconductors with high carrier concentrations where interelectronic collisions are frequent enough to establish the described type of distribution function . Excitation of semiconductors with picosecond laser pulse generates high density carriers without causing any damage or heating the sample and makes it possible to study energy relaxation of degenerate hot carriers .

Information about the dynamics of hot carrier energy relaxation is important and fundamental in the design and fabrication of high speed devices . Time resolved absorption and luminescence spectroscopy of semiconductors provides direct information about the evolution of the carrier density as well as distribution function[4] . There are a variety of direct and direct techniques such as pump and probe[5] , optical Kerr gate[6] , upconversion gate[7] , and autocorrelation [8] to study the ultrafast processes in semiconductors . Each of these techniques has advantage as well as disadvantage . The streak camera offers the only direct method to measure the intensity profile on a picosecond time scale . The linear dependence of the detected light in this method avoids the confusion of nonlinear optical processes involved in the detection which is not offered in other techniques .

Energy relaxation of low density carriers in GaAs has been studied by Ulbrich by measuring the photoluminescence spectra under nanosecond laser pulse excitation[9]

. As tunable picosecond laser pulse became available , several groups (Smirl [10] , Leheny [11] , Von der Linde[12] and Alfano[13]) used these pulses to study the absorption and luminescence of semiconductors on picosecond time scale . They were able to obtain information about carrier carrier energy relaxation at intermediate excitation regime (photogenerated carrier density of less than $10^{18} cm^{-3}$) and concluded that electron gas cools to within 100 K of the lattice temperature in about 2-5 ps . From the results of picosecond reflection measurements Shank at el.[14] concluded that in GaAs , carriers with initial energy of .6 ev lose their energy in about 2 ps . In polar semiconductors like GaAs , $Ga_{1-x}In_xP$, the dominant mechanism for energy relaxation is carrier - LO phonon scattering[15] . Shah and coworkers[11] found modest slowing of energy lose rate at $10^{18} cm^{-3}$ carrier density . They attributed this reduction this reduction of energy relaxation to the screening of electron phonon interaction . Yoffa at el.[16] based on Random Phase Approximation approach calculated the effect of screening on the energy loss rate . She concluded when photogenerated carrier density exceeds the a critical value n_c , the interaction between carriers and LO phonons is reduced . Seymour at el.[17] studied the screening of hot carriers in GaAs by measuring the rise time of emission at different excitation power . He observed that the rise time of emission increased with excitation power as a result of the screening of the interaction of carriers and LO phonons . Similar work has been done by Yao at el.[18] in the case of GaSe which is a layered semiconductor and he observed that phonon emission rate by holes decreased with increasing excitation power . At the same time Van Driel[19] presented another argument that under high power excitation , enough optical phonons could be created to raise the optical phonon temperature into equilibrium with the partially cooled e-h plasma . In most of the experiments done to date , the semiconductor samples were excited at low temperature . There has not been that much information available in the literature about the carrier energy relaxation at room temperature even though most of the devices fabricated from semiconductors

are used at room temperature .

This thesis deals with the physics of high density carriers in $Ga_x In_{1-x} P$ and $GaAs_{1-x} P_x$ under picosecond laser pulse excitation at room temperature . The dynamics of carriers in optically pumped $Ga_x In_{1-x} P$ were studied by means of time resolved photoluminescence spectroscopy . The radiative and nonradiative recombination processes in $GaAs_{1-x} P$ were studied experimentally . In chapter 2 , the experimental set up including the laser system , detection system , and data storage and analysis system are explained . The generation of single pulse , selection and second harmonic generation of laser pulse will be discussed . The streak camera with the white cell delay unit will be covered in the detection system . The digitized data for time resolved fluorescence stored in the DEC Minc 11 minicomputer are analyzed by the scientific programs . The dynamics of carriers in $Ga_{.5} In_{.5} P$ under picosecond laser pulse excitation is presented in chapter 3 . The time evolution of carrier density , carrier temperature and the output photon density at different spectral region is calculated by solving the appropriate differential equations . The effect of stimulated emission in the output of the optically pumped semiconductor $Ga_{.5} In_{.5} P$ will be discussed and the computer simulation of the detected output at different wavelengths is presented . The screening of hot carrier energy relaxation in $Ga_x In_{1-x} P (x = .56)$ at room temperature is studied by analysis of the time resolved photoluminescence spectra measured by a streak camera is presented in chapter 4 . Time resolved photoluminescence spectra at different times following the excitation pulse were determined experimentally and were fitted to direct transition expression to obtain the reduced band gap , carrier density and carrier temperature . Theoretical time evolution of carrier temperature assuming M . B . distribution , F . D . distribution is calculated and the results are compared with the experimental data . In chapter 5 the radiative and nonradiative processes were studied in $GaAs_{1-x} P_x$ under high excitation power . The radiative and nonradiative rates , bimolecular and Auger rates have been

determined by studying the intensity dependence of the time resolved photolumines-cence profiles .

References

1 D . J . Oliver , Phys. Rev. 127 , 1045 (1962) .

2 R . S . Crandal , Phys. Rev. B1 ,730 (1970) .

3 R . Stratton , Proc. Roy. Soc. (London) , A 246 , 406 (1958) .

4 Semiconductors probed by Ultrafast Laser Spectroscopy , R.R.Alfano , Academic press , (1984) .

5 C . V . Shank , R . L . Fork , R . Yen , J . Shah , A . C . Gossard ,C . Wiesbuch , Solid State Comm. 47 , 981 (1983) .

6 M . A . Duguay , J .W . Hansen , Appl. Phys. Lett . 15 , 192 (1969) .

7 H . Mahr , M . D . Hirsch , Opt. Comm. 13 , 96 (1975) .

8 H . P . Weber , J. Appl. Phys. 39 , 6041 (1968) .

9 R . G . Ulbrich , Solid State Elec. 21 , 51 (1978) .

10 A . Elci ,A . L . Smirl , C . Y . Leung , M . O . Scully , Solid State Elec. 21 , 151 (1978) .

11 R . F . Lehny , J . Shah , R . L . Fork , C . V . Shank , A . Migus , Solid State Comm. 31 , 809 (1979) .

12 D . von der Linde , R . Lambrich , Phys. Rev . Lett. 41 , 1090 (1979) .

13 S . S . Yao , J . Buchert , R . R . Alfano , Phys. Rev. B 25 , 6534 (1982) .

14 C . V . Shank , D . H . Auston ,E . P . Ippen , O . Tesechki , Solid State Comm. 26 , 567 (1978) .

15 K . Kash , J . Shah , Appl. Phys. Lett. 45 , 401 (1984) .

16 E . Yoffa , Phys. Rev. B 23 , 1901 (1981) .

17 R . J . Seymour , M . R . Junnarkar , R . R . Alfano , Solid State Comm. 41 , 657 (1982) .

18 S . S . Yao , R . R . Alfano , Phys. Rev. B 26 , 4781 (1982) .

19 H . M . van Driel , Phys. Rev. B 26 , 2147 (1982) .

CHAPTER 2

EXPERIMENTAL TECHNIQUES

The experimental setup used for this research is described in this chapter . A brief introduction to the concept of mode-locking , pulse selection technique , second harmonic generation is given in the subsequent sections . The detection system (streak camera) is described at the end of this chapter .

2 . 1 Steady State Photoluminescence Setup

This setup has been used to characterize the samples under study . The photoluminescence spectra of samples under low excitation power have been studied using the setup which is shown in Fig. 2 . 1 . 1 .

The excitation source can be a lamp or gas ion laser . The output of an Argon laser at 488 nm was chopped and focussed onto the sample under study . The photoluminescence from samples was collected by a combination of lenses and imaged to the slit of Spex double spectrometer , and detected by a RCA S-20 photomultiplier and measured by a lock-in amplifier .The output of lock-in amplifier can be either connected to a computer or X-Y recorder .

2 . 2 TIME RESOLVED EXPERIMENTAL SETUP

The experimental setup[1] used to study the time resolved photoluminescence is shown in Fig. 2 . 2 . 1 . It is composed of a laser cavity , pulse selector , amplifier , second harmonic generator , and , a detection system , and data storage and analysis system .

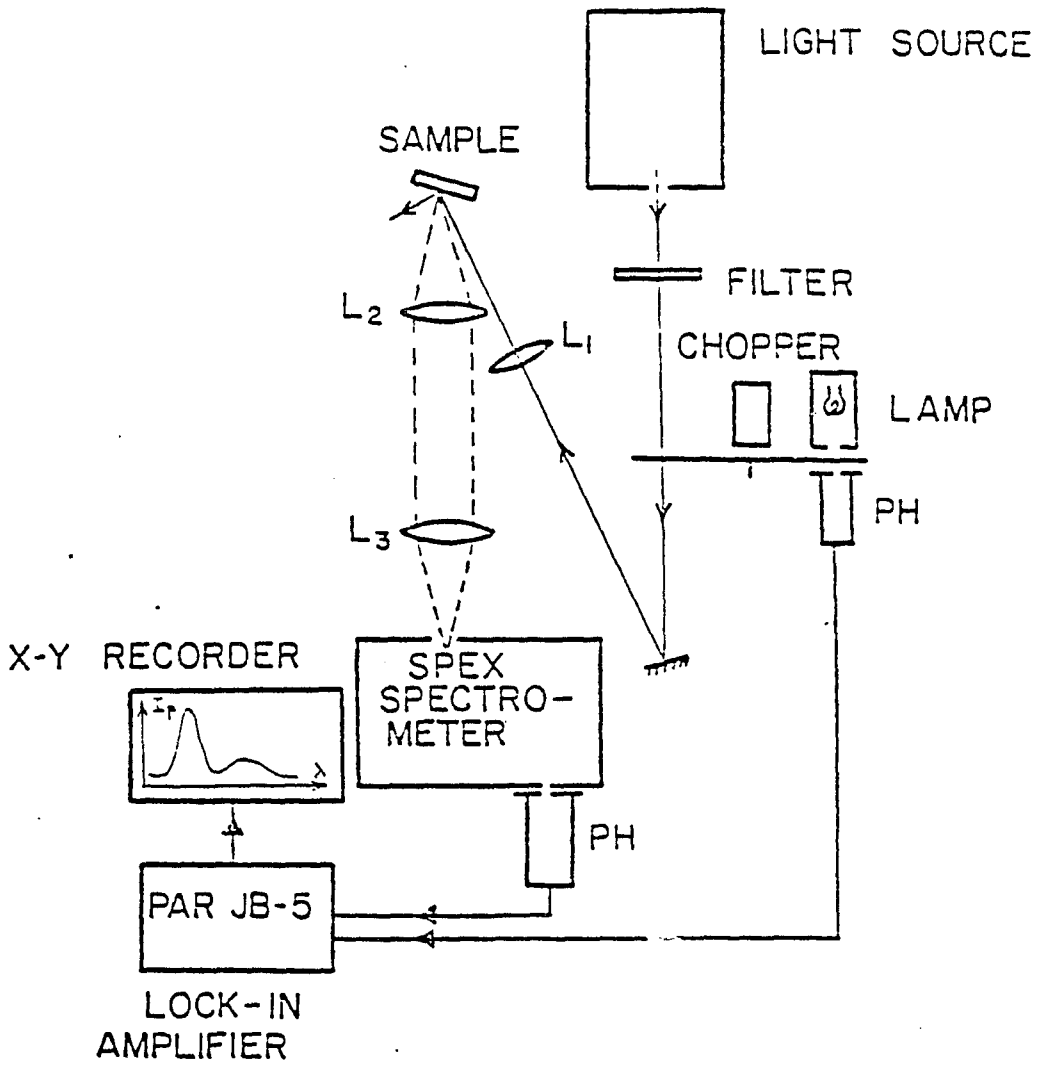

Fig. 2 . 1 . 1 Schematic diagram of the steady state luminescence setup (Ref. 1) .

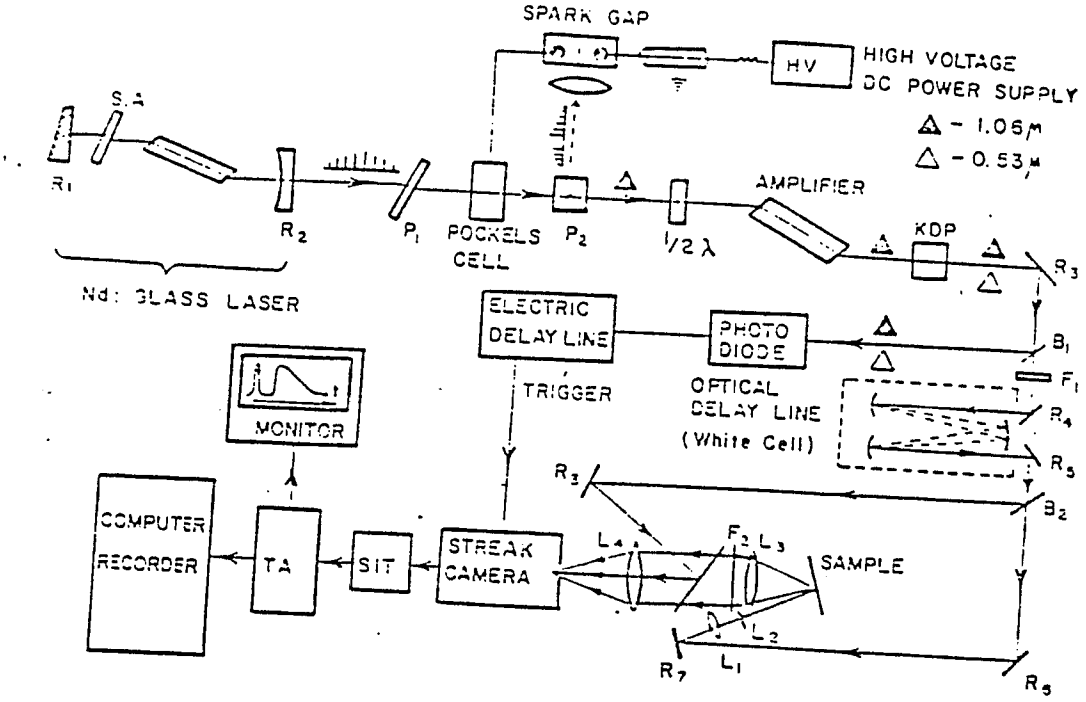

Fig. 2 . 2 . 1 Schematic diagram of picosecond time resolved spectroscopy setup (Ref. 1) .

2 . 2 . 1 Laser Resonator

A typical cavity design is shown in Fig. 2 . 2 . 2 . The lasing medium is Nd : glass rod pumped by a helical flash lamp connected to a power supply for optical excitation . The Nd : glass is a four level laser and its schematic energy level is shown in Fig. 2 . 2 . 3 . The excitation of laser rod with the flash lamp creates electrons in the excited states . The excited electrons can decay back to ground state either by spontaneous or stimulated emission . In practice , the electrons in the level 2 decay to the metastable level 3 by nonradiative transition . The metastable level acts as a trap and in the process of population inversion , the photon generated by spontaneous emission bounce back and forth in the laser cavity and they stimulate more atoms to emit photons of the same frequency , phase and direction[2] .

The light emitted by the laser is determined by the fluorescence band width , quantum yield of the lasing medium and the configuration of the laser cavity (Yarive et. al [3]) . Usually the fluorescence spectrum of the lasing medium is broad and from all the possible frequencies only some are allowed in the laser cavity which are called modes[4] . There are two types of modes in the laser cavity ; longitudinal and transverse modes . The longitudinal modes differ from each other only in frequency , and transverse modes are different from each other in the distribution of the field as well as the frequency . The allowed longitudinal modes in the cavity is governed by the equation of a standing wave which is given by

$$n\ \lambda_j = L \qquad (2.2.1)$$

where L is the length of the cavity , λ_j is the wavelength of an allowed mode and n is an integer . The number of active modes in the laser cavity is generally high (order of 10^4) for a 1- meter cavity . The number of transverse modes (TEM_{mn}) in the cavity is lower than longitudinal modes . The output of the laser cavity is usually is noise like

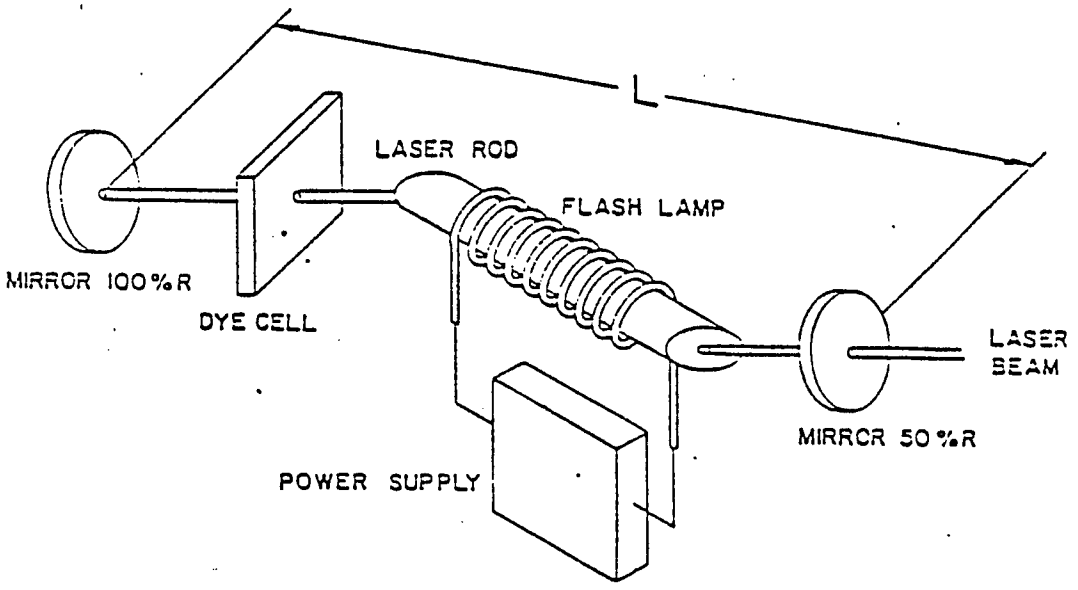

Fig. 2 . 2 . 2 Configuration of the optical cavity resonator (Ref. 1) .

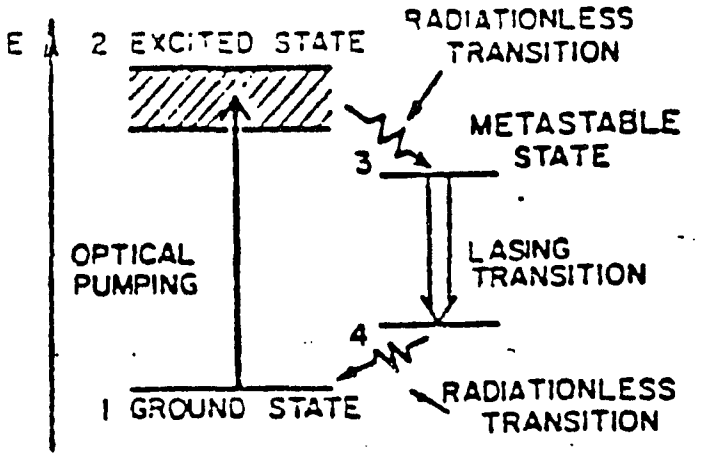

Fig. 2 . 2 . 3 Energy level of Nd : glass laser (Ref. 2) .

and it has a pulse width of a few microseconds (time duration of the flash lamp) . To obtain a short pulse , all the different modes are forced to oscillate in phase by placing a saturable absorber in the cavity . This process is called mode-locking . Mocker and Collins[5] and DeMaria[6] were the first to produce mode-locked pulses using a saturable absorber . It is a combination of lasing medium and the saturable absorber which produces the short pulses . The pulse width of the generated laser pulse is determined by the recovery time of the dye typically 10 ps . The initial noise like modes are absorbed by the saturable absorber and only modes above the background will get through the dye . When gain increases , the high intensity modes will bleach the dye . In general one can say that the saturable absorber acts as an optical shutter closing and opening at frequency equal to the difference in frequency of two adjacent modes ($C / 2L$).

2 . 3 Single Pulse Selection and Pulse Width Measurement

A schematic diagram of the experimental apparatus is shown in Fig. 2 . 3 . 1 . The single pulse can be selected from the train by a pair of cross polarizers placed between a Pockell cell and a spark gap . The spark gap is filled with Nitrogen gas under pressure and connected to the high voltage power supply through a 10 $M\Omega$ resistor by a double sheathed cable which forms the transmission lines from the electrode of the spark gap. The output of the Pockells cell was dumped into a 50 Ω resistor through a 15 ft long cable to eliminate the high voltage pulse reflection from returning to the Pockell cell. A 4 cm focal length cylindrical lens was used to focus the laser pulses into the spark gap. The first polarizer is polarized along the direction of polarization of the output laser train at 1.054 μm from the cavity. When the first few pulses pass through the first polarizer and Pockells cell , they get reflected by the second polarizing prism and focused into the spark gap, the Nitrogen gas in the spark gap is ionized by the first few laser pulses and the avalanche breakdown across the

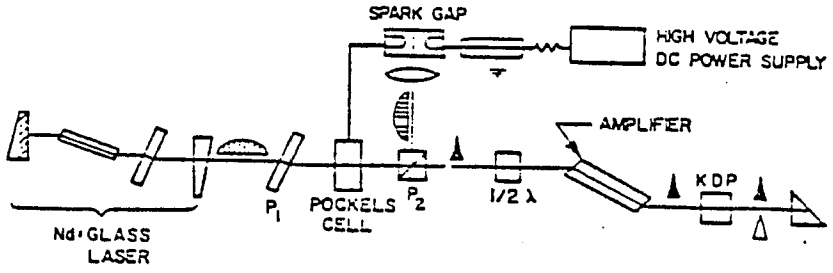

Fig. 2 . 3 . 1 Nd : glass laser with second harmonic generation and amplifier (Ref. 1) .

electrode appears to form a conductive path for high voltage . Because of the impedance matching between two ports of the cable, a high voltage pulse 8 kv, 5 ns is then applied to the Pockell cells . The axes of the index ellipsoid of refraction of the crystal (KDP) inside the Pockells cell are rotated because of the nonlinear electro-optical effect. The polarization of the next subsequent incoming laser pulse just after the first few pulses is then rotated to match the polarization direction of the second prism polarizer and escape through it. Since the high voltage (8 kv) applied to the Pockcells cell lasts for about 5 ns, there is not a long enough time period to have another single pulse being transmitted. Actually, the time separation between two adjacent single pulses is about 7 ns, which is longer than the time period for the Pockells cell to be functioning. Fig. 2 . 3 . 2 shows the typical picture of the train and a selected pulse as measured by fast oscilloscope .

The amplification of selected pulse can be obtained by passing the selected pulse through a laser rod same as the one used in the oscillator . However the diameter of the rod in the amplification stage should be larger than the rod employed in the oscillator , typically 3/4 inch . Also the amplifier rod has to be doped at lower concentration for more uniform pumping .

The pulse width of the selected pulse can be measured by a variety of methods such as second harmonic generation[7] and two photon fluorescence [8] and streak camera . In our lab we used the (TPF) technique to measure the pulse width . The experimental arrangement for the TPF is shown in Fig. 2.3.3 . The beam is split into two beams by a 50 % transmission beam splitter and directed into a cell containing a dye which does not absorb at the laser wavelength . The dye molecules however may absorb two photons simultaneously which leads to fluorescence . A camera is placed in front of the bright spot and measures the width of the spot . The measured value of the pulse width in our setup at $1.06\mu m$ was ~ 8 ps .

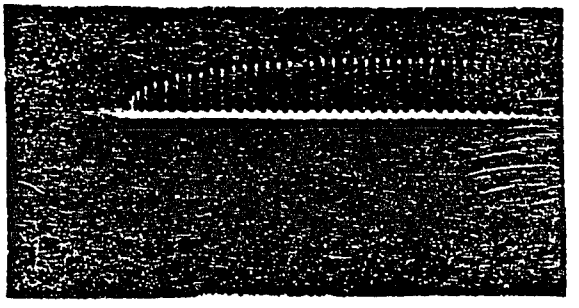

Fig. 2 . 3 . 2 (a) - The picture of the picosecond laser pulse train with one pulse selected .

(b) - The picture of a selected laser pulse .

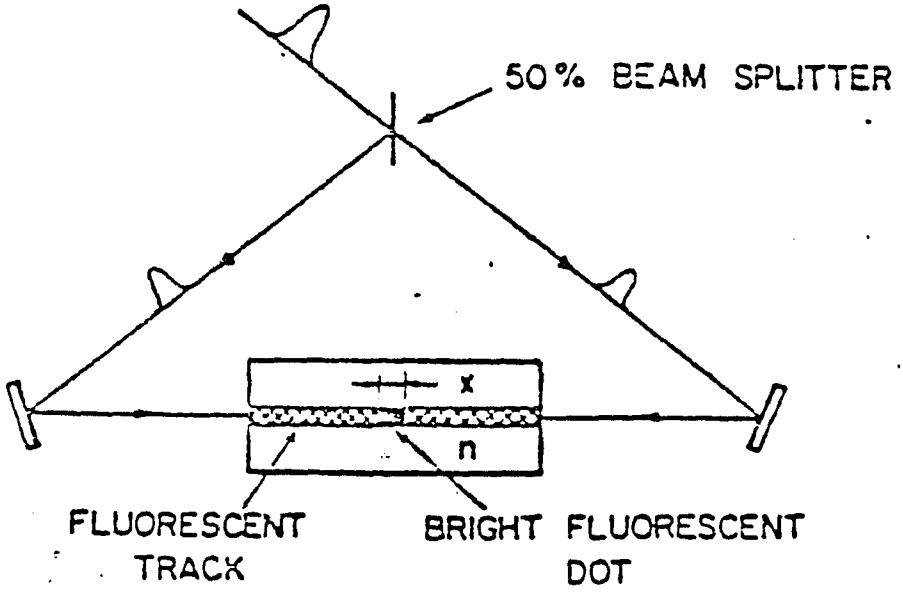

Fig. 2 . 3 . 3 Schematic diagram of the setup for two photon fluorescence measurements (Ref. 2) .

2 . 4 Second Harmonic Generation

In order to photoexcite the electrons in a semiconductor from valence band to conduction band , the energy of the exciting photons must exceed the band gap of the semiconductor under investigation . Since most of the semiconductors have a band gap greater than photon energy of 1.06μm (1.17 ev) , the conversion of 1.06μm pulses to .53μm is desirable . The pulses of 530 nm can be obtained by passing the 1.06μm through a KDP (Potassium Dihdrogen Phosphate) crystal .

The intensity of the second harmonic is given by

$$I\ (\ 2\omega\ ,L\ ) = (X^{2\omega})^2 \left[\frac{\sin^2 \frac{\Delta k L}{2}}{(\frac{\Delta k L}{2})^2} \right] I^2\ (\ \omega\ ) \qquad (2.4.1)$$

where Δk is expressed as

$$\Delta k\ =\ |\ k_2 - 2k\ | = (\frac{2\omega}{c})\ (\ n_{2\omega} - n_{\omega}\ )$$

In Eq. 2.4.1 , $I\ (\ \omega\ ) , I\ (\ 2\omega\ )$ are the intensity of the laser and generated second harmonics , L is the crystal length , k , n_{ω} and $n_{2\omega}$ are the wave vector and index of refraction of the crystal at laser and its second harmonics and finally X is the susceptibility constant . In Eq. 2.4.1 when $\Delta k = 0$, the bracket is maximum and highest degree of conversion can be obtained . This condition is called phase matching . This can be satisfied by orientation of SHG crystal . In a properly phased matched condition the efficiency of conversion is about 10 % .

2 . 5 Streak Camera System

The detection system used in this research is a streak camera which offers the best way of directly measuring the time resolved photoluminescence in ps time scale .

The streak camera is a device which converts time information from a luminous

event to a spatial information[9]. In early 1970's the streak camera was introduced by Bradly[10] and Shelev[11] to study the transient photoluminescence . A simplified schematic diagram of the streak tube operation is shown in Fig. 2.5.2. The photoelectrons generated by light incident on the photocathode are proportion to the intensity of the light . These electrons are then accelerated into the streak tube by a accelerating voltage applied to the plates and at the mean time they are swept at a known rate over a known disance which converts the temporal information into spatial information[12] . The accelerated electrons then strike a microchannel plate capable of producing multiplication through secondary emission . These secondary electrons strike a phosphor screen forming the streak image . This image can be digitized to store the information in a computer for data analysis .

Because of the nonlinearity of the streak tube each streak camera has to be calibrated . To do this a 8 ps , 530 nm laser pulse is passed through a pair of partially reflecting mirrors (etalon) with transmission coefficient of T . The result is a series of pulses separated in time by $\Delta\tau = 2d / c$, where c is the speed of light and d is the spacing of the mirrors . The intensity of each pulse decreases respect to the previous pulse by a factor of $(1-T)^2$. In general the envelope of these pulses decays exponentially according to the following equation

$$I = = I_0 \exp\left\{ \frac{t_k}{\Delta\tau} \ln (1 - T)^2 \right\} \qquad (2.5.1)$$

where $t_k = k\ \Delta\tau$ and k is an integer . Fig. 2.5.1 shows the intensity profile of these pulses which can be used to calibrate the time axes of the streak camera . The sweep rate $\frac{\Delta T}{\Delta X}$ per channel versus the channel number can be used to calibrate the time axes and intensity calibration can be done according to the following equation

$$I(t) = I(x)\frac{\Delta X}{\Delta t} \qquad (2.5.2)$$

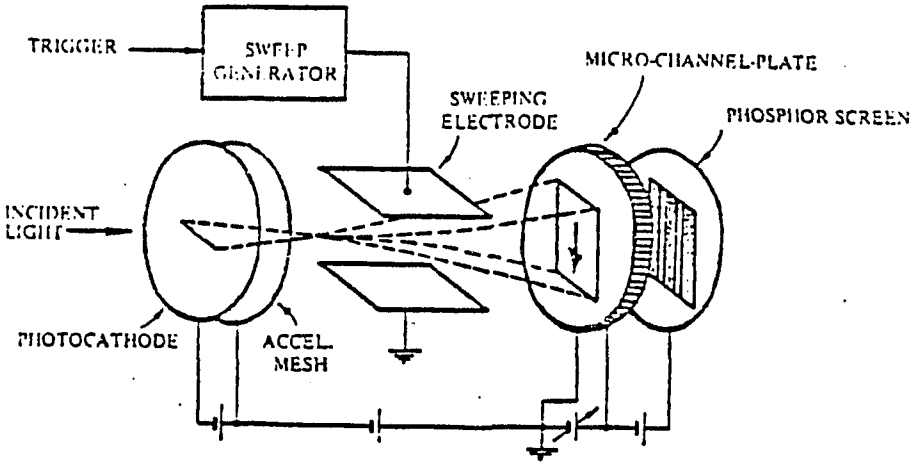

Fig. 2.5.2. Schematic diagram of a streak camera tube (Ref. 1)

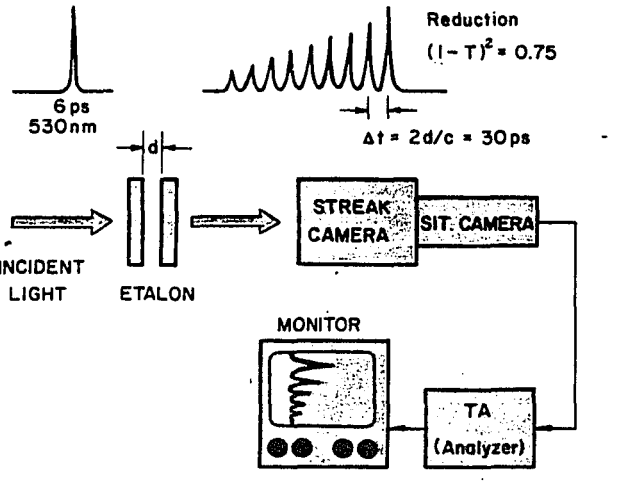

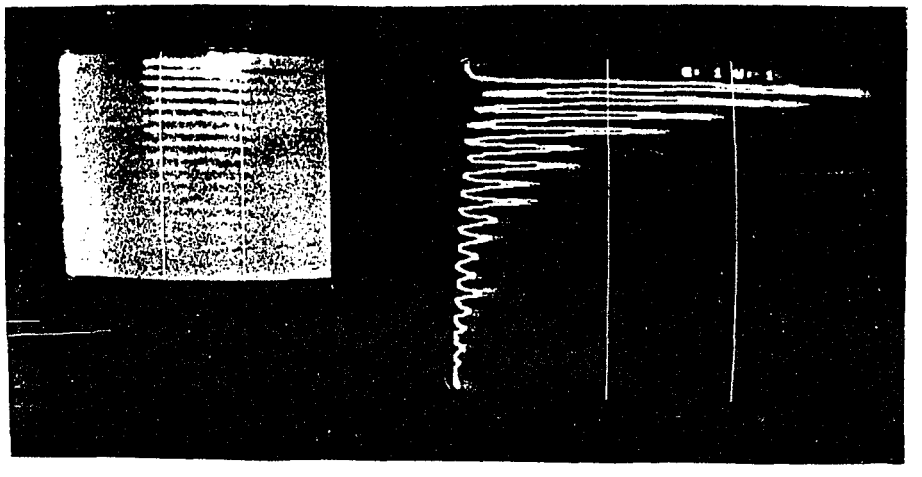

Fig. 2.5.1 (a) - Schematic diagram of calibration technique for a streak camera .

(b) - Graphic representation of the intensity profile for a 8 ps laser pulse passing through a 30 ps etalon .

where ΔX is the number of channels between peaks and $\Delta \tau$ is fixed for a given etalon mirrors .

The total time resolution of a streak camera deponds on many factors such as initial velocities of the photoelectrons , spatial resolution of the slit and time spread occurring between the photocathode and mesh electrode . The temporal resolution is defined as the *FHWM* of the streak image . This is measured by allowing a sufficiently short pulse to enter the streak camera and recording the *FHWM* of the image . If we assume the temporal resolution of the streak camera is T_s and the *FHWM* of the incident pulse to be T_p then the measured *FHWM* time T is given by[12]

$$T = (T_s^2 + T_p^2)^{\frac{1}{2}} \qquad (2.5.3)$$

Therefore if T_p is known then it is possible to determine the T_s which is the temporal resolution of the streak camera . The overall resolution of the streak camera used for this research is 12 ps .

A DEC Minc 11 minicomputer was used to store the digitized data from the temporal analyzer and this data was transfered to a VAX 11/780 for curve fitting and data reduction .

References

1 P . Y . Lu, P . P . Ho, and R . R . Alfano, IEE., J . of Quan. Electron. QE-15, 406 (1979) .

2 Biological Events probed by Ultrafast Laser spectroscopy , Chapter 17 , A.G. Doukes , J. Buchert , R.R. Alfano , Academic press , Newyork (1982) .

3 A . Yarive ," Quantum Electronics " , 2nd edition , Wiley , NewYork (1975) .

4- A . G . Fox , T. Li , Bell Syst. Tech. J . 40 , 453 (1961) .

5- M . Mocker , R . J . Collins , Appl. Phys. Lett. 7 , 270 (1965) .

6- A . J . DeMaria, D . A . Stetser, W . H . Glenn, Jr., Science 156, 1559 (1967) .

7- E . P . Ippen , C . V . Shank ," Ultrafast Laser Pulses " , edited by S.L.Shapiro , p 83 (1977) .

8- J . A . Giordmaine , P . M . Rentzepis , S.L. Shapiro , K.W.Wecht ,Appl. Phys. lett. 11 , 216 (1967) .

9 N . H . Schiller , R . R . Alfano , Laser Focus Magazine , p 43-45 (1982) .

10 D . J . Bradley and Geoffrey H . C . New, Proceed. of IEEE , 62 ,313 (1974) .

11 M . Y. Shelev , M . C . Richardson , A . J . Alcock , Appl. Phys. Lett. 18 , 18 (1971) .

12 N . H. Schiller , Y . Tsuchiya , E . Inuzuka , K . Kamiya , H . Iida , R . R . Alfano , Opt. Spect. 14 , 55 (1980) .

CHAPTER 3

Picosecond Carrier Dynamics in optically Pumped Semiconductor $Ga_{.5}In_{.5}P$

3.1 - Experimental Observation of Unusual Time Resolved Photoluminescence in $Ga_{.5}In_{.5}P$ under Picosecond Laser Pulse Excitation.

Before embarking on the discussion of the experimental aspects of picosecond optically pumped semiconductors, it should be noted that the objective of this chapter is to explain and interpret the unusual behavior of time resolved photoluminescence in $Ga_{.5}In_{.5}P$ semiconductor under picosecond laser pulse excitation. Fig 3 . 1 . 1 shows the time resolved photoluminescence profiles of $Ga_{.5}In_{.5}P$ under excitation power of $10 MW / cm^2$. The two curves represents the output at two different spectral regions with the same pumping power. These spectrally resolved temporal profiles were obtained by placing filters in front of streak camera. The important feature is the different temporal behavior at different wavelengths . Time resolved profile at short wavelengths is shown in Fig 3 . 1 . 1 (a) . This corresponds to the temporal profile at wavelengths shorter than 620 nm($\lambda < 620 nm$ or E > 2 ev) or another words the time resolved profile of high energy portion of the photoluminescence spectra . The decay profile is exponential with decay time of 18$\pm$2 ps . Fig. 3 . 1 . (b) shows the temporal profile for wavelengths longer than 620 nm (λ > 620 nm or E < 2 ev) or one can say the time resolved profile at lower energy portion of the photoluminescence spectra . The decay time of this curve is about 40 $\pm$5 ps . When excitation power increased to $\sim 50 MW / cm^2$, the general trend was again the same as Fig. 3 . 3 . 1 but

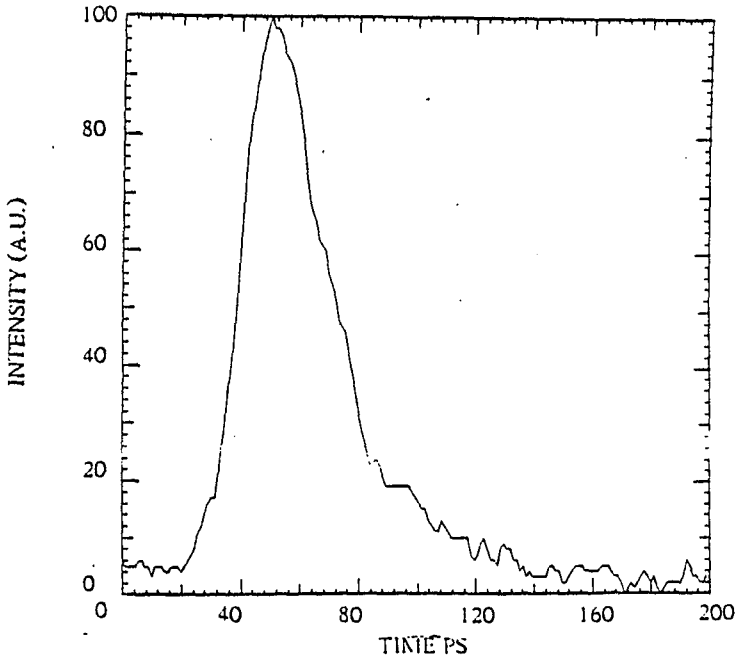

Fig. 3 . 1 . 1 (a) - Time resolved photoluminescence profile of $Ga_{.5}In_{.5}P$ at short wavelengths ($\lambda < 620nm$) for excitation fluence of $10MW / cm^2$.

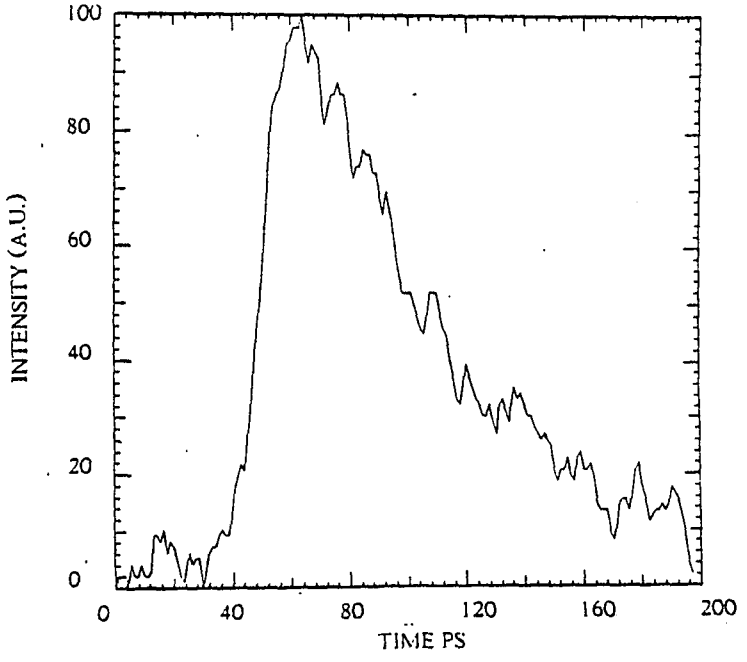

Fig. 3 . 1 . 1 (b) - Time resolved photoluminescence profile of $Ga_{.5}In_{.5}P$ at long wavelengths $\lambda > 620\ nm$ for excitation fluence of $10MW / cm^2$.

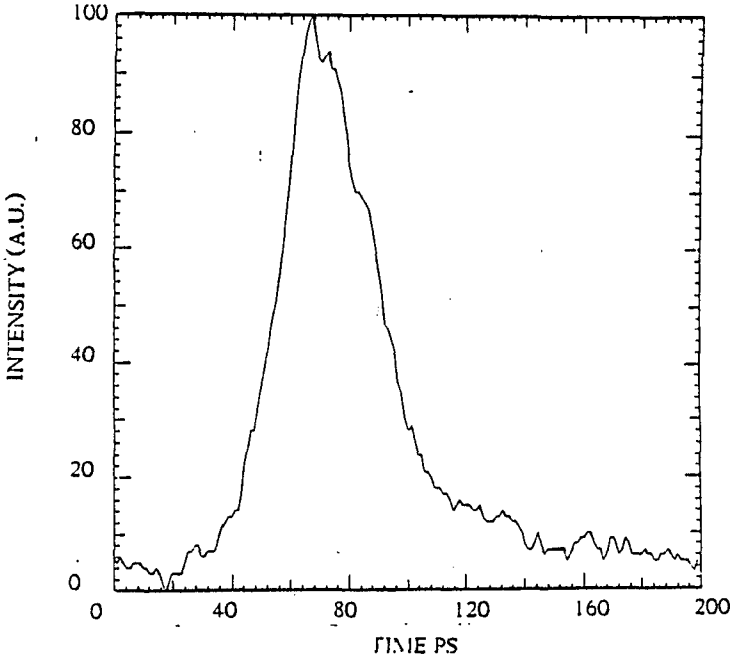

Fig. 3 . 1 . 2 (a) - Time resolved photoluminescence profile of $Ga_{.5}In_{.5}P$ at short wavelengths $\lambda < 620nm$ for excitation fluence of 50 MW / cm^2

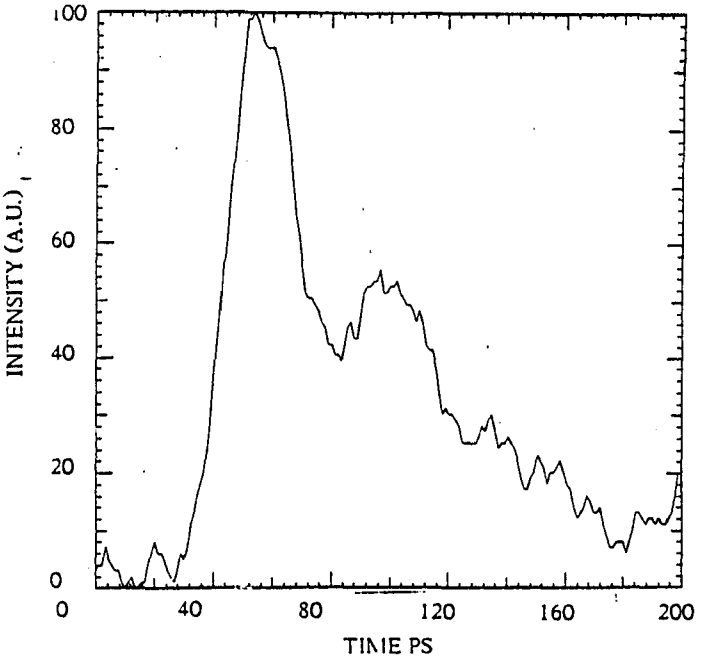

Fig. 3 . 1 . 2 (b) - Time resolved photoluminescence profile of $Ga_{.5}In_{.5}P$ at long wavelengths $\lambda > 620\ nm$ for excitation fluence of $50MW / cm^2$.

several interesting features began to appear. As expected from band filling, shorter wavelength time resolved profile is the same as the low excitation power (compare Fig 3.1.1 a and Fig 3.1.2 b) but at longer wavelengths there is an unusual temporal profile . At longer wavelengths , the time resolved profile acquired a distinct tail as excitation power increased even to the point of developing a secondary peak at longest wavelength of emission (see Fig 3 . 1 . 2 b) . In order to explain the results of the measurements shown in Fig. 3.3.1 and Fig. 3.3.2 one has to calculate the time evolution of carrier density and carrier temperature . This is because the time dependence of output photon density depends on these two dynamical variables . In the remaining of this chapter , I have tried to explain, interpret and also present a computer simulation of output of optically pumped $Ga_{.5}In_{.5}P$ under picosecond laser pulse excitation . Before concentrating on the dynamical equations for carrier density , carrier temperature and output photon density, the experimental method involved in this chapter will be given and then band structure of $Ga_x In_{1-x} P$ is discussed to give a background about the sample .

Experimental Method

The experimental setup used here is described in detail in chapter 2 . A second harmonic (527 nm) of Nd : glass laser pulse of 8 ps duration was used to excite the sample of $Ga_{.5}In_{.5}P$ on the front surface . The sample was 1 μm thick , n doped ($\sim 1\times10^{17} cm^{-3}$) and grown by MBE on a GaAs substrate . The composition of sample was determined from the calibration of the band gap versus composition[12] . The band gap of the sample was determined to be 1.87 ev at room temperature from the direct transition relationship $E_g = h\nu_p - \frac{1}{2}kT$ where $h\nu_p$ is the peak energy in the low power steady state photoluminescence spectra and $\frac{1}{2}kT$ accounts for the direct transition of the carriers . The photoluminescence from sample was collected by a combination of

lenses and imaged to a 30 μm slit of a Hamamatsu streak camera . The time resolution of detection system was approximately 10 ps . The excitation area was measured to be $5\times10^{-3}\ cm^{-2}$ and excitation power fluence was varied between 5 to 50 MW / cm^2 by placing ND filters in the path of the exciting laser pulse . In order to measure the time resolved photoluminescence at different energies various filters were placed in front of the streak camera . For example the time resolved photoluminescence profiles shown in Fig. (3.1.1 -a) and Fig. (3.1.2 -a) which are correspond to high energy portion of the photoluminescence spectra were obtained by placing a SP 620 in front of the streak camera . Similarly , the time resolved profiles shown in Fig. (3.1.1 - b) and Fig. (3.1.2 - b) were obtained by placing a R62 filter in front of the streak camera . These profiles are coresopnd to low energy portion of the photoluminescence spectra .

3 . 2 - The Band Structure of $Ga_x In_{1-x} P$

It is well known that direct band gap semiconductors have inherently short radiative life time and high radiative efficiency. Unfortunately, such direct band gap semiconductors have low band gap, leading to emission in IR or near IR . In order to increase the direct band gap and shifting the emission to visible region of the spectrum, ternary semiconductor have been prepared from a small band gap like InP and an indirect large band gap like GaP leading to production of $Ga_x In_{1-x} P$ ternary alloys . In spite of the large mismatch of the binary components InP (5.8688 A^o) and GaP (5.4512 A^o) and the difficulty in the synthesis of the alloy by means of both Vapor Phase Epitaxy [1] (VPE) and Liquid Phase Epitaxy [2] , progress has been made in the preparation of $Ga_x In_{1-x} P$ by Molecular Beam Epitaxy [3].

The band structure of GaP and InP have been calculated theoretically and band structure parameters of these semiconductors have been determined thoroughly from a large number of experiments[4,5] . However the band structure of $Ga_x In_{1-x} P$ has been controversial especially determination of crossover composition. It is important to

determine the behavior of the conduction bands (Γ and X band edges) as a function of the composition x, particularly the location of $\Gamma-X$ crossover ($E_\Gamma = E_X$, $x = x_c$). There has been disagreement about the value of crossover composition (x_c) . From the measurements on diodes , Lorenz at el. [6] determined $x_c = .8$. Measurements of band edge absorption coefficient as a function of photon energy by Rodot at el. [7] determined $x_c = .63$. This value has been confirmed by Williams at el.[8] using the photoluminescence spectra and by Hakki at ei. [9] using hydrostatic pressure measurements. Using the cathodoluminescence peaks at 300 K as the position of the band gap, Lorentz assigned the value of $x_c = .74$ to the crossover composition with a parabolic empirical variation of the band gap which is given by [6]

$$E_g = 1.34 + 1.426\,x + .758\,x\,(x-1) \qquad (3.2.1)$$

Onton and Chickota [10] confirmed the results of Lorentz based on low temperature photoluminescence spectra. In GaP an InP, the indirect band gap $E_i = X_1^c - \Gamma_8^v$ is nearly the same, so that the disagreement on the value of x_c is mainly due to discrepancy on the variation of lowest direct band gap $E_d = \Gamma_8^c - \Gamma_8^v$ versus the composition. In order to determine the precise electronic structure of GaInP and to clarify the discrepancy , Alibert et al. [11] and coworkers applied the modulation spectroscopy technique to InP and GaP and GaInP alloy system since it is generally recognized that this method represents the most accurate process for determining transition energies of interband critical points. The sharp optical structures obtained by modulation method is usually not washed out by alloy composition fluctuations. They performed Electro-Reflectance (ER) experiments on high purity and very homogeneous materials at room temperature. The important results obtained by them are given by empirical formula for variation of direct band gap which is given by

$$E_d = 1.345 + 1.435\,x + .5\,x\,(x-1) \qquad (3.2.2)$$

and they assigned the value of $x_c = .63 \pm .015$ to crossover composition with

$E_c = 2.14 \pm .01$ ev . One of the reason behind the discrepancy of determining the cross-over composition is attributed to the poor quality of the samples. The higher estimate of x_c has been based primarily upon photoluminescence measurements while electro reflectance has given usually a lower estimate. Also photoluminescence measurements are sensitive to donor and acceptor impurities which yield transitions below the band edge. R. J. Nelson and N. Holonyak Jr. at el. [12] used both absorption and photo-luminescence measurements on high quality lattice matched GaInP grown by constant temperature Liquid Phase Epitaxy on GaAsp substrate. These crystals were of sufficient quality and low enough impurities ($<3\times10^{16}cm^{-3}$) to permit the first observation of Γ exciton peak in the absorption measurements at T=77 K . Fig 3.2.1 shows the absorption curve for an x=.69 of $Ga_x In_{1-x} P$ sample. At 77 K the exciton peak occurs at 5530 A (2.242 ev) but as shown in Fig 3 . 2 . 1 this peak is not present at room temperature. To determine the direct band gap at Γ point they used the Elliot's expression for the absorption coefficient for $E > E_\Gamma$ assuming the optical transition was direct between nondegenerate parabolic energy band including the exciton effect. According to Elliot's theory, the absorption coefficient at energy E can be described as

$$\alpha(E) = \alpha'(E_\Gamma) \exp\left(\frac{z}{2}\right) \sinh z \qquad (3.2.3)$$

where $z = \pi \left[\frac{E_{exc}}{E - E_\Gamma}\right]^{\frac{1}{2}}$, $\alpha'(E_\Gamma)$ is the value of absorption coefficient at the energy gap and E_{exc} is the exciton binding energy. At 77k where exciton peak is resolved they determined the band gap by adding the exciton energy to the exciton peak energy. To obtain the exciton binding energy they have fitted the experimental data of Fig.3.2.1 to the Eq. (3.2.3) where $\alpha'(E_\Gamma)$ was set equal to the minimum value of the absorption coefficient on the high energy side of the exciton peak. At 300 K where the exciton peak was not resolved they varied both E_Γ and E_{exc} to obtain the best fit to the experimental data. In summary, they found the variation of band gap with composition at

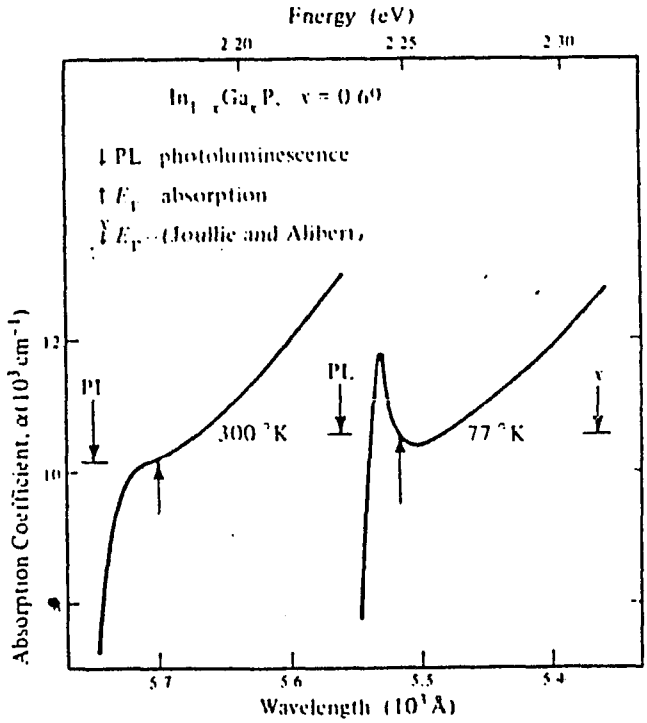

Fig. 3 . 2 . 1 - Absorption coefficient of $Ga_x In_{1-x} P$ (x=.69) at 77 and 300 K . The position of direct band edge (E_Γ) is shown by arrow . Also indicated are the photoluminescence peaks (Ref. 12) .

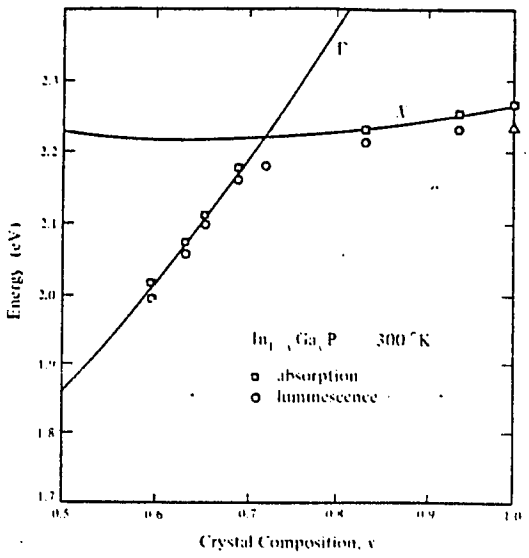

Fig. 3 . 2 . 3 - Dependence of absorption edge and photoluminescence peak energy on alloy composition in $Ga_x In_{1-x} P$ at T=300 K . The absorption band edges are indicated by squares and photoluminescence peak energies by circles (Ref. 12) .

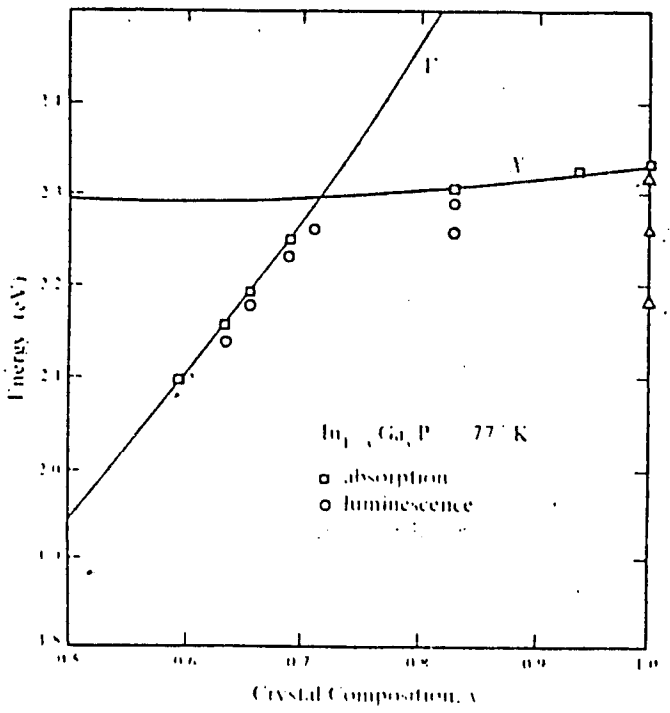

Fig. 3 . 2 . 2 - Dependence of absorption edge and photoluminescence peak energy on alloy composition in $Ga_x In_{1-x} P$ at T=77 K . The absorption band edges are indicated by squares and photoluminescence peak energies by circles (Ref. 12) .

T=77 K can be expressed as

$$E_\Gamma = 1.414+1.452x +.758x\,(x-1) \tag{3.2.4}$$

For T=300k, the band gap is given by

$$E_\Gamma = 1.351 + 1.429\,x + .786\,x\,(x-1) \tag{3.2.5}$$

The Eqs. (3.2.4) and (3.2.5) for the Γ energy gap are more accurate than those previously reported by luminescence and modulation reflection measurements where the exciton peak was not resolved. Fig. 3 . 2 . 2 and Fig 3 . 2 . 3 shows the experimental plot of the absorption edge in GaInP at 77 and 300k respectively. Therefore on can see from Eq. (3.2.5) that band gap of GaInP ternary semiconductor increases from 1.351 ev (x=0 , direct gap) to 2.78 ev (x=1 , indirect gap) and at x=.73 the direct -indirect crossover occurs. The band structure of GaInP is shown in Fig. 3 . 2 . 4 . The direct band gap, hereafter referred to as E_Γ is given by Eq (3.2.5) for T=300k. The spin orbit splitting is located about .1 ev below the light and heavy hole valence band. The central Γ valley effective mass is given by [13]

$$m_\Gamma(x) = (\,.068 + .052\,x\,)\,m^*_0 \tag{3.2.6}$$

The effective mass of heavy hole, light hole and split off holes in $Ga_{.5}In_{.5}P$ can be determined by interpolation between the values in InP and GaP and are calculated to be .51, .16, .1 respectively. There are effectively 6 X valleys in the [111] symmetry directions at the Brillouin zone edge and they are located higher than Γ valley . In $Ga_{.5}In_{.5}P$ the separation of X and Γ valley is ΔE = .34 ev .

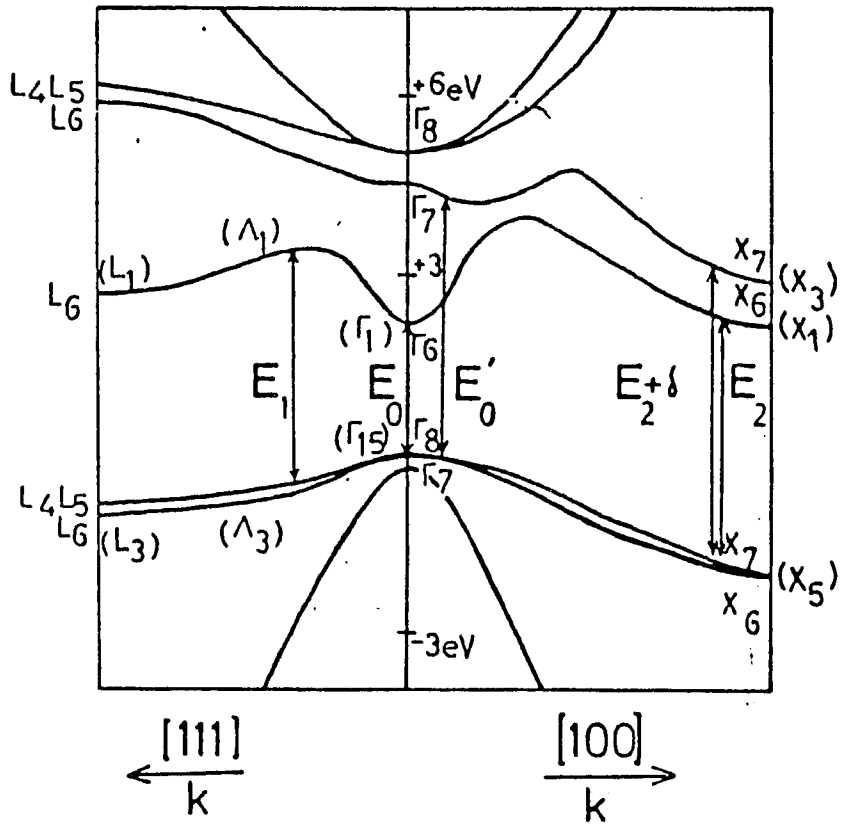

Fig. 3 . 2 . 4 Simplified band structure of $Ga_x In_{1-x} P(x=.5)$.

3 . 3 - Carrier Dynamics in $Ga_{.5}In_{.5}P$ under picosecond Laser Pulse Excitation

In general, the state of the semiconductor can be described by giving the occupation number of k states in the various bands in the form of distribution function $f_j(k)$ for each band j , where we can write

$$n = 2\int \frac{d^3\vec{k}}{(2\pi)^3} f_j(\vec{k}) \tag{3.3.1}$$

where n is the number of carriers in the band j . In most of the situations , because of the parabolic nature of the conduction and valence band the Eq. (3.3.1) can be converted into the energy space as

$$n = \int_0^\infty \rho(E) f(E) dE \tag{3.3.2}$$

where $\rho(E)$ is the density of states and is given by

$$\rho(E) = 4\pi(\frac{2m}{h})^{\frac{3}{2}}(E-E_g)^{\frac{1}{2}} \tag{3.3.3}$$

and $f(E)$ is the Fermi-Dirac distribution function and in given by

$$f(E) = \left\{ 1+\exp(E-F_c)/\ KT_c \right\}^{-1} \tag{3.3.4}$$

If we choose $\epsilon = \frac{E-E_g}{KT_c}$ and $\frac{F_c}{KT_c} = \eta$ then the Eq. (3.3.2) becomes

$$n = N_c \int_0^\infty \frac{\epsilon^{\frac{1}{2}}}{1+e^{\epsilon-\eta}} d\epsilon \tag{3.3.5}$$

where $N_c = 2(\frac{2\pi m_c^* kT_c}{h^2})^{\frac{3}{2}}$ and sometimes it is called the effective density of states. The integral in Eq. (3.3.5) is called Fermi-Dirac integrals and unfortunately there is no analytical solution for this integral. However tables do exist for these integrals including the various powers of the reduced energy multiplying the Fermi-Dirac dis-

tribution function. The actual integrals are in the form of

$$F_j(\eta) = \frac{1}{\Gamma(j+1)} \int_0^\infty \frac{\epsilon^j \, d\epsilon}{1+e^{\epsilon-\eta}} \tag{3.3.6}$$

When carrier density exceeds a certain value n_{deg} , the quasi-Fermi level moves into the band and carrier distribution is called degenerate[14]. Fig. 3 . 3 . 1 shows the degenerate and nondegenerate electron distributions . The equation establishing the degenerate condition in a parabolic band can be used to calculate approximately the degenerate carrier concentration which is given by

$$n_{deg} = \left(\frac{\pi}{3}\right) \left[\frac{8KT_c m^*}{h^2} \right]^{\frac{3}{2}} \tag{3.3.7}$$

where k is the Boltzmann constant,m^* is the effective mass of carrier and T_c is the carrier temperature. For $Ga_{.5}In_{.5}P$ we obtain $n_{deg} = 4.5\times10^{17} cm^{-3}$ at T =300 K and $n_{deg} = 7\times10^{16} cm^{-3}$ at T=78 K . Fig (3.3.1) shows the electron distribution for both low density (nondegenerate) and high density (degenerate) cases . Because F_e and F_h are related to carrier temperature and carrier density through the Fermi integrals , to calculate these Fermi levels at a given carrier density and temperature one has to calculate $F_{1/2}(\eta)$ from the relation $F_{1/2}(\eta) = \frac{n}{N_c}$ and then referring to the tables for Fermi integrals finding out the value of η for which the Fermi integral is computed. For example to calculate the Fermi level in GaInP at RT for the carrier density of $5\times10^{18} cm^{-3}$, one has to calculate the value of N_c which is equal to $7.23\times10^{17} cm^{-3}$. Therefore , $F_{1/2}(\eta) = \frac{5\times10^{18}}{7.23\times10^{17}} = 6.9$ and by referring to the Fermi integrals we see that $\eta = 4.2$. Hence , the fermi level is calculated by multiplying the η by the kT which is 25 mev , $F_e = 25\times4.2 = 108$ mev . This is very inconvenient in many situation of fitting procedures which requires the value of the Fermi level. Fortunately , there is an approximate analytical expression which eliminates the need for the Fermi integrals. This approximate analytical expression for η is given by [15]

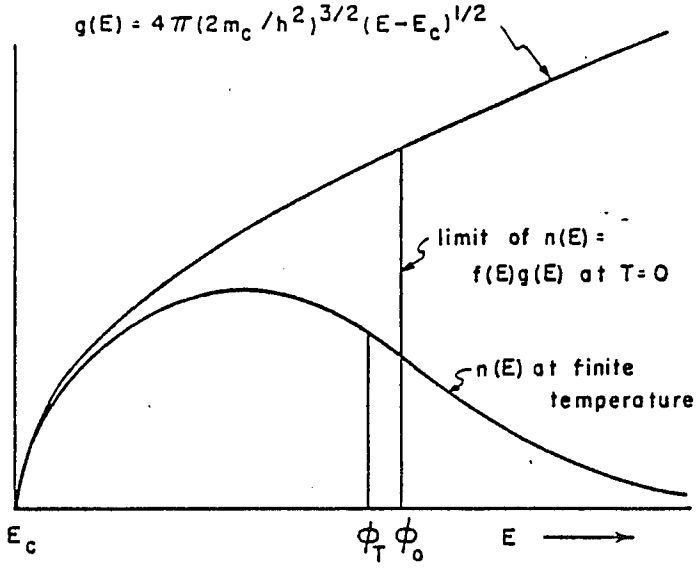

Elcctron density distribution in a highly degenerate case.

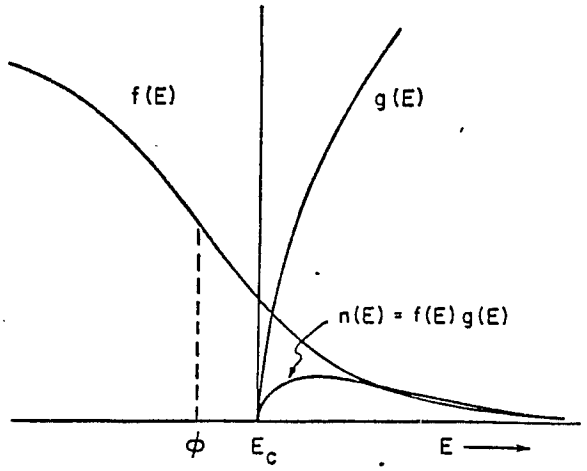

Electron density distribution in a non-degenerate case.

Fig. 3 . 3 . 1 Degenerate and non-degenerate electron distributions n (E) . The density of states , g (E) is also shown . For the non-degenerate case the Fermi function f (E) is shown . ϕ is the Fermi level . Note , in non-degenerate case the Fermi level is below the conduction band edge and in degenerate case the Fermi level in the conduction band (Ref. 14) .

$$\eta = \ln(\frac{n}{N_c}) + 353\,(\frac{n}{N_c}) - 4.95\times10^{-3}\,(\frac{n}{N_c})^2 + 1.48\times10^{-4}(\frac{n}{N_c})^3 - 4.42\times10^{-6}\,(\frac{n}{N_c})^4 + \ldots . \tag{3.3.8}$$

This expression is accurate at low carrier densities $(\frac{n}{N_c})<1$ and at high carrier densities $(\frac{n}{N_c}) \sim 15$ there is less than 5% error calculation of Fermi levels. Fig. 3 . 3 . 2 shows the comparison between the exact calculated value of Fermi level by Fermi integrals Eq. (3.3.6) and the approximate analytical expression Eq. (3.3.8) at room temperature .

3 . 4 - Energy Loss Mechanisms of Photogenerated Carriers

Photoexcitation of a semiconductor with band gap of E_g by a picosecond laser pulse of energy $\hbar\omega$ creates electrons with initial energy of $\Delta E_e = \frac{m_h}{m_e + m_h}(\hbar\omega - E_g)$ in the conduction band and holes with excess energy of $\Delta E_h = \frac{m_e}{m_e + m_h}(\hbar\omega - E_g)$ in the valence bands . The photogenerated carriers lose their energy and thermalize with lattice as a result of various interactions and scatterings .

There are four possible mechanisms in which carriers lose their energy and can be divided into two groups . The first group which includes electron-electron interaction and plasmon emission redistributes the excess energy of the photogenerated carriers among the system of carriers with no loss of the energy as a whole and carriers thermalize with each other to a temperature which is usually higher than lattice temperature . The second group , are mainly the interaction of carriers with phonons (optical and acoustical phonon) results to loss of energy from carriers to phonon system and lattice .

The energy relaxation via electron-electron interaction is given by[16]

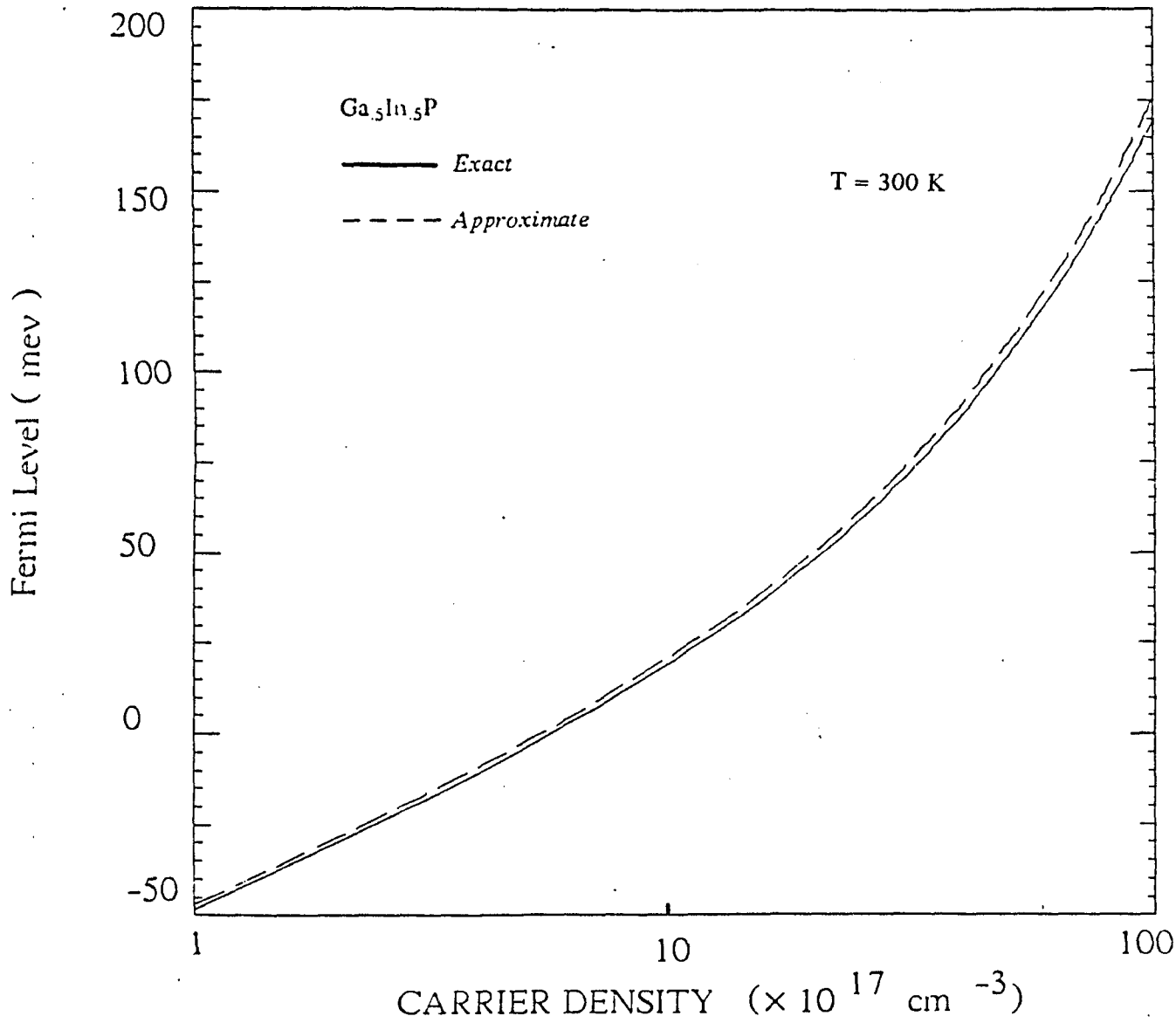

Fig. 3 . 3 . 2 Fermi level (in mev) in $Ga_x In_{1-x} P(x=.5)$ calculated from Fermi integral Eq. 3 . 3 . 5 (solid line) and approximate value calculated from Eq. 3 . 3 . 8 (dashed line) .

$$\frac{dE}{dt} = -\frac{4\pi n_e e^2}{\epsilon^2 (2m_e^* E)^{\frac{1}{2}}} \tag{3.3.9}$$

where n_e is the number of electrons at energy E , m_e^* is the effective mass of electron and ϵ is the dielectric constant . For an electron in the central Γ valley of $Ga_{.5}In_{.5}P$ with effective mass of .094 injected .34 ev over the band edge by a 527 nm picosecond laser pulse in the case of free carrier density of $5\times10^{18}cm^{-3}$, this yield an energy loss rate of $\sim$1.1 ev /ps as calculated from Eq. 3.3.9 . Another words the carriers thermalize with each other in about .3 ps . This rate increases as the electrons cool and thus in a small fraction of a picosecond , the electron has given its excess energy to the other electrons . In general it is possible to characterize the state of electrons in the Γ valley with an electron density of n_e and a temperature T_e . Electron-electron collisions are fast enough to ensure that also electrons in X valley system have the same temperature T_e . Because the momentum must be conserved , the electron-electron scattering is ineffective in transferring the electrons into and out of X valley system . Transfer of electrons from one valley to other ($\Gamma \rightarrow X$, $X \rightarrow \Gamma$) is accomplished via phonon emission and absorption and this occurs on a picosecond time scale . In practice , this means the Γ and X valley electrons will be characterized by the same temperature but Fermi levels for each valley will be independent , and relative population of the two valley must be calculated dynamically and these rate equations will be part of a set of differential equations which will be discussed in later sections .

The energy loss rate of a hole to other holes is also given by Eq. (3.3.9) with m_h^* should be substituted for m_e^* . The rate is then slower by the square root of the mass ratio . However , since the holes excess energy are usually lower than electrons , the equilibration rate are effectively almost the same as electrons and time scale would be on the order of subpicosecond. In our discussion we assume here that hole-hole collision is effective in maintaining a distribution among the light and heavy valence bands.

Electron - hole energy transfer can be calculated by modifying Eq. (3.3.9) to take into account the mass ratio . For energy loss of electrons to holes , one has to multiply the Eq. (3.3.9) with mass ratio of $\frac{m_e}{m_h}$, which brings the electron - hole equilibration rate up to a picosecond time scale . The electron loss rate to the light holes would be faster , but because the population of light holes is much smaller , then the rate would be almost the same as order of ps . To calculate an estimate for the energy loss of electrons to holes , we can use the results from two temperature plasma theory with Maxwell Boltzmann distribution . The average energy loss of an electron to the hole is given by [17]

$$\frac{d\bar{E}_e}{dt} = -\frac{8\pi e^4 n_e (T_e - T_h)}{\sqrt{2\pi k}\, m_e m_h \epsilon^2 \left[\frac{T_e}{m_e} + \frac{T_h}{m_h}\right]^{\frac{3}{2}}} \tag{3.3.10}$$

where k is the Boltzmann constant , ϵ is the dielectric constant and T_e and T_h are the electron and hole temperatures . The average hole energy loss rate is simply given by

$$\frac{dE_h}{dt} = -\frac{dE_e}{dt} \tag{3.3.11}$$

However , since the electron-electron and hole-hole collision is very fast (typically 10^{12} collisions per second) , it is reasonable to assume that electrons and holes reach thermal equilibrium in about 1 ps and for the remaining of this chapter we assume the electrons and holes have the same temperature namely T_e .

The second group of energy loss mechanisms , is optical and acoustical phonon scattering . In polar semiconductors like GaAs and $Ga_{.5}In_{.5}P$, the dominant mechanism responsible for carrier energy loss is the interaction of carriers with LO phonons as long as carrier temperature is above 40 K .

The general Hamiltonian for the electron-phonon interaction is given [16]

$$H = \int \frac{d^3k}{(2\pi)^3} \left[M_{\vec{q}} a_{\vec{q}} e^{i\vec{q}\cdot\vec{r}} + M_{\vec{q}}^{*} a_{\vec{q}}^{+} e^{-i\vec{q}\cdot\vec{r}} \right] \tag{3.3.12}$$

where $a_{\vec{q}}$ and $a_{\vec{q}}^{+}$ are the annihilation and creation operators for phonons of wavevector $\vec{q}$, and H is the Hamiltonian interaction for the electrons at $\vec{r}$. For the polar longitudinal optical phonon the matrix element is $M_q = \frac{C}{q}$ where C is given by

$$C = i \left(\frac{2\pi\hbar\omega_{LO} e^2}{\bar{\epsilon}} \right)^{\frac{1}{2}} \tag{3.3.13}$$

and $\hbar\omega_{LO}$ is the optical phonon energy , and the $\bar{\epsilon}$ is given by

$$\frac{1}{\bar{\epsilon}} = \frac{1}{\epsilon_\infty} - \frac{1}{\epsilon_s} \tag{3.3.14}$$

where ϵ_∞ and ϵ_s are the high frequency and static dielectric constants , respectively . The rate of change of electron energy is

$$\frac{d\epsilon_e}{dt} = \sum_{k,\sigma} \epsilon^{\sigma_k} \frac{\partial f(k)}{\partial t} = \sum_{k,\sigma} \sum_{k',\sigma'} W_{k \to k'} \epsilon_k^{\sigma} f_k^{\sigma}(k) \left[1 - f^{\sigma'}(k') \right]$$

$$- \sum_{k,\sigma} \sum_{k',\sigma'} W_{k' \to k} \epsilon_k^{\sigma'} f^{\sigma'}(k') \left[1 - f^{\sigma}(k) \right] \tag{3.3.15}$$

where σ is the spin index , and $f^{\sigma}(k)$ is the occupation number of electron state σ, k and $W_{k \to k'}$ is the transition rate given by Fermi Golden rule as

$$W_{k \to k'} = \frac{2\pi}{\hbar} \sum_{\{n\}} | \langle k', \sigma', \{n'\} | H' | k, \sigma, \{n\} \rangle |^2 \delta(\epsilon_k - \epsilon_{k'} + E\{n\} - E\{n\}) \tag{3.3.16}$$

where $\{n\}$ denotes the set of phonon occupation numbers and $E\{n\}$ is the energy of whole phonon states associated with these numbers . The polar longitudinal optical interaction is spin conserving , and because H contains only the first power of a_q and $a_q^{\dagger}$, $\{n\}$ can only change ± 1 . The matrix element insures the momentum conservation and the result becomes

$$W_{k\to k'} = \frac{2\pi}{\hbar} |M_q|^2 \{ n_{k'\to k}\, \delta(\epsilon_k - \epsilon_{k'} + \hbar\omega_{LO})\delta_{\sigma,\sigma'} + (n_{k\to k'}+1)\delta(\epsilon^{\sigma}_{k} - \epsilon^{\sigma}_{k} - \hbar\omega_{LO})\delta_{\sigma,\sigma'} \} \tag{3.3.17}$$

where the first term in the bracket is the phonon absorption and the second term represents phonon emission . The energy delta function are converted to delta function in k space , summations are converted to integrals and after some algebra the average energy loss of the carriers due to interaction with LO phonon in the case Maxwell Boltzmann distribution becomes[16]

$$<\frac{d\epsilon}{dt}>_{M.B.} = -P_0 \left[\frac{e^{x_0 - x_c} - 1}{e^{x_0} - 1} \right] \left[\frac{(x_c/2)^{\frac{1}{2}} e^{x_c/2} K_0(x_c/2)}{\sqrt{\pi}/2} \right] \tag{3.3.18}$$

The parameter P_0 is independent of carrier temperature and is given by

$$P_0 = eE_0 \left(\frac{2\hbar\omega_{LO}}{m^*}\right)^{\frac{1}{2}} \tag{3.3.19}$$

and E_0 is defined as

$$E_0 = \frac{m^* e \hbar\omega_{LO}}{\hbar^2} \left\{ \frac{1}{\epsilon_\infty} - \frac{1}{\epsilon_s} \right\} \tag{3.3.20}$$

In Eq. (3.3.18) , the $x_0 = \frac{\hbar\omega_{LO}}{KT_L}$ and $x_c = \frac{\hbar\omega_{LO}}{KT_c}$ nad K_0 is the modified Bessel function of order zero . The parameter P_0 can be simplified to

$$P_0 = 3.54\times10^{11} \left[\hbar\omega_{LO}(mev) \right]^{\frac{3}{2}} \qquad ev/sec \tag{3.3.21}$$

The Eq. (3.3.18) is derived for nondegenerate case ($\eta < 0$) and is independent of the density of carriers . In $Ga_{.5}In_{.5}P$ the distribution of electrons at room temperature is degenerate when $n_e > 4.5\times10^{17} cm^{-3}$ and one has to consider the carrier dependent cooling rate . The cooling rate in the case of degenerate Fermi Dirac distribution is calculated by Bauer and Kahlert following Conwell and is given by[18]

$$<\frac{d\epsilon}{dt}> = -P_0 x_c^{\frac{1}{2}}(\frac{2}{\sqrt{\pi}})\frac{1}{F_{1/2}(\eta)}\left\{N_q\int_o^\infty f(\epsilon)\left|1-f(\epsilon+x_c)\right|\sinh^{-1}(\frac{\epsilon}{x_c})^{\frac{1}{2}}\,d\epsilon\right.$$

$$\left.-(N_q+1)\int_0^\infty f(\epsilon+x_c)\left|1-f(\epsilon)\right|\sinh^{-1}(\frac{\epsilon}{x_c})^{\frac{1}{2}}\,d\epsilon\right\} \qquad (3.3.22)$$

where $F_{1/2}$ is the Fermi integral and N_q is given by

$$N_q = \frac{1}{e^{\frac{\hbar\omega_{LO}}{KT}}-1} \qquad (3.3.23)$$

Again the first term in the bracket is due to phonon absorption and the second term represents the phonon emission . Fig. 3 . 3 . 3 shows the electron energy loss rate to lattice via phonon emission as a function of carrier temperature for Maxwell Boltzmann distribution calculated from Eq. 3.3.18 and Fermi Dirac distribution from Eq. 3.3.22 at carrier densities of 1×10^{18} , 5×10^{18} and $1\times10^{19}cm^{-3}$. For the above calculation we used the following parameters $m_c=.094$, $\hbar\omega_{LO}=48mev$, $\epsilon_s=9.1$, $\epsilon_\infty=11.6$. The Maxwellian result is independent of carrier density . Fig. 3.3.3. shows that at given carrier temperature the cooling rate decreases with increasing carrier density . Fig. 3.3.4 shows the logarithmic plot of carrier energy loss as a function of carrier density in $Ga_{.5}In_{.5}P$ for temperatures 500 , 1000 , 2000 K . The reduction of cooling rate is due to Fermi Dirac statistic is more clear at high carrier densities .

Screening of Hot Carriers

At high carrier densities achievable by picosecond laser pulse , the energy loss rate will be reduced as a result of the the screening of the interaction between carriers and phonons[19,20] . The Hamiltonian in this case is derived by considering the interaction of electrons with the charge density $\rho_{eff}=-\vec{\nabla}.\vec{P}$ which results from a polarization wave $\vec{P}$. In the presence of a large free carrier density , this effective charge is screened by carriers via Thomas Fermi or Debye dielectric constant which is given by

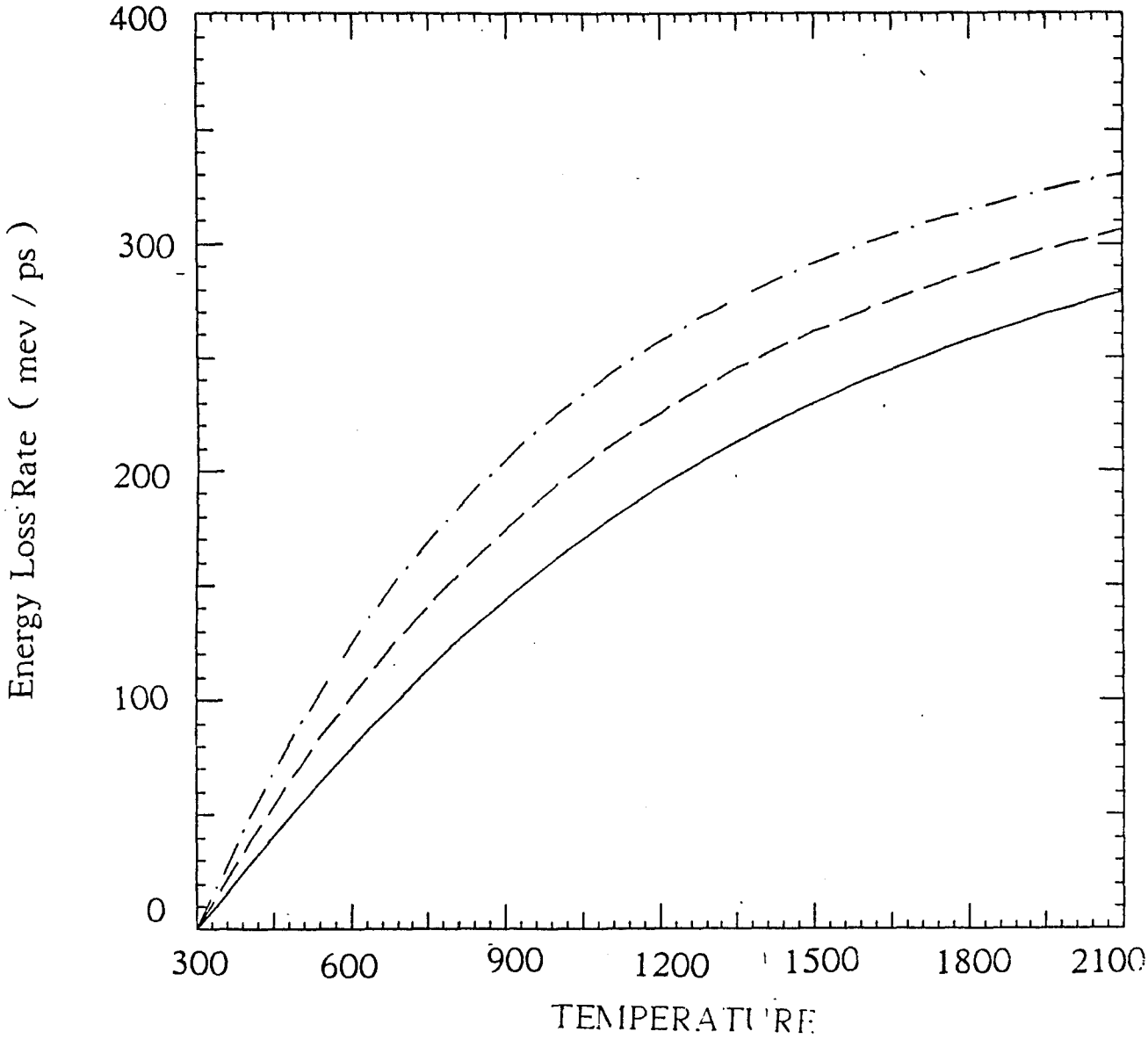

Fig. 3 . 3 . 3 Electron energy loss rate in $Ga_x In_{1-x} P(x=.5)$ as a function of electron temperature calculated from Eq. 3 . 3 . 18 for 1×10^{18} (dot-dash) , 5×10^{18} (dashed) and $1\times10^{19} cm^{-1}$ (solid line) . The Maxwellian result is independent of electron density .

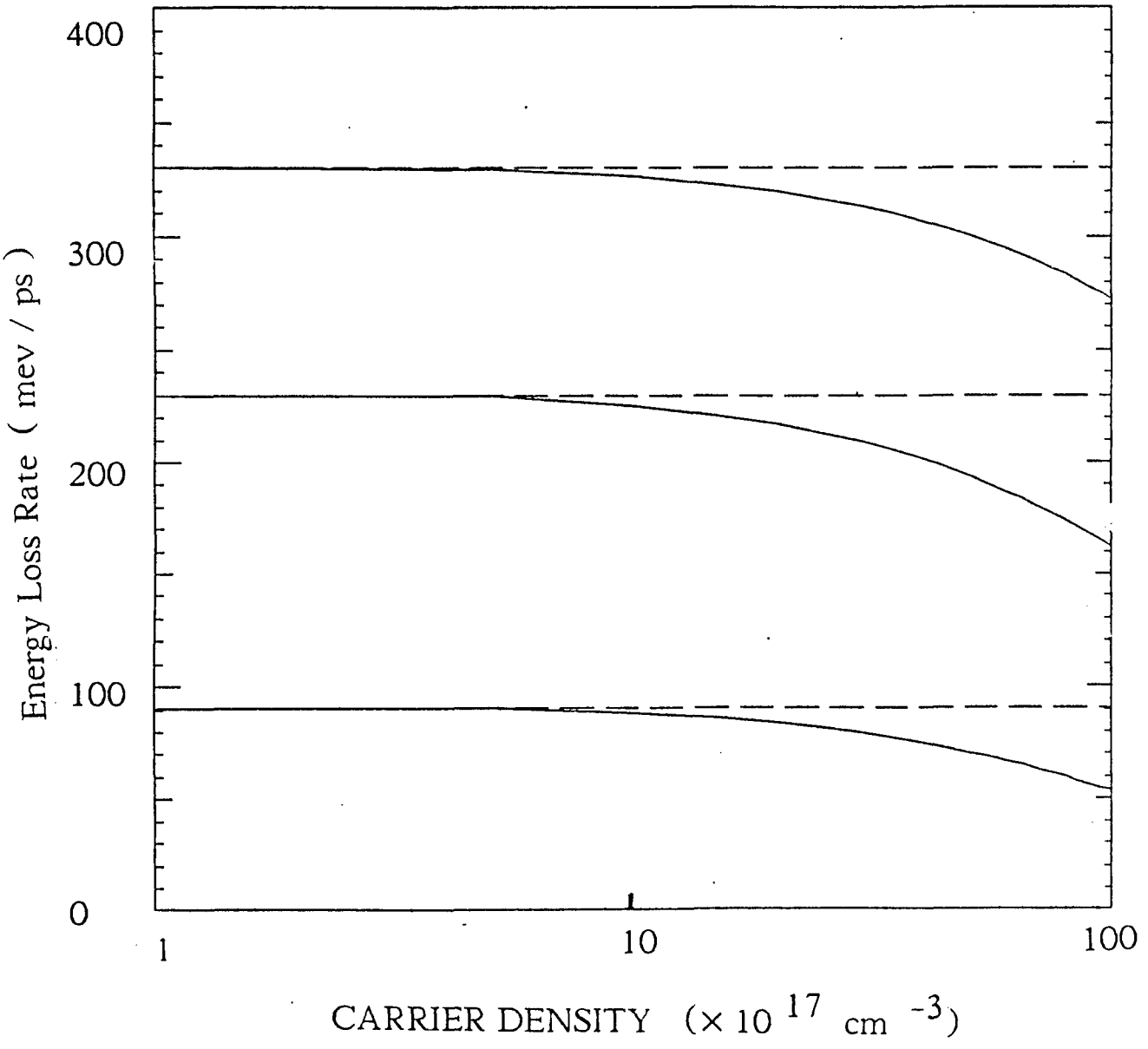

Fig. 3 . 3 . 4 Electron energy loss rate vs electron density in $Ga_x In_{1-x} P(x=.5)$ on semi-log scale for 500 , 1000 , 2000 K calculated from Eq. 3 . 3 . 22 . The lowest curve corresponds to 500 K and dashed lines are for Maxwell distribution case .

$$\epsilon(q) = \left| 1+\frac{Q^2}{q^2} \right| \tag{3.3.23}$$

where Q is the Debye screening wave vector . In this case , the general Hamiltonian for the electron-phonon interaction becomes

$$H' = \int \frac{d^3\vec{k}}{(2\pi)^3} \frac{q}{Q^2+q^2} \left[C a_{\vec{q}}^{i\vec{q}\cdot\vec{r}} + C^* a_{\vec{q}}^{+} e^{-i\vec{q}\cdot\vec{r}} \right] \tag{3.3.25}$$

Here , the transition rate from state k to k' can be calculated from Fermi Golden rule which is given by

$$W_{k\to k'}^{\sigma\to\sigma'} = \frac{2\pi}{\hbar} |C|^2 \frac{|k'-k|^2}{/\ |k'-k|^2+Q^2\ /^2} \Big\{ n_{k'-k}\, \delta(\epsilon^{\sigma_k} - \epsilon_k^{\sigma'} + \hbar\omega_{LO})\, \delta_{\sigma,\sigma'}$$

$$+ (n_{k-k'}+1)\, \delta(\epsilon_k^{\sigma} - \epsilon_k^{\sigma'} - \hbar\omega_{LO})\, \delta_{\sigma,\sigma'} \tag{3.3.26}$$

Again , if we convert the delta function into the k space and substituting Eq. (3.3.26) into Eq. (3.3.15) and some algebra we obtain the cooling rate in the presence of screening and the result is given by[21,22]

$$\left\langle \frac{d\epsilon}{dt} \right\rangle = \frac{-m_e^* e^2(\omega_{LO})^2}{2\pi^2\bar{\epsilon}} \left[N_{LO}(T_c) - N_{LO}(T_L) \right] \int_0^\infty k dk \left| f\left(\frac{\epsilon_k}{kT_c}\right) - f\left(\frac{\epsilon_k+\hbar\omega_{LO}}{kT_c}\right) \right|$$

$$\left\{ \ln \left| \frac{(k+\sqrt{k^2+2m_e\omega_{LO}/\hbar})^2+Q^2}{(k-\sqrt{k^2+2m_e\omega_{LO}/\hbar})^2+Q^2} \right| - \frac{Q^2}{(k-\sqrt{k^2+2m_e\omega_{LO}/\hbar})^2+Q^2} \right.$$

$$\left. + \frac{Q^2}{(k+\sqrt{k^2+2m_e\omega_{LO}/\hbar})^2+Q^2} \right\} \tag{3.3.27}$$

where $N(T_c)-N(T_L)$ is the difference in phonon occupation at the carrier temperature and lattice temperature and is equal to

$$N(T_c)-N(T_L)=\frac{1}{e^{\frac{\hbar\omega_{LO}}{kT_c}}-1}-\frac{1}{e^{\frac{\hbar\omega_{LO}}{kT_L}}-1} \tag{3.3.28}$$

where Q is the Debye screening wavevector and is given by[23]

$$Q=\left(\frac{32\pi e^2 n_e}{\epsilon_0 k_B T_c}\right)^{\frac{1}{2}} \tag{3.3.30}$$

For example at carrier density of $6\times10^{18}cm^{-3}$ and $T=500K$ the value of Q is calculated to be $1.25\times10^{7}cm^{-1}$. In Eq. (3 . 3 . 27) the value of $\bar{\epsilon}$ is given by

$$\frac{1}{\bar{\epsilon}}=\frac{1}{\epsilon_\infty}-\frac{1}{\epsilon_s} \tag{3.3.29}$$

where ϵ_∞ and ϵ_s are the optical and static dielectric constants. At low carrier densities where screening is not important $Q\rightarrow 0$ and in addition the Maxwell Boltzmann statistics can apply the the electron distribution becomes

$$f\left(\frac{\epsilon_k}{kT_c}\right)=\exp\left(\eta_e-\frac{\epsilon_k}{kT_c}\right)=\frac{n_e}{2}\left(\frac{h^2}{2\pi m_e kT_c}\right)^{\frac{3}{2}}\exp\left(\frac{-\hbar^2k^2}{2m_e kT_c}\right) \tag{3.3.30}$$

Under these conditions , the integral in Eq. (12) can be worked out analytically to give the equation

$$<\frac{d\epsilon}{dt}>=n_e\ <\frac{d\epsilon}{dt}>_{M.B.} \tag{3.3.31}$$

where $<\frac{d\epsilon}{dt}>_{MB}$ is given by Eq. (3 .3 .18) . Fig. 3 . 3 . 5 shows the electron energy loss rate to lattice in $Ga_{.5}In_{.5}P$ as a function of electron temperature with screening effects included for carrier densities of 1×10^{18} , 5×10^{18} and $1\times10^{19}\ cm^{-3}$, respectively . The parameters used for this calculation has been described before . As shown in the Figure , the cooling rate at a given temperature decreases with increasing carrier density .

The variation of energy loss rate as a function of carrier density is shown in log-log scale in Fig. 3 . 3 . 6 for the case where the effects of screening has been taken into

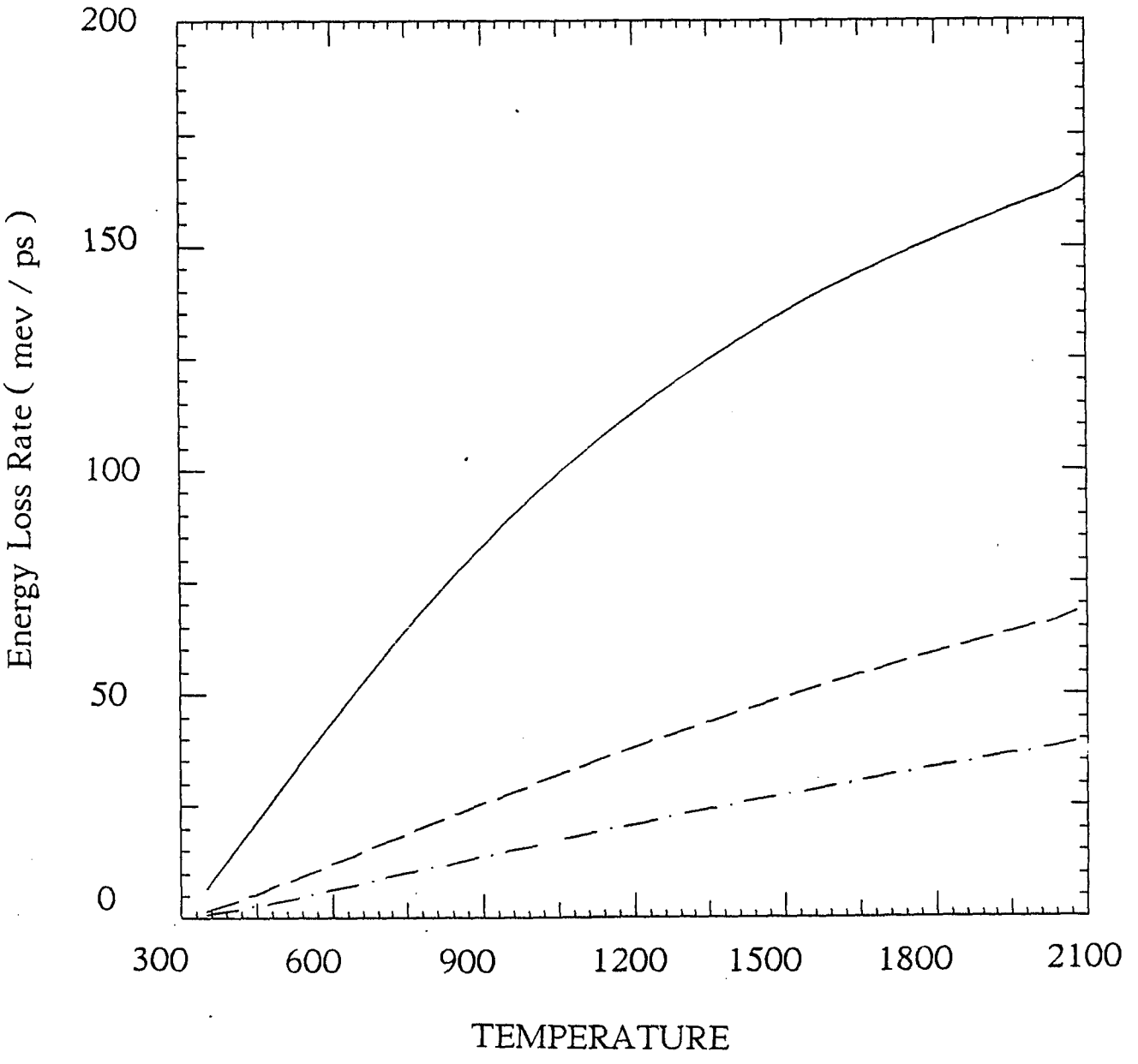

Fig. 3 . 3 . 5 Electron energy loss rate to lattice via optical phonon interaction as a function of temperature with screening effects included as calculated from Eq. 3 . 3 . 27 for $n = 1\times10^{18} cm^{-3}$ (solid line), $5\times10^{18} cm^{-3}$ (dashed line), $1\times10^{19} cm^{-3}$ (dot-dashed line)

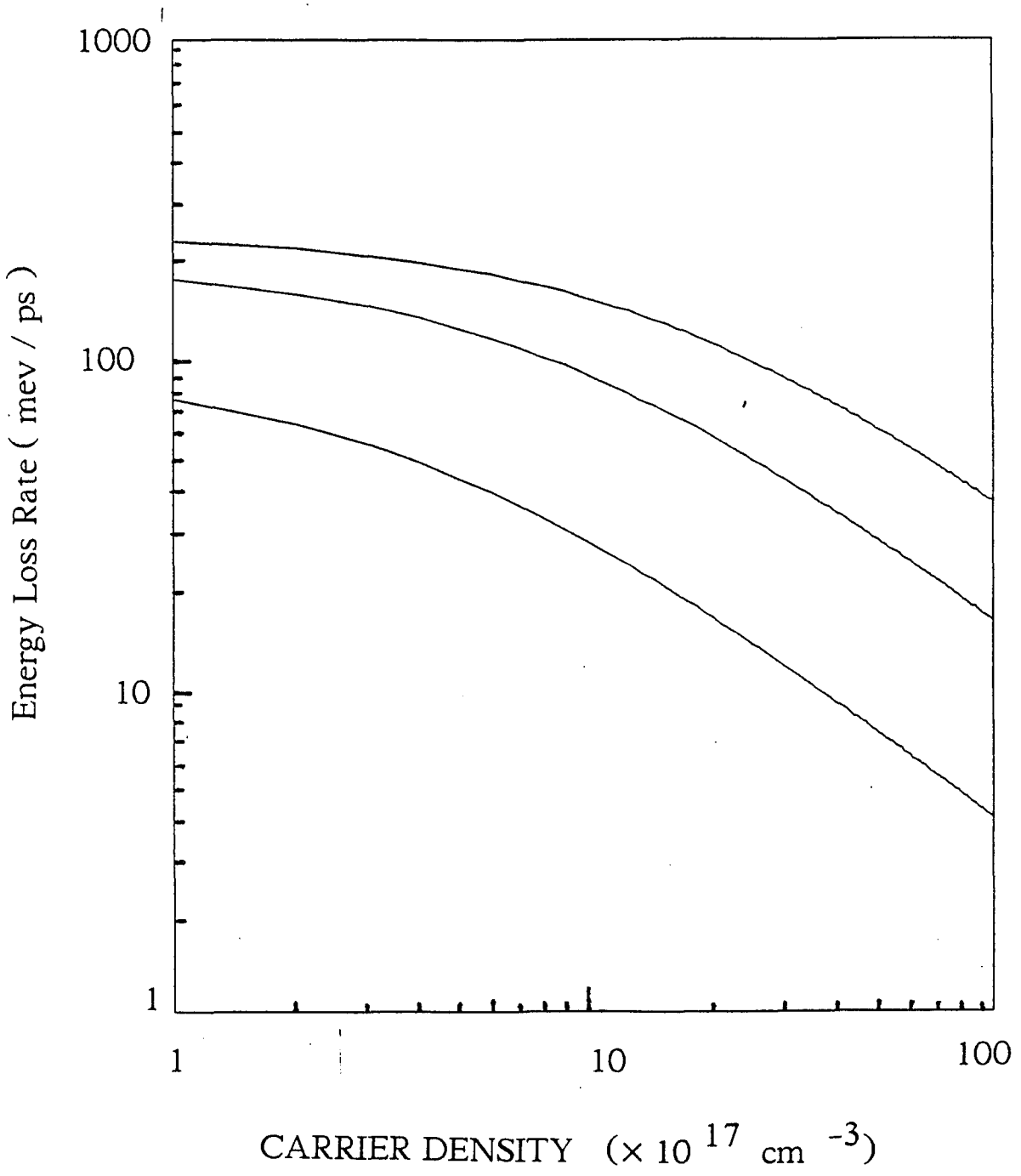

Fig. 3 . 3 . 6 Electron energy loss loss rate to lattice via optical phonon interaction , with screening effect included on a logarithmic scale . The three curves are for T=500 , 1000 , 2000 K , respectively . The upper curve is for T=2000 K and the lower curve is for T=500 K .

account as calculated from Eq. 3.3.27 for T=500 , 1000 and 2000 K .

Intervalley Scattering

In order to have a complete set of equations describing the dynamical behavior of carrier density , one also has to take into account the intervalley scattering rate from $\Gamma \rightarrow X$ and $X \rightarrow \Gamma$ valley . The intervalley scattering time as a function of carrier energy is given by[16]

$$(\tau_{\Gamma X})^{-1}(x) = \frac{D^{2\Gamma X}(\hbar\omega_{LO})^{\frac{1}{2}} m_X^{\frac{3}{2}}}{\sqrt{2}\pi\hbar^3\rho\omega_i(e^{x_i}-1)} \left[(x + x_1 - x_\Delta)^{\frac{1}{2}} + e^{x_i}(x - x_1 - x_\Delta)^{\frac{1}{2}} \right] \qquad (3.3.33)$$

where $D_{\Gamma X}$ is the deformation potential associated with coupling between Γ and X valleys , ρ is the material density , $\hbar\omega_i$ is the phonon energy (optical or acoustic) required to provide the momentum necessary for a transfer from Γ to X valleys , $x_i = \frac{\hbar\omega_i}{KT}$, $x_1 = \frac{\hbar\omega_i}{\hbar\omega_{LO}}$, $x = \frac{\epsilon_c}{\hbar\omega_{LO}}$ and $x_\Delta = (\frac{E_X - E_\Gamma}{\hbar\omega_{LO}}) = \frac{\Delta E}{\hbar\omega_{LO}}$. The $x \mp x_1$ terms in Eq. 3.3.33 correspond to phonon absorption and emission , respectively . It is also understood that in Eq. 3.3.33 , the electronic energy involved in phonon emission are $x \geq (x_\Delta + x_1)$, where x_Δ is the normalized energy separation .

The total rate of electron transfer from Γ to X valleys can be written as[13]

$$\frac{dn_\Gamma}{dt}\Big|_{\Gamma \rightarrow X} = \int \frac{\partial f_\Gamma(x)}{\partial t} d^3k \qquad (3.3.34)$$

The time rate of change of the distribution of electrons in the Γ valley is written as

$$\frac{\partial f_\Gamma(x)}{\partial t}\Big|_{\Gamma \rightarrow X} = \frac{f_\Gamma(x)}{\tau_{\Gamma \rightarrow X}(x)} \qquad (3.3.35)$$

Substituting Eq. 3.3.35 into Eq. 3.3.34 gives the rate at which electrons are transferred from Γ to X valleys . These equations were used by Conwell to evaluate the intervalley rate of transfer in GaAs when an impressed field increased the electron temperature above the lattice temperature . Under low excitation power where the distribution

of electrons is Maxwellian the integration can be performed to give the analytical expression for the transfer rate . However, in our experiments since we are in the high excitation regime and the distribution of electrons is described by Fermi-Dirac statistics, computer evaluation of the integral is necessary. The important parameter entering the calculation of the transfer rate is the phonon energy $\hbar\omega_i$ associated with those phonons imparting the necessary momentum to the electrons. In GaAs , Γ to X transfer takes place via electron interaction with LO phonons [16]. In other binary semiconductors it is necessary to resort to group theory in order to determine which phonons participate in intervalley transfer of electrons. Birman et al. [24] concluded that the selection rule for phonons depend on the ratio of the group V atomic mass m_v to group III mass m_{III} of the binary. In the case of GaP and InP it is LA phonons that take part in $\Gamma \rightarrow X$ transitions. It is also possible that in ternary semiconductors, the phonon selection rule is relaxed such as in GaAsP, thereby allowing both LA and LO take part in the $\Gamma \rightarrow X$ transfer. For GaInP, it is LA phonons that are important in intervalley transfer [13]. Since LA phonon energies for InP and GaP are 25 and 33 mev , respectively . one can determine the LA phonon energy in $Ga_xIn_{1-x}P$ by interpolation . only parameter which is not known for $Ga_{.5}In_{.5}P$ is the deformation potential and for the calculations we use the value of 5×10^8 ev/cm used by Conwell in GaAs . Using the material density of $4.455 gr/cm^3$ and LA phonon energy the $\hbar\omega_i$ = 29 mev, the Eq. (3.3.34) can be written as

$$\frac{dn_\Gamma}{dt}\Big|_{\Gamma\rightarrow X} = 1.12\times10^{32} \int_{x_\Delta+x_1}^{\infty} x^{\frac{1}{2}} \frac{1}{1+e^{x-\eta}} \frac{1}{e^{x_i}-1} \left| (x-x_\Delta+x_1)^{\frac{1}{2}} + e^{x_i}(x-x_\Delta-x_1)^{\frac{1}{2}} \right|$$

$$= \frac{n_\Gamma}{\tau_{\Gamma X}} \qquad (3.3.36)$$

Similarly , we can write the total rate at which electrons are transferred from X to Γ valley . The transfer time as a function of carrier energy is given by

$$\tau_{X\to\Gamma}^{-1}(x) = \frac{D_{\Gamma X}^{\,2}(\hbar\omega_{LO})^{\frac{1}{2}} m_{\Gamma}^{\frac{3}{2}}}{\sqrt{2}\pi\hbar^3\rho\omega_i(e^{x_i}-1)} \left| (x+x_1)^{\frac{1}{2}} + e^{x_i}(x-x_1)^{\frac{1}{2}} \right| \qquad (3.3.37)$$

Again we can write

$$\frac{dn_X}{dt}\Big|_{X\to\Gamma} = \int \frac{\partial f_X}{\partial t} d^3k = \int \frac{f_X(x)}{\tau_{X\to\Gamma}(x)} d^3k \qquad (3.3.38)$$

Substituting Eqs. (3.3.37) into Eq. (3.3.38) and converting the integral from k space to energy we obtain[13]

$$\frac{dn_X}{dt}\Big|_{X\to\Gamma} = \frac{2}{\sqrt{\pi}} X_0^{\frac{3}{2}} N_X \int_{x_1}^{\infty} \frac{f_X(x)}{\tau_{X\to\Gamma}} dx = \frac{n_X}{\tau_{X\Gamma}} \qquad (3.3.39)$$

Here , the lower limit of integration is dictated by the minimum energy required for phonon emission . Again using the parameters used for the evaluation of $\tau_{\Gamma X}$, the Eq. 3.3.39 can be written as

$$\frac{dn_\Gamma}{dt}\Big|_{X\to\Gamma} = 7.62\times10^{30} \int_{x=1}^{\infty} x^{1/2} \frac{1}{1+e^{x-\eta}} \frac{1}{e^{x_i}-1} \left| (x+x_1)^{\frac{1}{2}} + e^{x_i}(x-x_1)^{\frac{1}{2}} \right| \qquad (3.3.40)$$

Fig. 3 . 3 . 7 shows the intervalley scattering times ($\tau_{\Gamma X}$, $\tau_{X\Gamma}$) in $Ga_{.5}In_{.5}P$ as a function of carrier temperature for the carrier density of $1\times10^{18} cm^{-3}$ calculated from Eqs. (3.3.36) and (3.3.40) , respectively . It should be point out that intervalley scattering time is very weak function of carrier density and as is seen from the Fig. 3.3.7 it is however strongly depends on carrier temperature .

The other factors which effects th dynamics of the carriers in semiconductors are band filling , dynamical Burstein shift , recombination and gain/loss which have to be taken into account.

GAIN / LOSS

The absorption coefficient at photon energy $h\nu$ and at carrier density n_c and carrier temperature T_c is described by

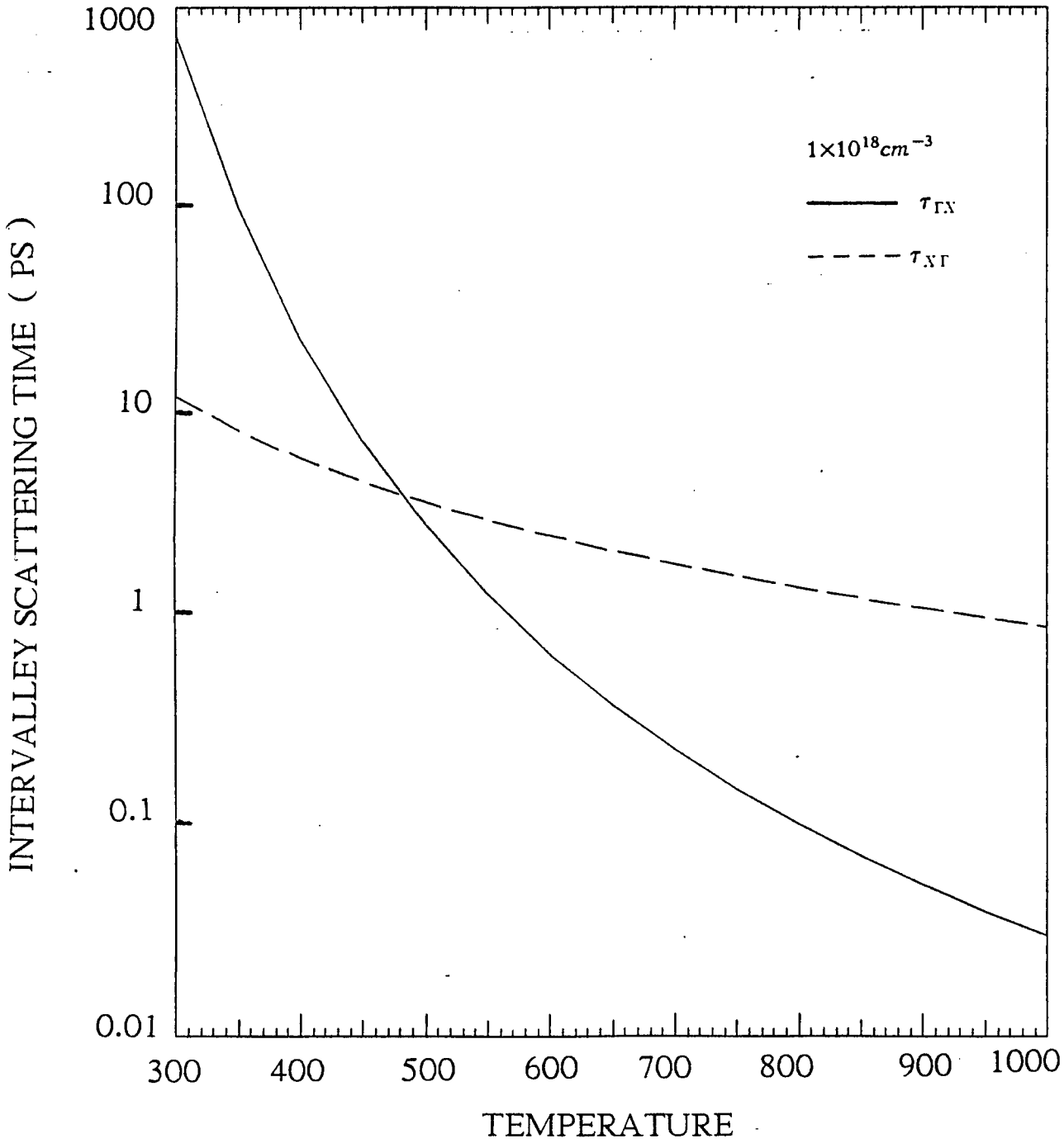

Fig. 3 . 3 .7 Intervalley scattering time in $Ga_{.5}In_{.5}Pas$ a function of electron temperature .

$$\alpha(\nu, n_e, T_c) = A\,(h\nu - E_g)^{\frac{1}{2}} \left\{ 1 - f_c(Z_e, \eta_e) - f(Z_h, \eta_h) \right\} \tag{3.3.41}$$

where $f(x, y)$ is the Fermi Dirac distribution and is given by

$$f(x, y) = \left\{ 1 + e^{x-y} \right\}^{-1} \tag{3.3.42}$$

In equation (3.3.42), the parameter Z_e is equal to

$$Z_e = \frac{m_r}{m_e} \frac{(h\nu - E_g)}{KT_c} \tag{3.3.43}$$

and

$$Z_h = \frac{m_r}{m_h} \frac{(h\nu - E_g)}{KT_c} \tag{3.3.44}$$

where m_r is the reduced mass of the carriers and is given by

$$\frac{1}{m_r} = \frac{1}{m_e} + \frac{1}{m_h} \tag{3.3.45}$$

The constant A is expressed as

$$A = \left(\frac{2m_r}{\hbar^2}\right)^{\frac{3}{2}} \frac{2e^2}{m_0^2 cn\omega} \left| \langle c, \vec{k} = 0 | \vec{\epsilon} \cdot \vec{p} | v, \vec{k} = 0 \rangle \right|^2 \tag{3.3.46}$$

where $\vec{p}$ is the electron momentum and ϵ is the optical polarization vector. In practice the value of A is determined experimentally by fitting the measured absorption coefficient versus the photon energy to the Eq. (3.3.41) at energies share the band gap, and the value we used in our calculation is $2\times10^4\ cm^{-1}ev^{-\frac{1}{2}}$. At low excitation power where the distribution of carriers is nondegenerate ($\eta<0$) the absorption coefficient given by Eq. (3.3.44) is positive at all the photon energies. However, at high carrier densities where electron distribution is degenerate ($\eta>0$), the absorption coefficient could become negative . In general one can write

$$\alpha > 0 \quad \text{for} \quad h\nu > E_g + F_e + F_h \qquad \textit{Absorption} \tag{3.3.47}$$

$$\alpha < 0 \quad \text{for} \quad E_g + F_e + F_h > h\nu > E_g \qquad \textit{Gain} \tag{3.3.48}$$

Therefore at high pumping power one expect to observe the stimulated emission on the low energy side of the photoluminescence spectra . The spontaneous emission rate $r(\nu)$ into the frequency interval $d\nu$ about ν is given by [25]

$$r(\nu, n_e, T_c) = A(h\nu - E_g)^{\frac{1}{2}} \frac{8\pi n^2 \nu^2 d\nu}{c^2} f_e(Z_e, \eta_e)\, f_h(Z_h, \eta_h) \tag{3.3.49}$$

where n is the refraction index and the rest of the parameters have been defined previously. So far we have written all the equations describing the optical interactions and now we derive the temperature dynamics of carriers by considering and energy balance equations.

The rate of change of the average carrier energy U can be written as[26]

$$\frac{dU}{dt} = H(t) - L(t) \tag{3.3.50}$$

In Eq. (3.3.50) , H (t) describes the increase in the energy due to optical pumping and in our expermental situation can be written as

$$H(t) = \frac{W I_p(t)}{\int_{-\infty}^{t} I_p(\tau) d\tau} \tag{3.3.51}$$

where W is the excess energy of electrons which is equal to $\frac{m_h}{m_h + m_e}(h\nu - E_g)$ and $I_p(t)$ is the pump intensity which we assume Gaussian shape with FHWM of 8 ps . $L(t)$ is the energy loss rate due to relaxation, recombination and intervalley scattering which can be written

$$L(t) = \frac{d\epsilon}{dt}\Big|_{LO} + \frac{d\epsilon}{dt}\Big|_{intervalley} + \frac{d\epsilon}{dt}\Big|_{recombination} \tag{3.3.52}$$

where the first term is the carrier energy loss due to interaction with LO phonons

which we discussed in detail and is given by Eq. (3.3.27) and second term is intervalley contribution which is the rate which energy is transferred from Γ to X valley and the last term is loss of energy due to recombination . Note that each time an electron is transferred from the Γ to X valley system, the kinetic energy of electron is reduced by Δwhere Δ is the separation between Γ and X valley . Therefore we can write

$$\frac{d\epsilon}{dt}\Big|_{intervalley} = -\Delta \frac{dn_\Gamma}{dt}\Big|_{\Gamma\to X} \tag{3.3.53}$$

where $\frac{dn_\Gamma}{dt}\Big|_{\Gamma\to X}$ is given previously by Eq. (3.3.36) .

For a Fermi gas $\frac{dU}{dt}$ can be expressed as [26]

$$\frac{dU}{dt} = \frac{3}{2}k_B \left| \frac{\frac{5}{2}F_{\frac{3}{2}}(\eta) - \frac{3}{2}F_{\frac{1}{2}}(\eta)}{F_{\frac{1}{2}}(\eta) - F_{-\frac{1}{2}}(\eta)} \right| \frac{dT_c}{dt} \tag{3.3.54}$$

where F_j are the Fermi integrals of order j and $\eta = \frac{F_c}{KT_c}$

To complete the set of equations which describes the dynamical behavior of semiconductors one also has to include the rate of equation for output photon density $\phi(\nu)$ which at high excitation power is broad band .

In general in an optically isotropic lasing medium with (gain / loss) coefficient α , the propagation of the photon density along the direction of medium can be written as

$$\frac{d\phi(\nu)}{dz} = -\alpha\,\phi(\nu) \tag{3.3.55}$$

where z is along the length of the medium and α is the (absorption / gain) coefficient . If $\alpha > 0$ (absorption) , the photon density will exponentially decrease due to the absorption along the medium . In the case where $\alpha < 0$ (gain) , the photon density will be amplified exponentially as propagate through the lasing medium .

The Eq. 3.3.55 can be converted to time dependence by considering

$$\frac{d\phi}{dt} = \frac{d\phi}{dz}\frac{dz}{dt} = -\alpha\frac{C}{n}\phi(\nu) \tag{3.3.56}$$

The final set of integro-differential equations describing the time dependence of electron density n_e, carrier temperature T_c, photon density $\phi(\nu)$ are as follow :

$$\frac{dn_\Gamma}{dt} = (1-R)\,\alpha(\nu_p, n_\Gamma, T_c)\,I_p(t) - \frac{dn_\Gamma}{dt}\Big|_{\Gamma\to X} + \frac{dn_X}{dt}\Big|_{X\to\Gamma} - \frac{n_\Gamma}{\tau_t} \tag{3.3.57}$$

$$\frac{dn_X}{dt} = \frac{n_\Gamma}{\tau_{\Gamma\to X}} - \frac{n_X}{\tau_{X\to\Gamma}} \tag{3.3.58}$$

$$\frac{dT_c}{dt} = \left\{ \frac{WI_p(t)}{\int_{-\infty}^{t} I_p(\tau)d\tau} - \int_0^\infty r(\nu, n_e, T_c)h\nu d\nu - \Delta\frac{dn_\Gamma}{dt}\Big|_{\Gamma\to X} - \frac{d\epsilon}{dt}\Big|_{LO} \right\} \frac{1}{G(\eta)} \tag{3.3.59}$$

$$\frac{d\phi(\nu_i)}{dt} = -C_F\,\frac{c}{n}\alpha(\nu_i, n_\Gamma, T_c)\,\phi(\nu_i) \tag{3.3.60}$$

In all the equations we assume that electrons and holes have the same temperature namely T_c. Description of the equations describing the time dependence of the dynamical variable n_e ,T_c ,$\phi(\nu)$ are as follows : In Eq. (3.3.57) , R is the reflectivity constant and the first term is the generation term which depends on the actual shape of the exciting laser pulse ; the second term is the rate at which generated electrons from Γ valley will be transferred to X valley system ; the third term represents the electrons which are transferred from X valley to Γ valley ; and the last term represents the depletion of electrons by radiative and non radiative process .

The relation between the total life time (τ_t), radiative life time (τ_R) and non radiative life time (τ_{NR}) is in the form of

$$\frac{1}{\tau_t} = \frac{1}{\tau_R} + \frac{1}{\tau_{NR}} \tag{3.3.61}$$

In Eq. (3.3.58) the first term is the fraction of electrons in Γ valley transferred to X

valley ; and the second term represents the return of the electrons from X valley to Γ valley . In Eq. (3.3.59) , the first term is the rate at which laser pulse deposits energy into the system of carriers . This term has been introduced by D. von der Linde at el.[26] to study the time dependence of carrier temperature in GaAs in a pump and probe experiment , and the rest of terms represents energy loss routes which has been outlined previously and $G(\eta)$ is given by

$$G(\eta) = \frac{3}{2}k_B \left[\frac{\frac{5}{2}F_{\frac{3}{2}}(\eta) - \frac{3}{2}F_{\frac{1}{2}}(\eta)}{F_{\frac{1}{2}}(\eta) - F_{\frac{-1}{2}}(\eta)} \right] \tag{3.3.62}$$

The bracket in Eq. (3.3.62) is close to unity when $\eta < 2$, which implies at RT for carrier densities below $2\times10^{18} cm^{-3}$.

The integration in Eq (3.3.59) which is the rate which energy is lost due to recombination can be converted to discreate sum in the interval of 5 nm to simplify the computations. In Eq. (3.3.60) , the first term is the usual absorption of photons with frequency ν in a medium with loss/gain $\alpha(\nu, n_c, T_c)$. When α is positive, it is a loss process which implies the photons generated at frequency ν inside the semiconductor will be reabsorbed. However, when $\alpha(\nu, n_c, T_c)$ becomes negative , the gain would be established and the stimulated emission could occur which leads to the amplification of the generated photon density $\phi(\nu)$. The first term in Eq. (3.3.60) is the same as Eq. (3.3.56) but a confinement factor C_F is included . In the best double heterostructure laser where the stimulated emission is confined within the cavity of laser the confinement factor C_F varies between .1 to .5 . The Eq. (3.3.60) is a set of differential equations which extends from ν_1 to ν_{10}. The broad photon density was assumed to extend from the band gap to 1000 A above the band gap . This interval then is divided to 10 discreate wavelengths , the first wavelength which is very close to the band gap correspond to photon energy ν_1 and the 10th discreate wavelength

would correspond to photon energy ν_{10} . This set of differential equations which describes the time dependence of the dynamical variables of carrier density (n_c), carrier temperature (T_c) and output photon density ($\phi(\nu)$) can be solved numerically by the computer to obtain the time evolution of (n_c , T_c , $\phi(\nu)$) which are the dynamical variables . This model predicts almost all the observed features of the short and long wavelength output photon density at high and low excitation power. In particular, the strong λ dependence of the output photon density is correctly predicted , even in detail down to unusual shapes of the second peak shown Fig. 3.1.2 .

The process mainly responsible for the secondary peak at long wavelength is cooling of the plasma and downward motion of the Fermi levels . Another possible mechanism responsible for the observation of the second peak at long wavelength is the many valley effect which is included in Eq. (3.3.56) and Eq. (3.3.57) and shown schematically in Fig 3.3.8. Because of the high density of states in X valleys, the electrons are rapidly scattered there during the initial excitation when plasma is still hot and Γ valley Fermi level is high. After depletion of the central Γ valley by spontaneous emission , the X valley electrons return slowly because of the low density of states in Γ valley and they cool to the band edge to allow the long wavelength emission to continue .

In our calculation we assume the laser pulse in Gaussian and its time dependence is give by

$$I_p(t) = I_0 \exp\{-(\frac{t}{T})^2 \ln 2\} \qquad (3.3.63)$$

where T is the FHWM of the pulse which is centered at t = 0 and I_0 is the normalization constant which can be determined by $\int_{-\infty}^{\infty} I_p(t)\,dt$ = No. of photons in the pulse per unit area .

We use the T=8 ps as measured from two photon fluorescence technique (see chapter 2) . Fig. 3.3.9 shows the actual shape of the laser pulse which is calculated

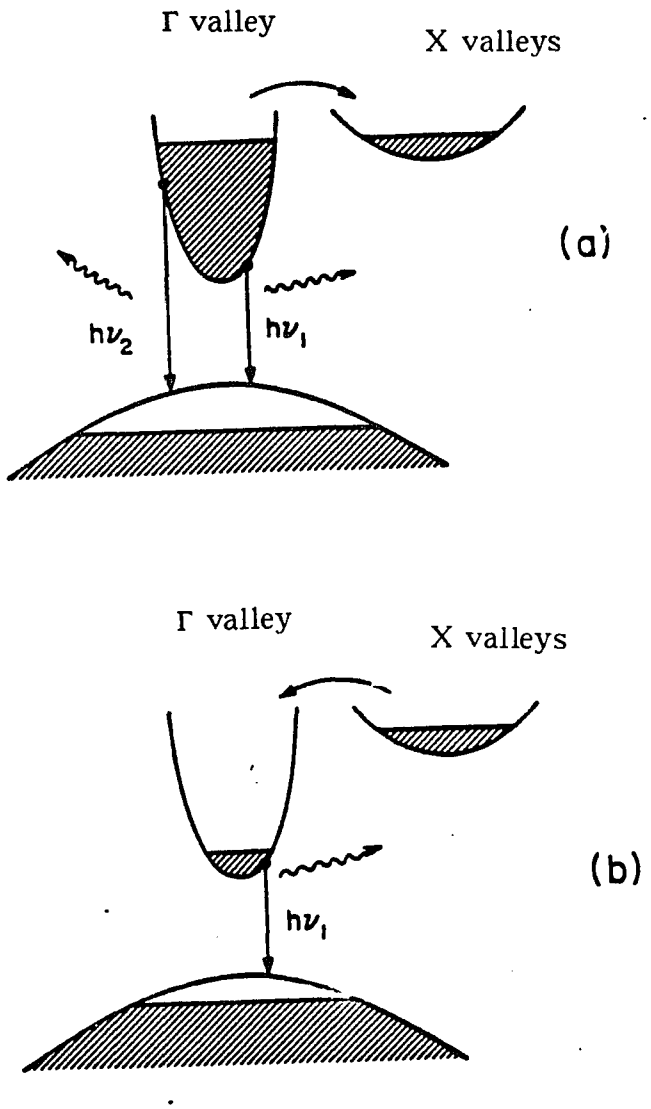

Fig. 3 . 3 . 8 Schematic diagram for many valley effects . In Fig. a . immediately following excitation the high density hot carriers spill over into the X valley system and emission begins at both long and short wavelengths . In Fig. b . after some time when Γ valley depleted the carriers in X valley slowly return back to Γ valley to allow the long wavelength emission to continue .

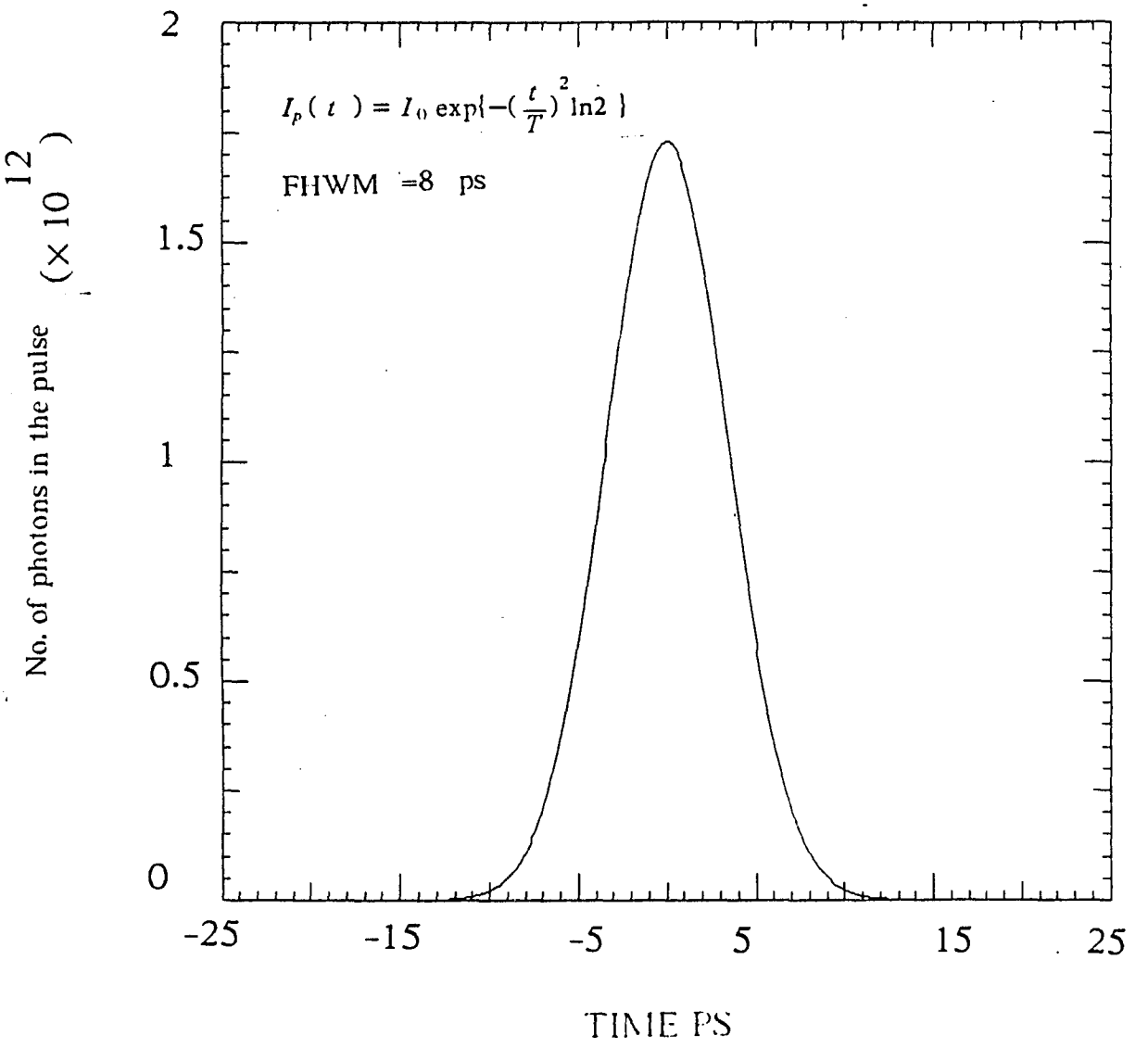

Fig. 3 . 3 . 9 The time dependence of a 8 ps laser pulse as calculated from Eq. 3.3.62 for 10 μj energy . The area under the curve is the number of photons in the pulse .

from Eq. (3.3.63) .

Fig. 3.3.10-a shows the electron density in the Γ valley as a function of time for excitation power fluence of 10 MW/cm^2. It shows in about 15 ps the electron density reaches its maximum value of $8\times10^{17}\ cm^{-3}$ and then it decays exponentially . The time dependence of electrons in X valley is shown in Fig. 3.3.10-b . It shows that electron density in X valley reaches the maximum value of $\sim1.4\times10^{16}\ cm^{-3}$ in about 30 ps , and then it decays much slower than the electrons in Γ valley . Fig. 3.3.11 shows the time evolution of electron temperature as calculated from Eq. 3.3.59 for excitation power of $10MW/cm^2$ It shows in about 1 ps the electron temperature reaches 1100 K and then it cools down to lattice temperature in about 20 ps .

The computed normalized output photon density at short (610 and 620 nm) and long (630 and 640 nm) wavelengths are shown in Fig. 3.3.12 a-d , respectively for excitation power fluence of 10 MW/cm^2 . For the above calculation we used τ = 40 ps which is the decay time of the time resolved at long wavelength near the band edge emission (see Fig 3.3.1 a) and we assume the photon density reaches its maximum value in about 5 ps following the excitation pulse and then it decays according to Eq. 3.3.60 . The value of confinement factor used for the calculation is set to be $C_F = 3\times10^{-3}$. As can be seen from the Fig. 3.3.12 there is no secondary peak present at long wavelengths . These curves are the computer simulation of the carrier density , carrier temperature and output photon density at four different wavelengths .

When excitation power fluence increased to $25MW/cm^2$, the results were similar to the case of low excitation power fluence of $10MW/cm^2$. The time dependence of electron density , carrier temperature and output photon density is shown in Fig. 3.3.13 , Fig. 3.3.14 and Fig. 3.3.15 a-d , respectively . The only feature which is different from the result of the low excitation power is the presence of a small tail at output photon density of $640nm$ which is shown in Fig. 3.3.15 d .

When excitation power fluence increased the level $\sim50\ MW/cm^2$ the calculated

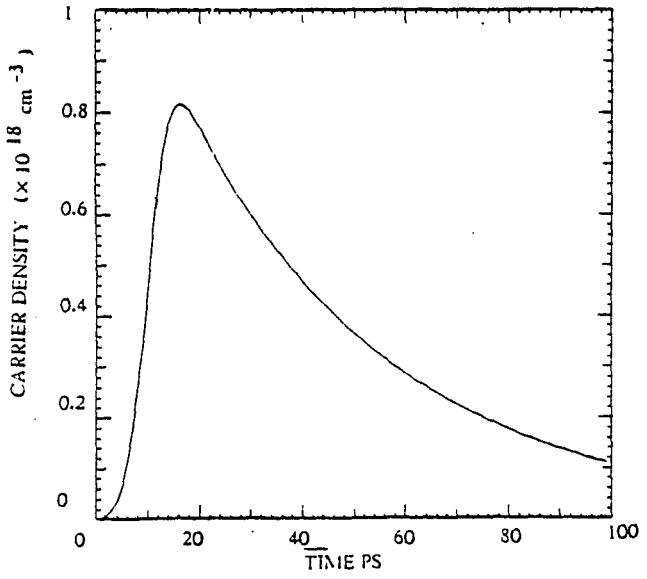

Fig. 3 . 3 .10 a - The electron density in Γ valley as a function of time for excitation fluence of $10MW/cm^2$ and $D_{\Gamma X} = 5\times10^8$ ev / cm .

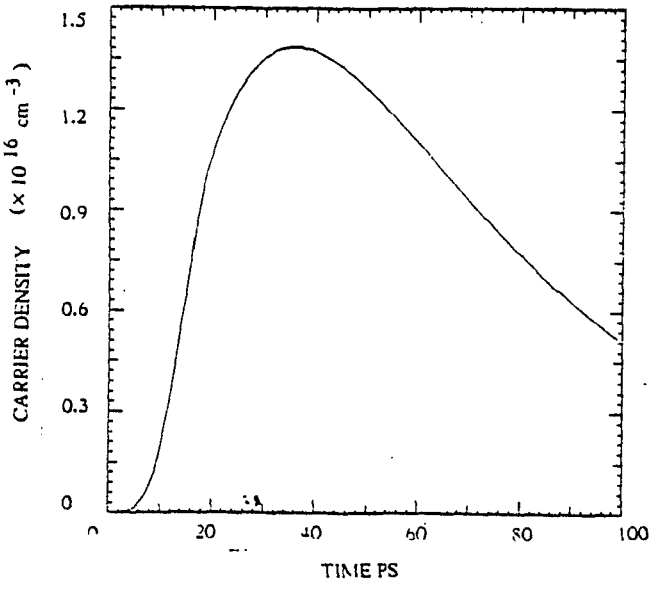

b - The electron density in X valley as a function of time for excitation power of $10MW/cm^2$ and $D_{\Gamma X} = 5\times10^8$ ev / cm .

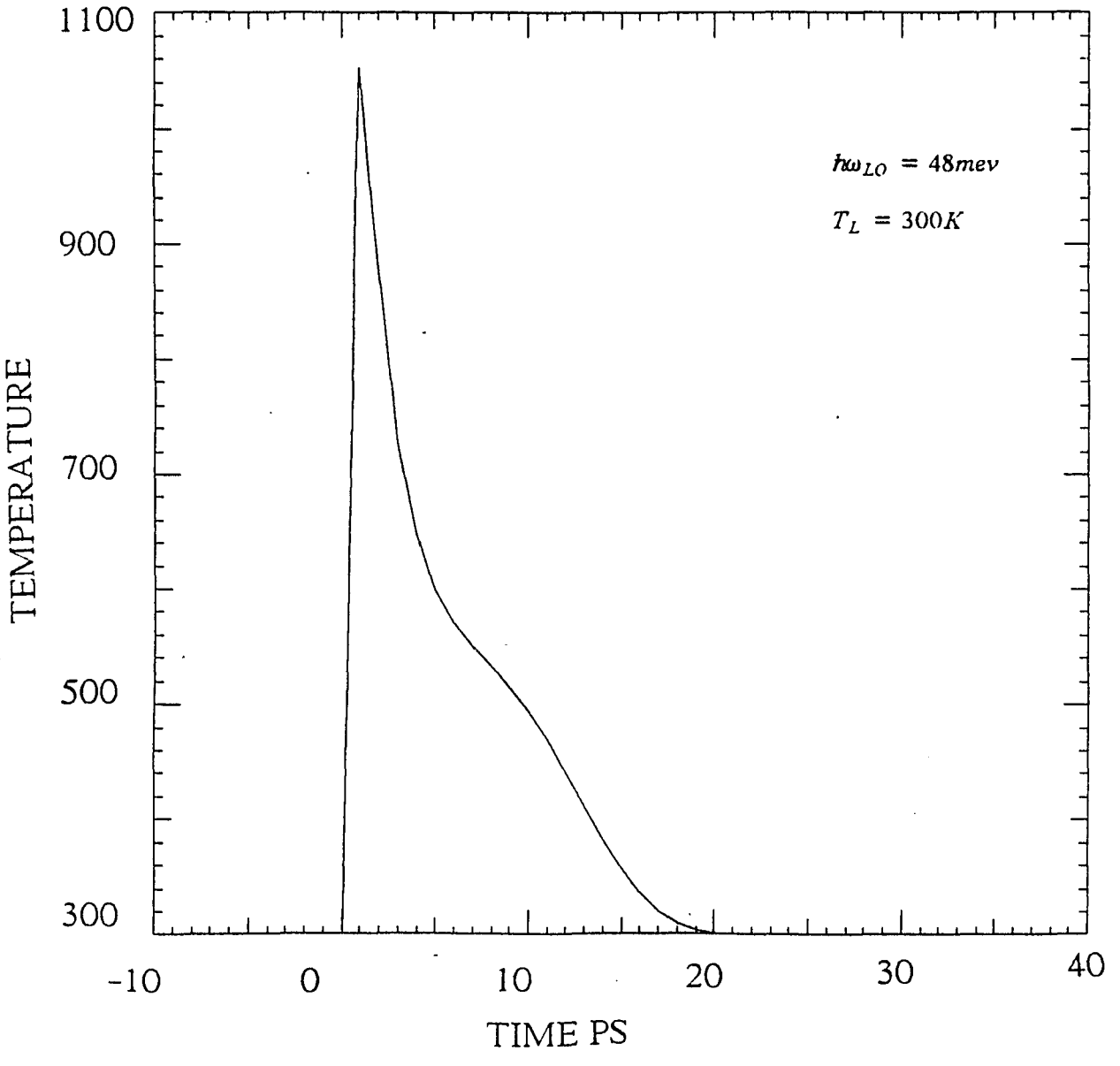

Fig. 3 . 3 .11 Electron temperature as a function of time as calculated from Eq. 3 . 3 . 59 for excitation power of $10MW/cm^2$.

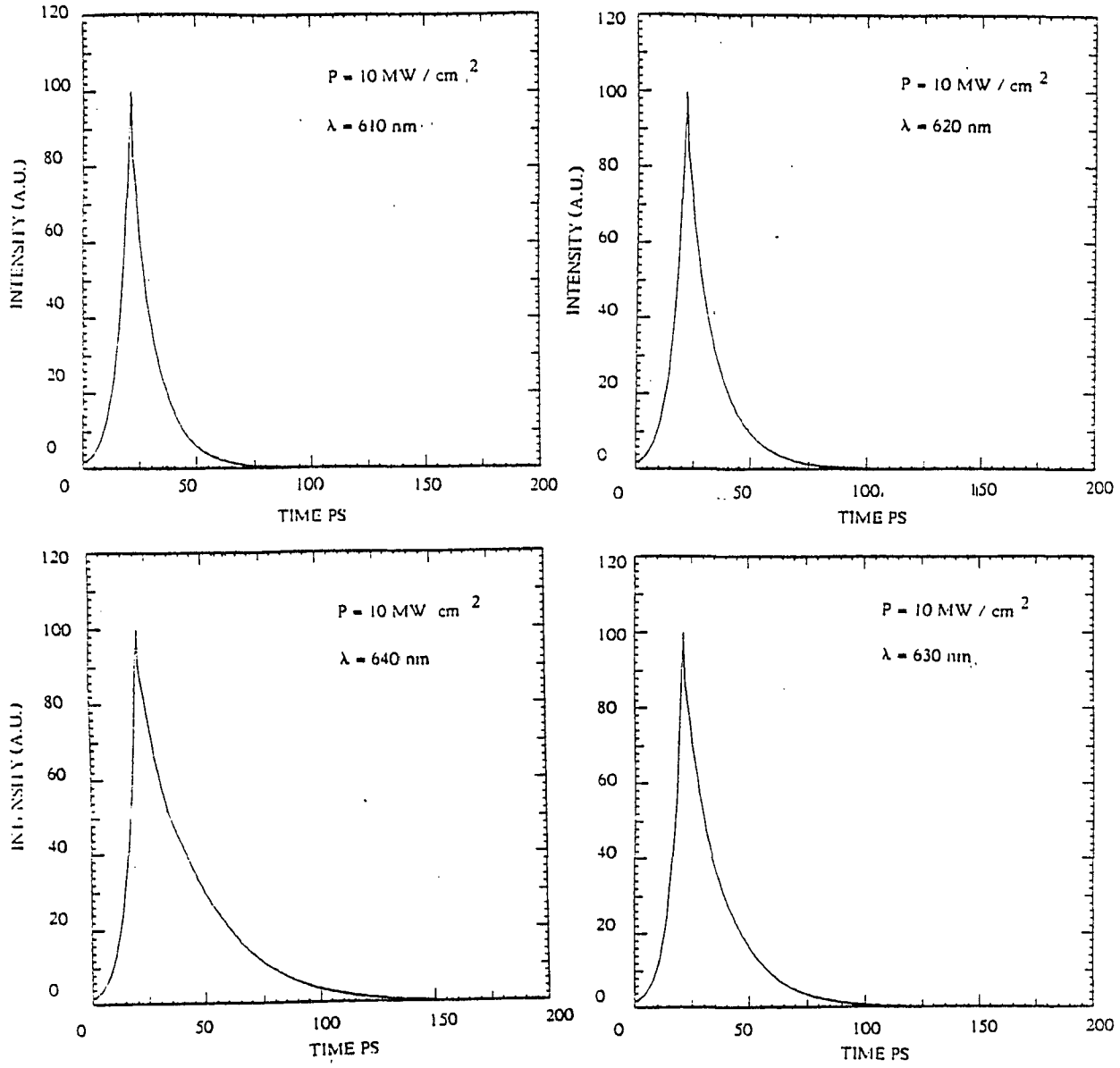

Fig. 3 . 3 . 12 (a) - The computed normalized output photon density at different wavelengths as a function of time for excitation of $P = 10 MW / cm^2$, $D_{TX} = 5 \times 10^8$ ev / cm and confinement factor of $C_F = 3 \times 10^{-3}$.

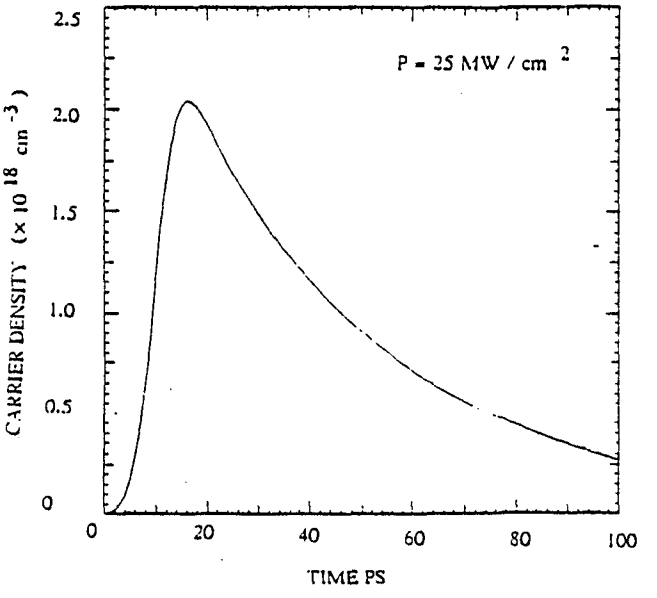

Fig. 3 . 3 . 13 a - The time dependence of electron density in Γ valley as a function of time for excitation power of $25MW/cm^2$, D_{TX} = 5×10⁸ ev / cm .

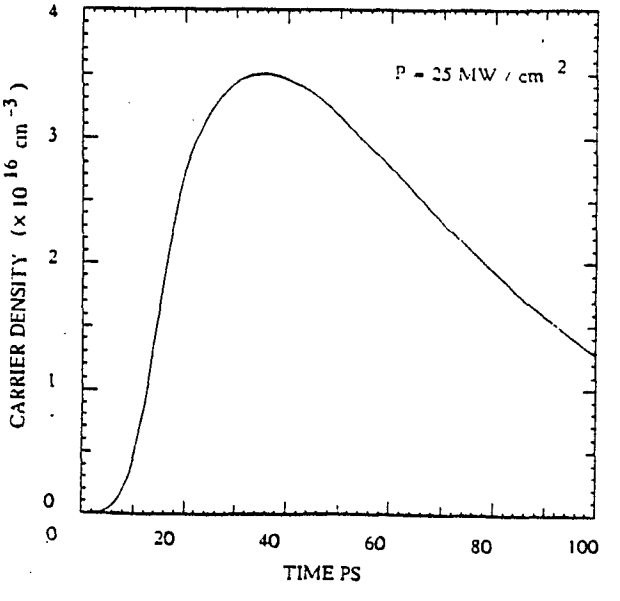

b - The time dependence of electron density in X valley as a function of time for excitation power of $25MW/cm^2$ and D_{TX} = 5×10⁸ ev / cm .

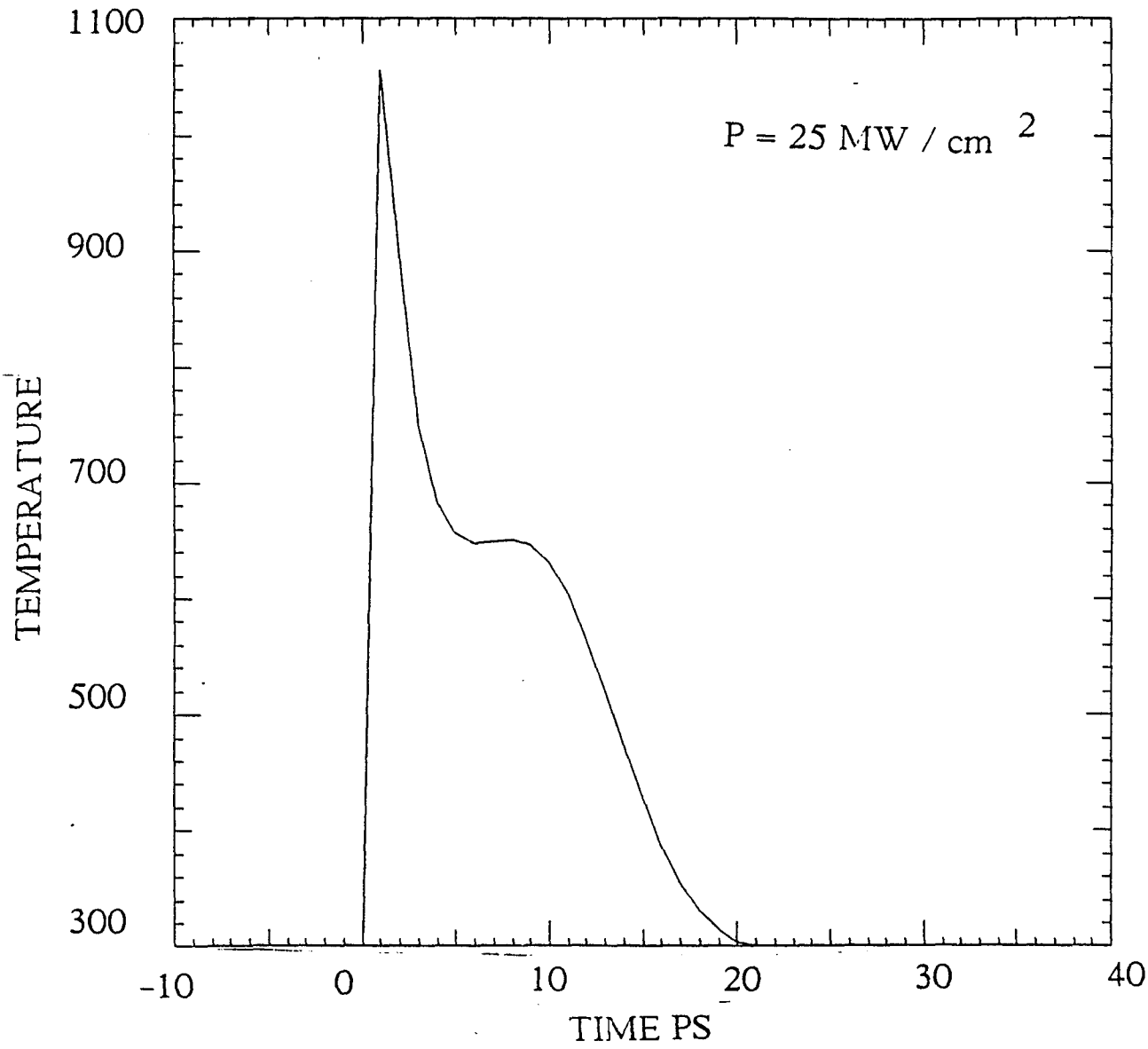

Fig. 3 . 3 . 14 The time dependence of electron temperature at excitation power of $25MW/cm^2$ and $D_{\Gamma X} = 5\times10^8$ ev / cm .

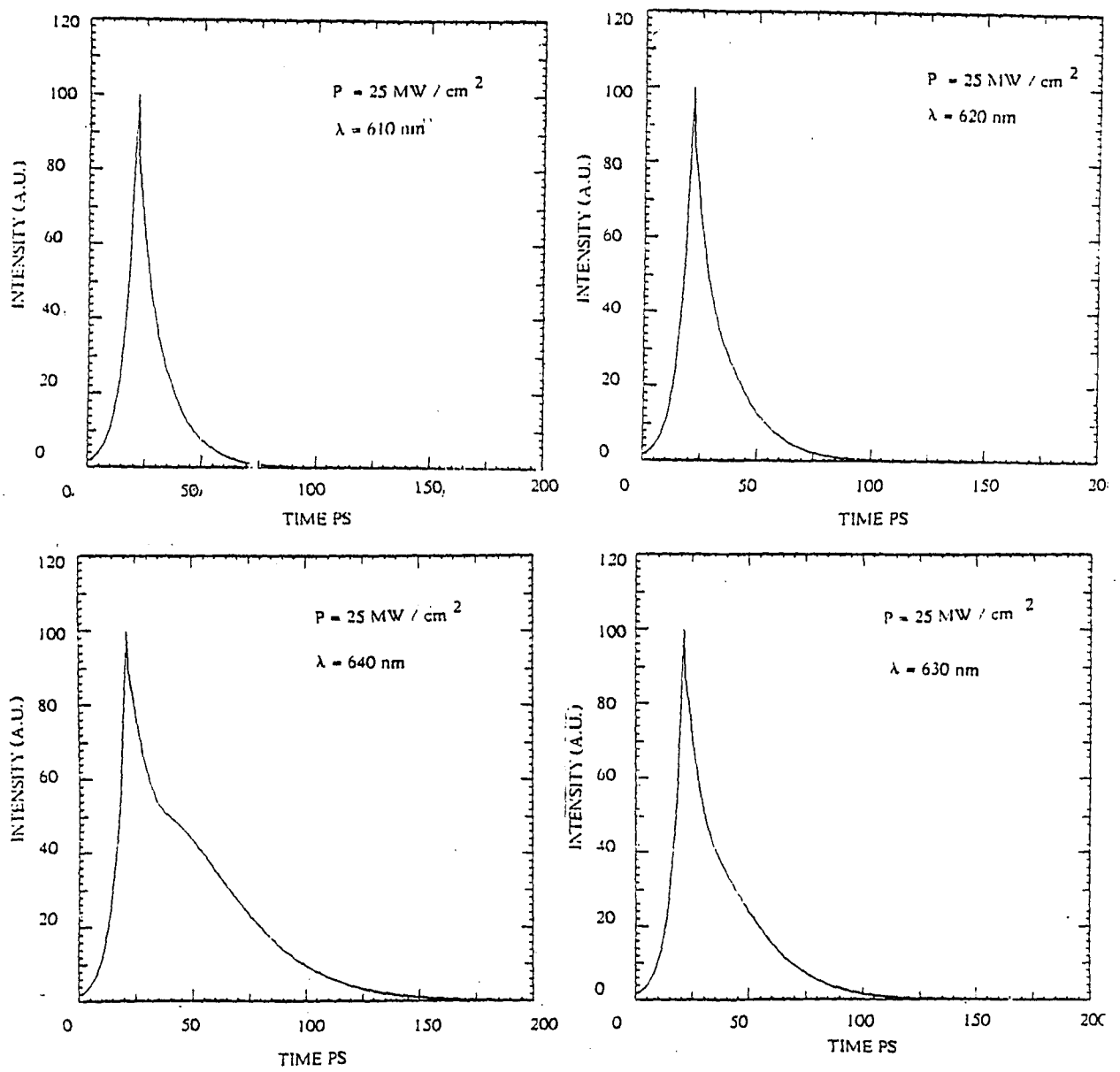

Fig. 3 . 3 . 15 The computed normalized output photon density at different wavelengths for excitation power of $25MW/cm^2$, $D_{TX} = 5\times10^8$ ev / cm and confinement factor of $C_F = 3\times10^{-3}$.

results were different. Fig 3.3.16 -a shows the time dependence of the electrons in the Γ valley . The electron density in Γ valley reaches the maximum value of $\sim 4\times10^{18} cm^{-3}$ in about 15 ps and then it decays exponentially . The time dependence of electron density in X valley is shown in Fig. 3.3.16 - b and it shows after 30 ps the electron density reaches the maximum value and then it decays exponentially . Fig. 3.3.17 shows the electron temperature as a function of time for excitation power fluence of $\sim 50 MW / cm^{-3}$. It shows in about 1 ps the electron temperature reaches 1100 K and then it cools for 5 ps and then it rises again for a while then it cools to lattice temperature in about 24 ps . This complex time dependence of temperature arises from the strong temperature dependence of intervalley scattering term .

The most interesting results of the computation is the time dependence of the output photon density . Fig. 3.3.18 shows the computed normalized output photon density at short (610 , 620*nm*) and long (630 , 640*nm*) wavelengths , respectively . At short wavelength of 610 , the general trend is the same as in the case of low power fluence of $5MW / cm^2$ (compare Fig. 3.3.12 -a and Fig. 3.3.18 -a) . However at long wavelength of 640 nm , the time dependence of output photon density is quite different . In this case , the unusual second peak is present and is separated from the main peak about 50 ps .

Comparing the computed results of the Fig. 3.3.12 and Fig. 3.3.18 with the experimental results which is shown in Fig. 3.1.1 and Fig. 3.1.2 shows that the the overall agreement between experiment and theory is seen to be quite good . In order to see the similarity of the experimental result and the theoretically calculated curves we have superimposed the experimental output photon density at long wavelength ($\lambda > 620 nm$) measured by streak camera shown in Fig. 3.1.2 -b and the computed result at long wavelength of 640 *nm* shown in Fig. 3.3.18-d . This is shown in Fig. 3.3.19 and it shows the theoretically calculated curve fits the experimental curve reasonably well .

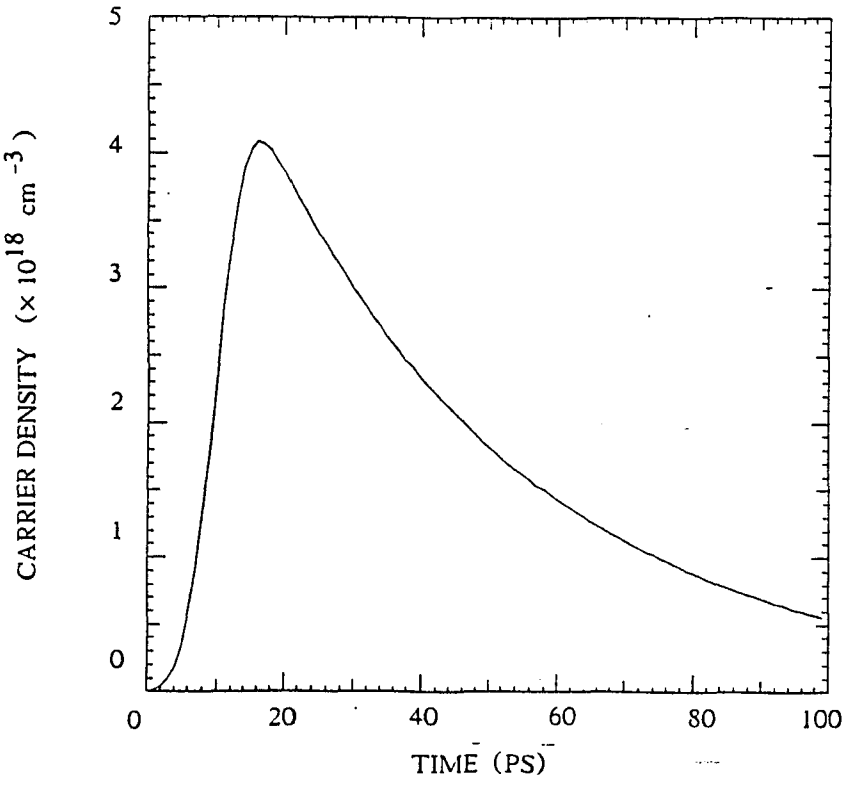

Fig. 3 . 3 . 16 a - The time dependence of electron density in Γ valley for excitation power of $50MW / cm^2$, $D_{\Gamma X} = 5\times10^8$ ev / cm .

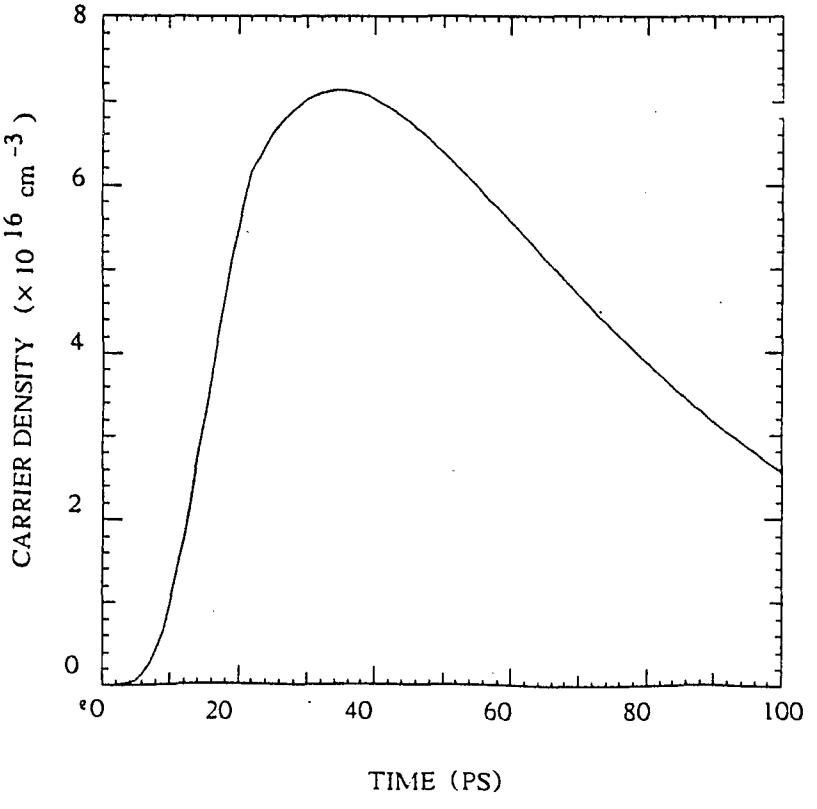

b - The time dependence of electron density in X valley for excitation power of $50MW / cm^2$, $D_{\Gamma X} = 5\times10^8$ ev / cm .

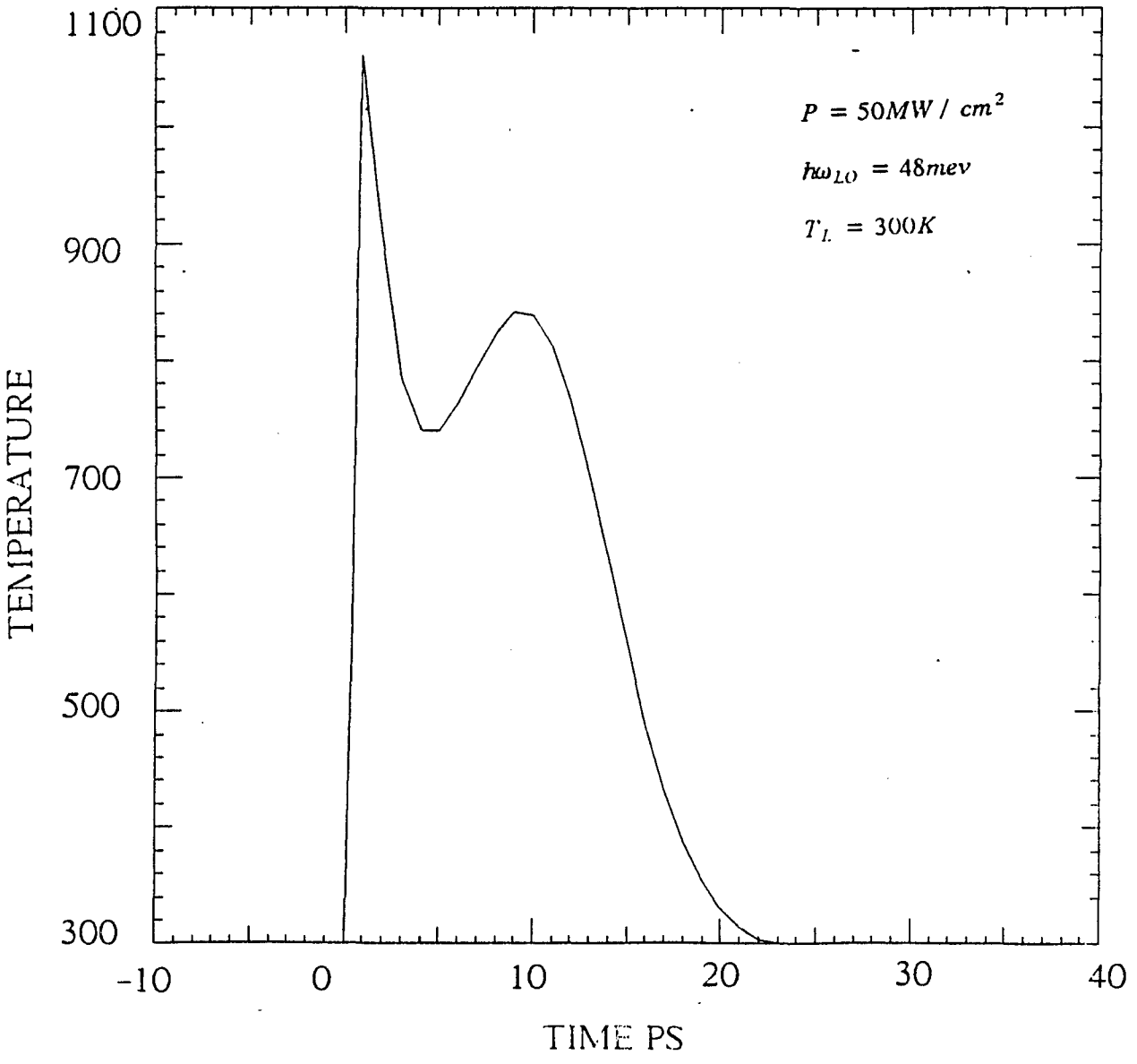

Fig. 3 . 3 . 17 Electron temperature as a function of time for excitation fluence of 50 MW / cm^2 , $D_{\Gamma X} = 5\times10^8$ ev / cm .

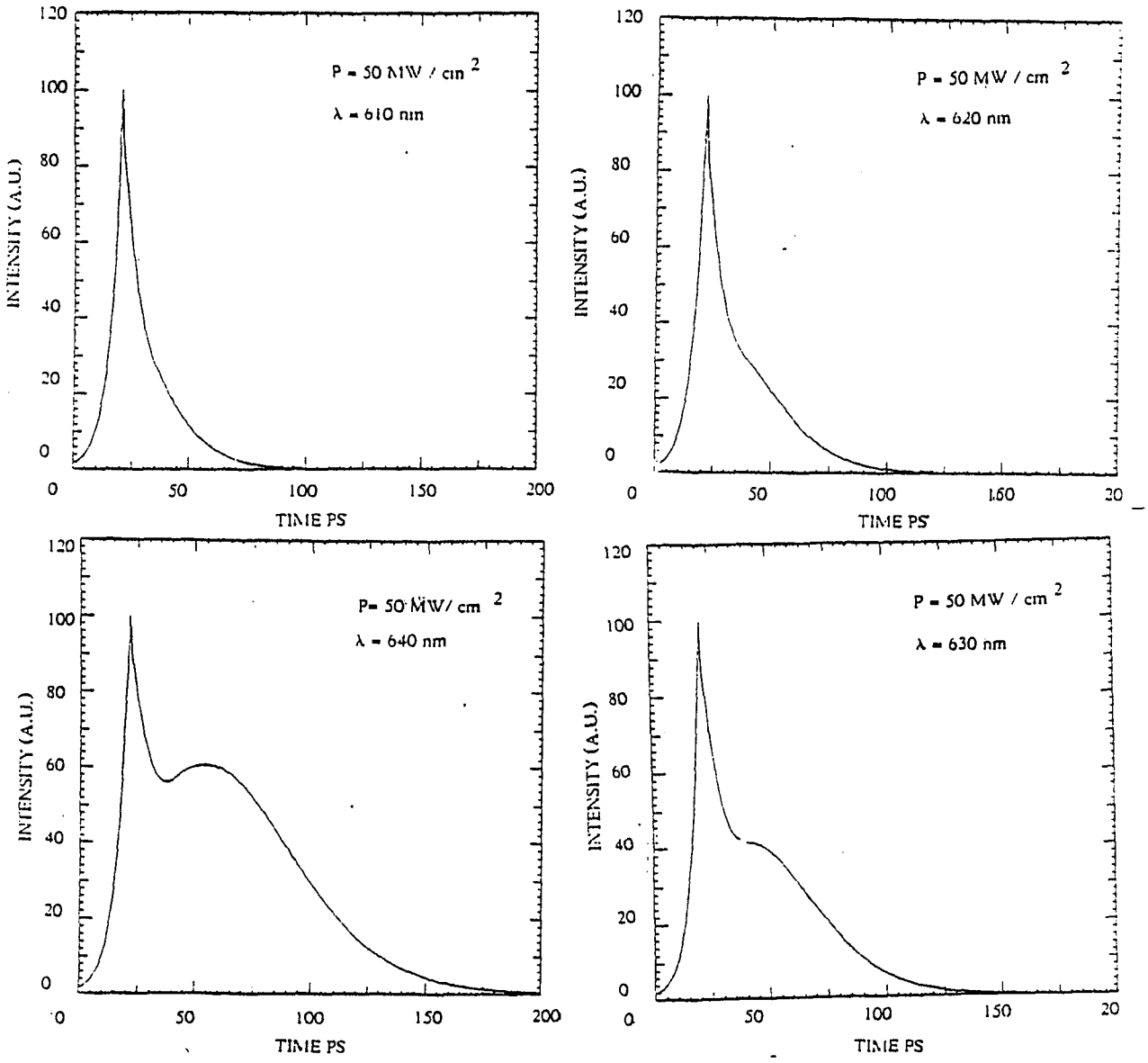

Fig. 3 . 3 . 18 The computed normalized output photon density at different wavelengths for excitation fluence of 50 MW/cm^2 , D_{TX} = 5×10^8 ev / cm and confinement factor of C_F = 3×10^{-3} .

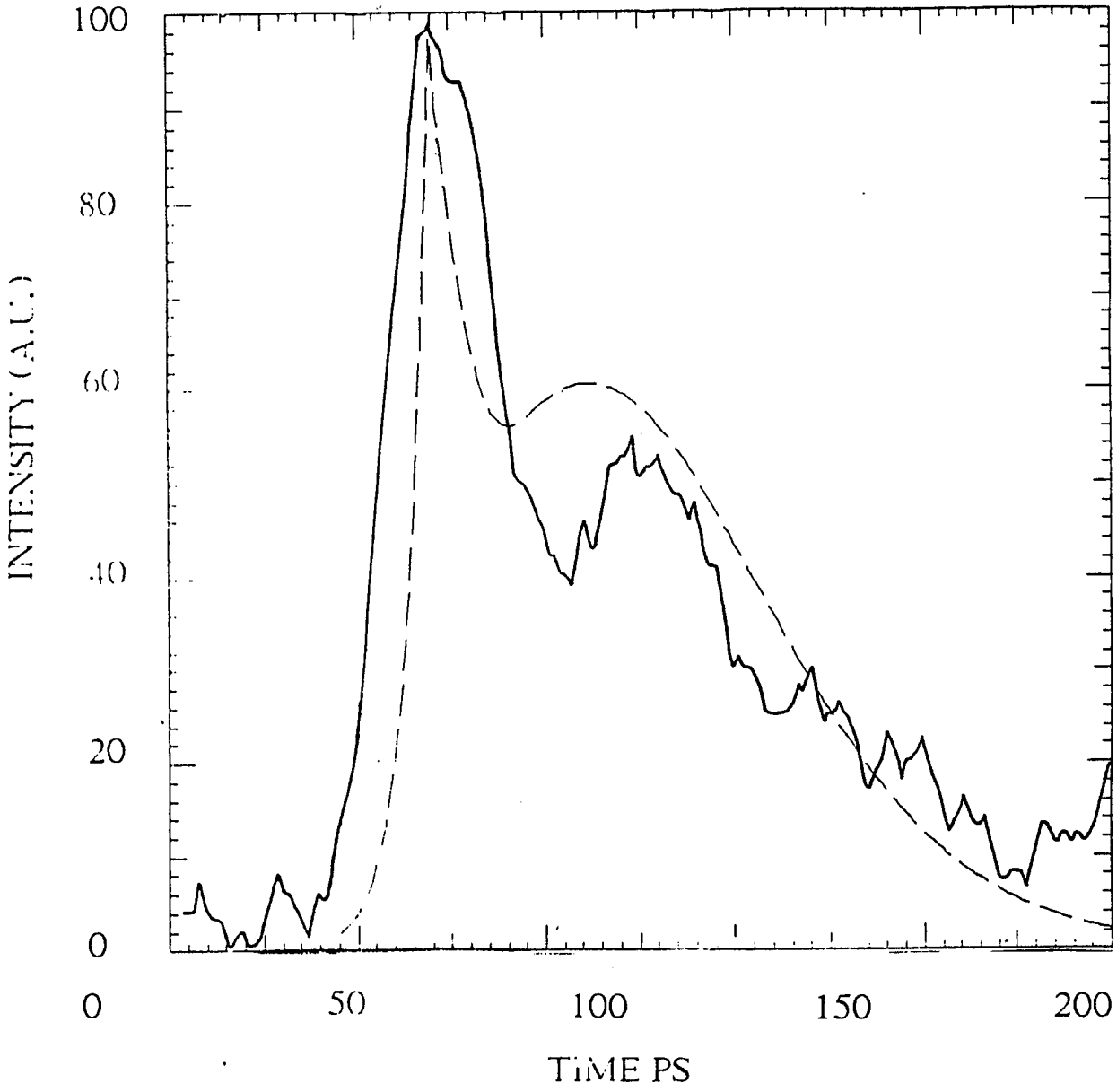

Fig. 3 . 3 . 19 The superposition of the experimental output photon density at $\lambda > 620nm$ (solid line) and the computed result at $\lambda = 640nm$ (dashed line) for excitation power of $50MW / cm^2$, $D_{\Gamma x} = 5\times10^8$ ev / cm and confinement factor of $C_F = 3\times10^{-3}$.

To investigate the effect of confinement variation on the shape of the output photon density , we also calculated the temporal profiles at different wavelengths for different confinement factors . Fig. 3.3.19 and Fig. 3.3.20 shows the output photon density at different wavelengths at excitation power of $50MW/cm^2$ for $C_F = 1.5\times10^{-3}$ and $C_F = 6\times10^{-3}$, respectively . By comparing the Fig. 3.3.20 and Fig. 3.3.21 we see that the smaller the confinement factor results to longer decay time at short wavelengths and higher intensity of secondary peak at long wavelengths .

The other factor which entered our calculation is the deformation potential $D_{\Gamma X}$. To investigate the effect of deformation potential variation in the theoretical calculations we changed the value of $D_{\Gamma X}$ by a factor of two . The time dependence of electron density, carrier temperature and output photon density is shown in Fig. 3.3.22 , Fig. 3.3.23 and Fig. 3.3.24 , respectively for deformation potential of $D_{\Gamma X} = 1\times10^9$ ev / cm . In this case the time dependence of electron density in Γ valley is very similar to the case of $D_{\Gamma X} = =5\times10^8$ ev / cm (compare Fig. 3.3.22- a and Fig. 3.3.10-a) . But the time dependence of electrons in X valley is different . In this case , the electron density reaches its maximum in about 60 ps and then they return back to the Γ valley much slower . As shown in Fig. 3.3.23 and Fig. 3.3.24 the time dependence of electron temperature and output photon density remained unchanged .

Similar calculations were performed for smaller deformation potential by a factor of two namely $D_{\Gamma X} = 2.5\times10^8$ ev /cm . The time dependence of electron density and electron temperature and output photon density is shown in Fig. 3.3.25 , Fig. 3.3.26 and Fig. 3.3.27 , respectively for excitation power of $50MW/cm^2$. In this case again as we can see the results are the same as before and only this time the electron density in X valley decays faster than before . From these calculations we can conclude that the variation of deformation potential will not effect the shape of the output photon density at different wavelengths . The factor which has a significant effect in the shape of the output photon density is the confinement factor C_F .

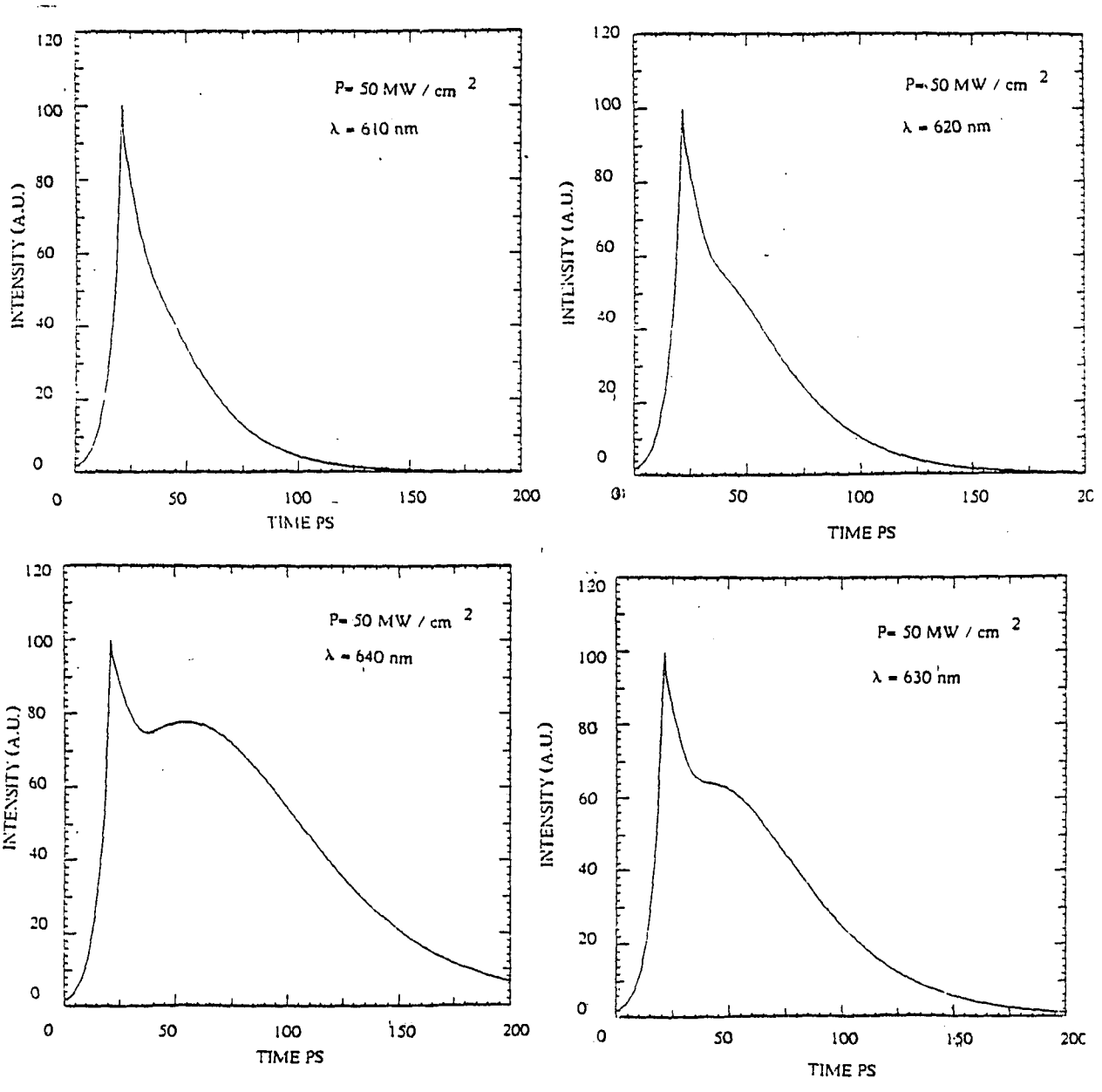

Fig. 3 . 3 .21 The computed normalized output photon density at different wavelengths for excitation power fluence of $50MW/cm^2$. $D_{TX} = 5\times10^{8}$ ev / cm and confinement $C_F = 6\times10^{-3}$.

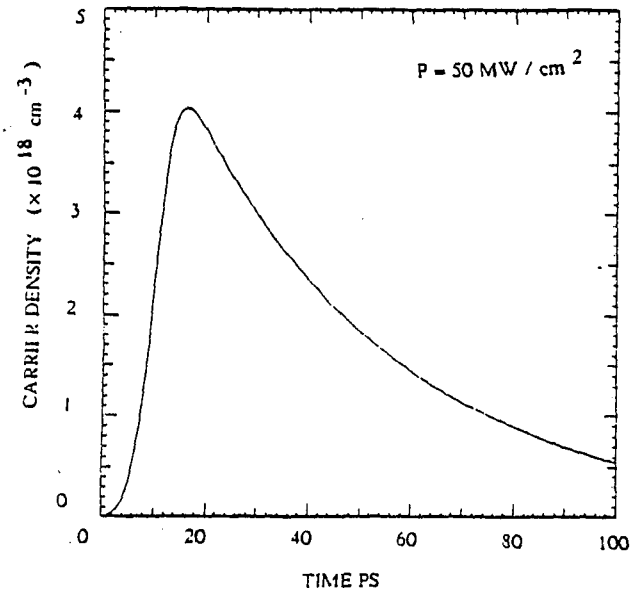

Fig. 3 . 3 . 22 a - The time dependence of electron density in Γ valley at excitation power of $50MW/cm^2$, $D_{\Gamma X} = 1\times10^9$ ev / cm .

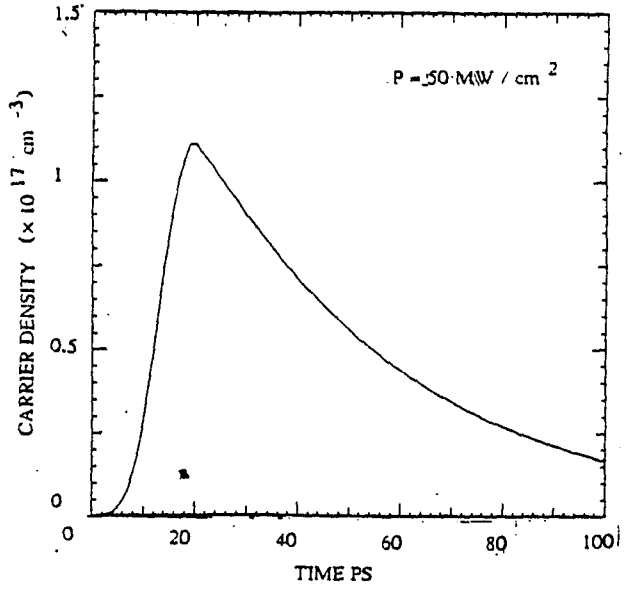

b- The time dependence of electron density in X valley at excitation power of $50MW/cm^2$, $D_{\Gamma X} = 1\times10^9$ ev / cm .

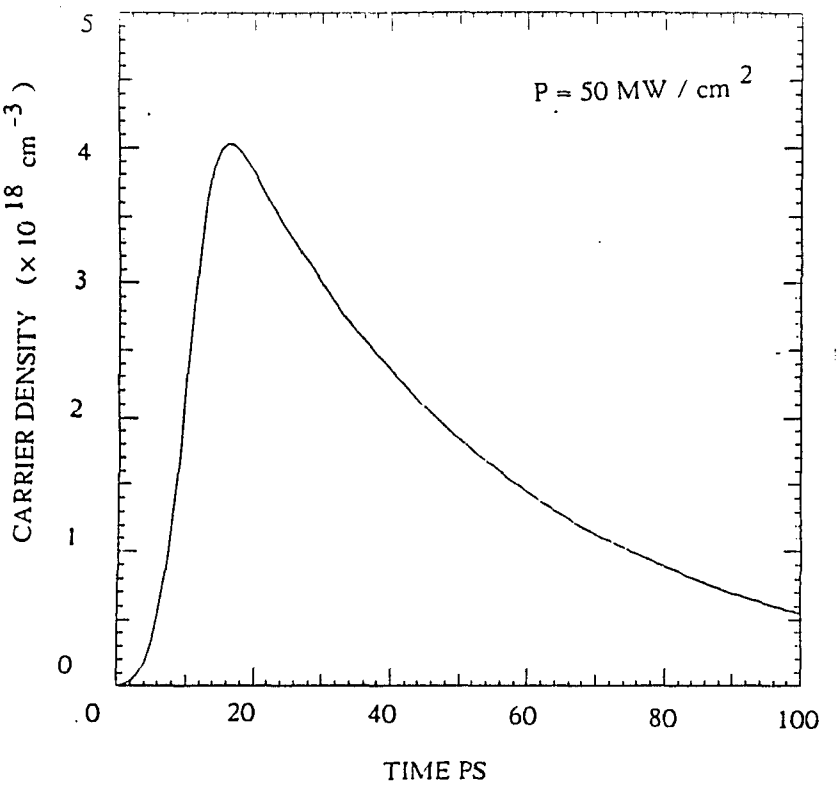

Fig. 3 . 3 . 22 a - The time dependence of electron density in Γ valley at excitation power of $50MW/cm^2$, $D_{\Gamma X} = 1\times10^9$ ev / cm .

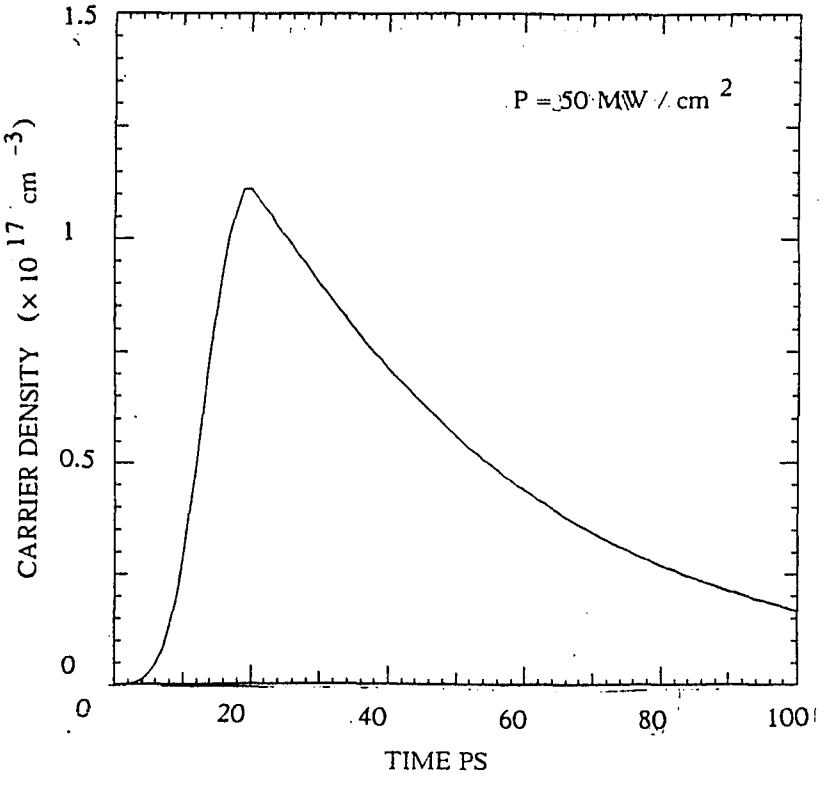

b- The time dependence of electron density in X valley at excitation power of $50MW/cm^2$, $D_{\Gamma X} = 1\times10^9$ ev / cm .

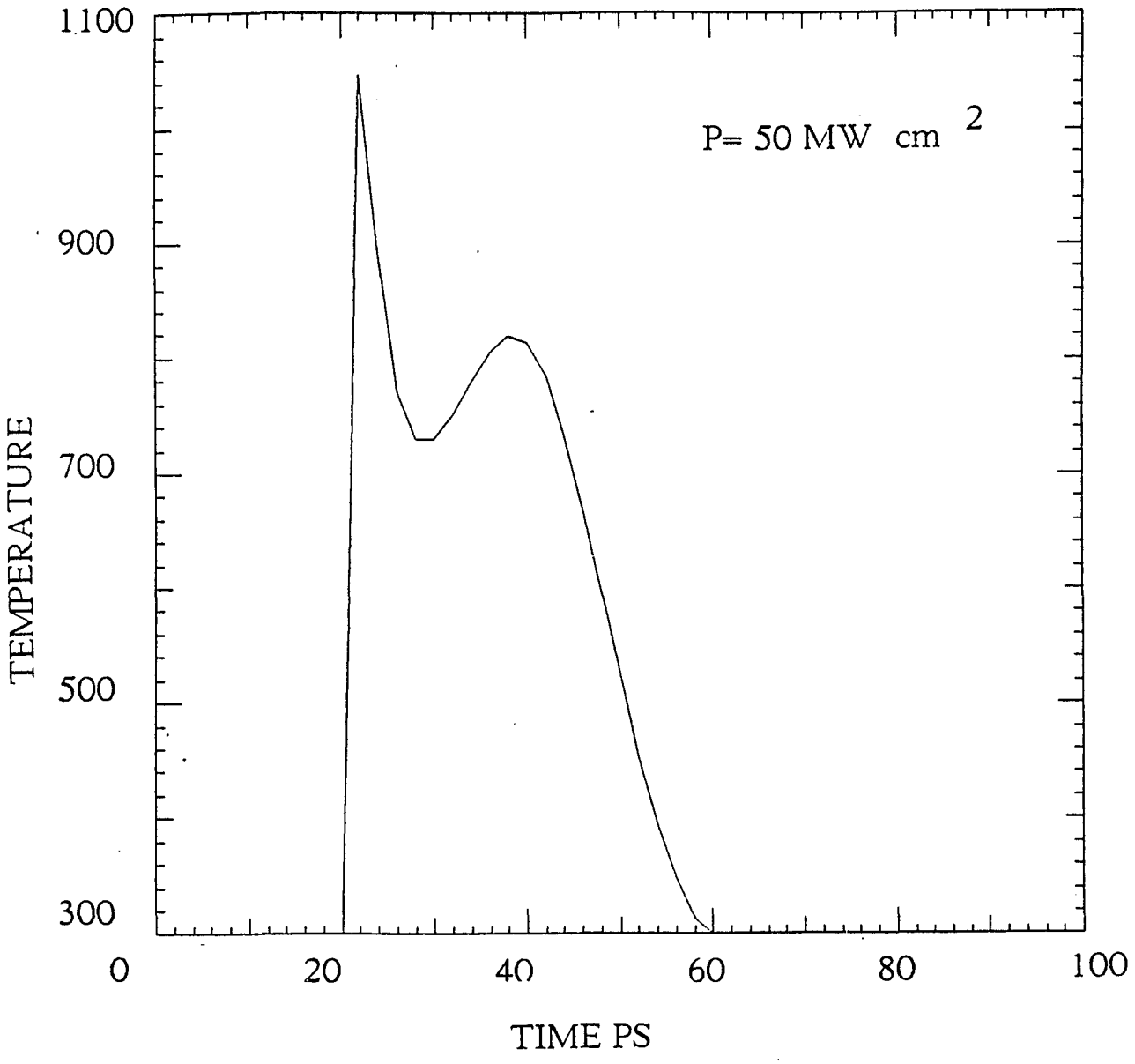

Fig. 3 . 3 . 23 The time dependence of electron temperature for excitation power of $50MW / cm$ and $D_{\Gamma X} = 1\times10^{9}$ ev / cm .

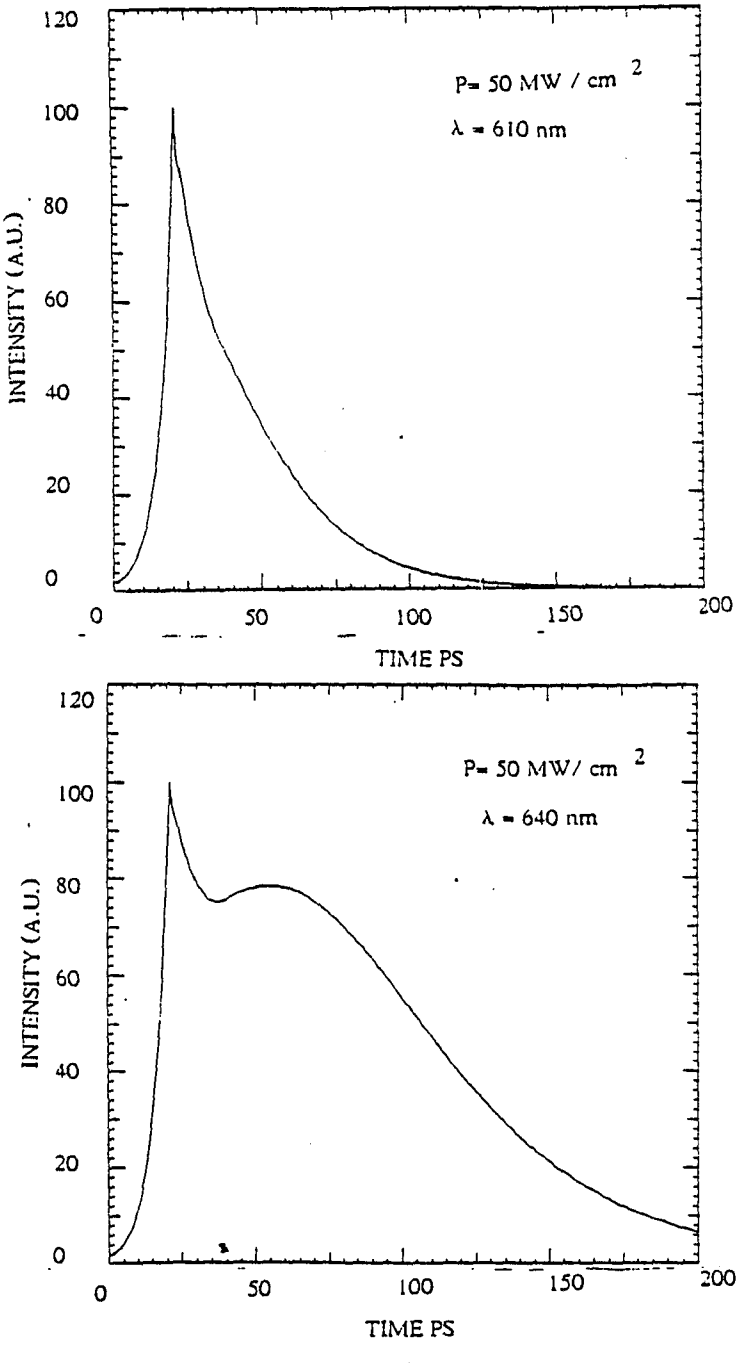

Fig. 3 . 3 . 24 The computed normalized output photon density at different wavelengths for excitation power of $50MW/cm^2$, $D_{TX} = 1\times10^9$ ev / cm and confinement factor of $C_F = 3\times10^{-3}$

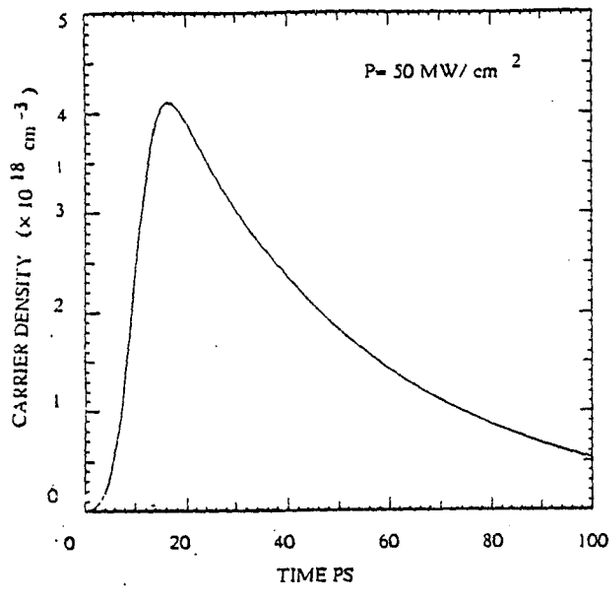

Fig. 3 . 3 . 25 a - The time dependence of electron density in Γ valley at excitation power of $50MW/cm^2$, $D_{\Gamma X} = 2.5\times10^8$ ev / cm .

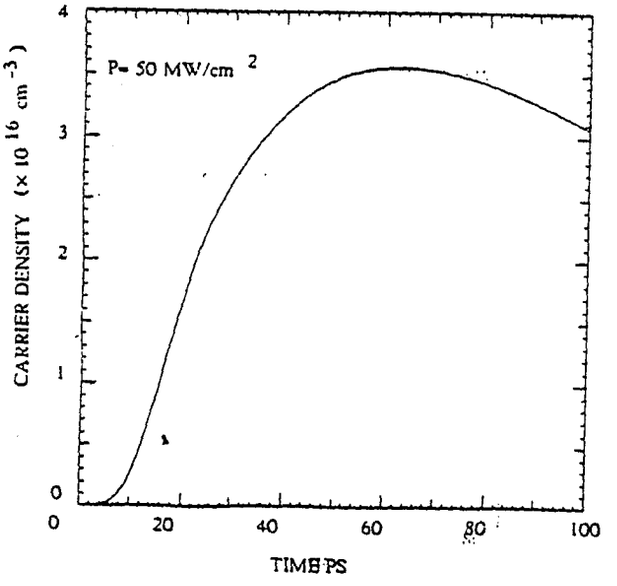

b - The time dependence of electron density in X valley at excitation power of $50MW/cm^2$, $D_{\Gamma X} = 2.5\times10^8$ ev / cm .

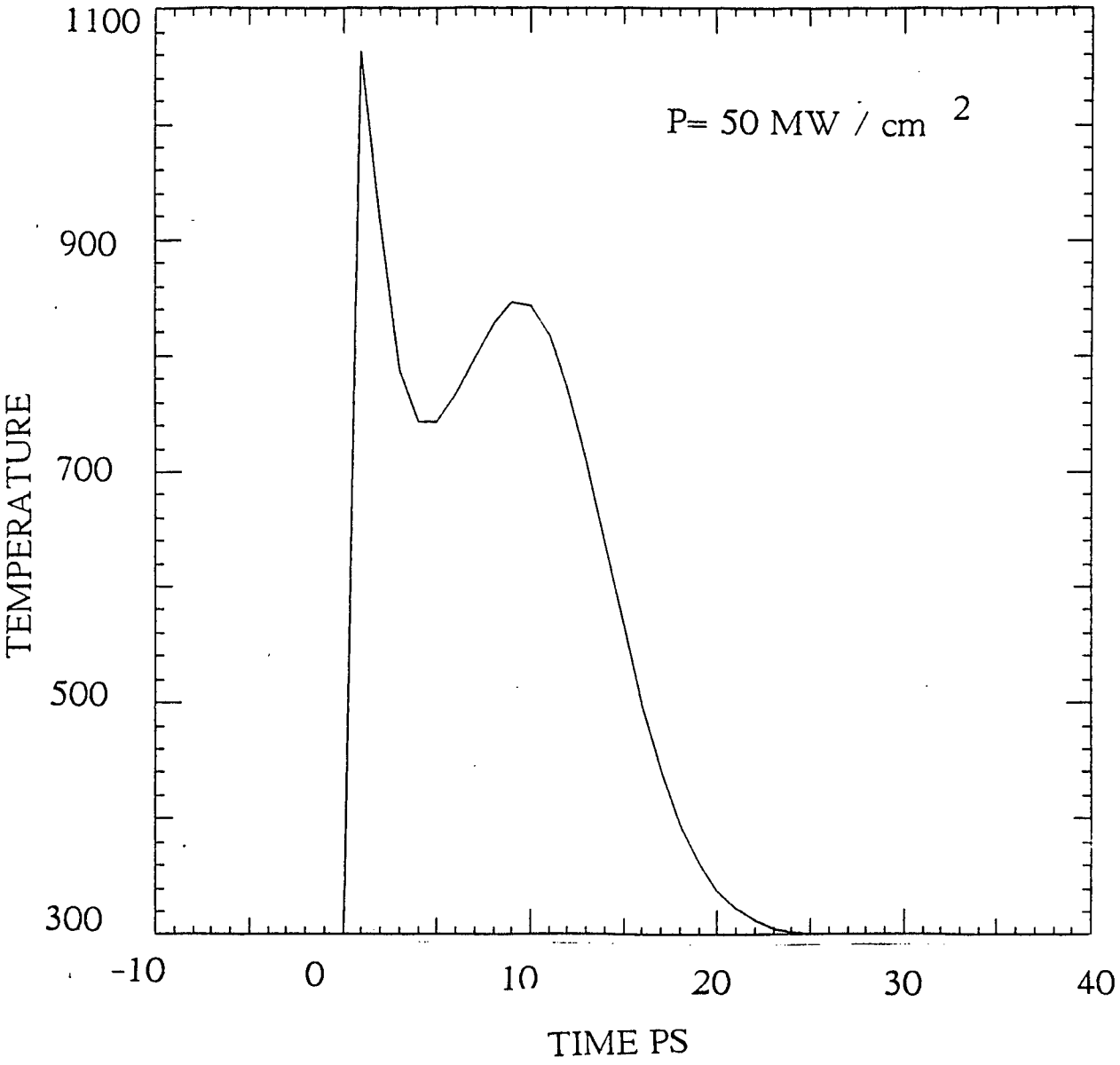

Fig. 3 . 3. 26 The time dependence of electron temperature for excitation power of $50MW / cm^2$,$D_{\Gamma X} = 2.5\times10^8$ ev / cm .

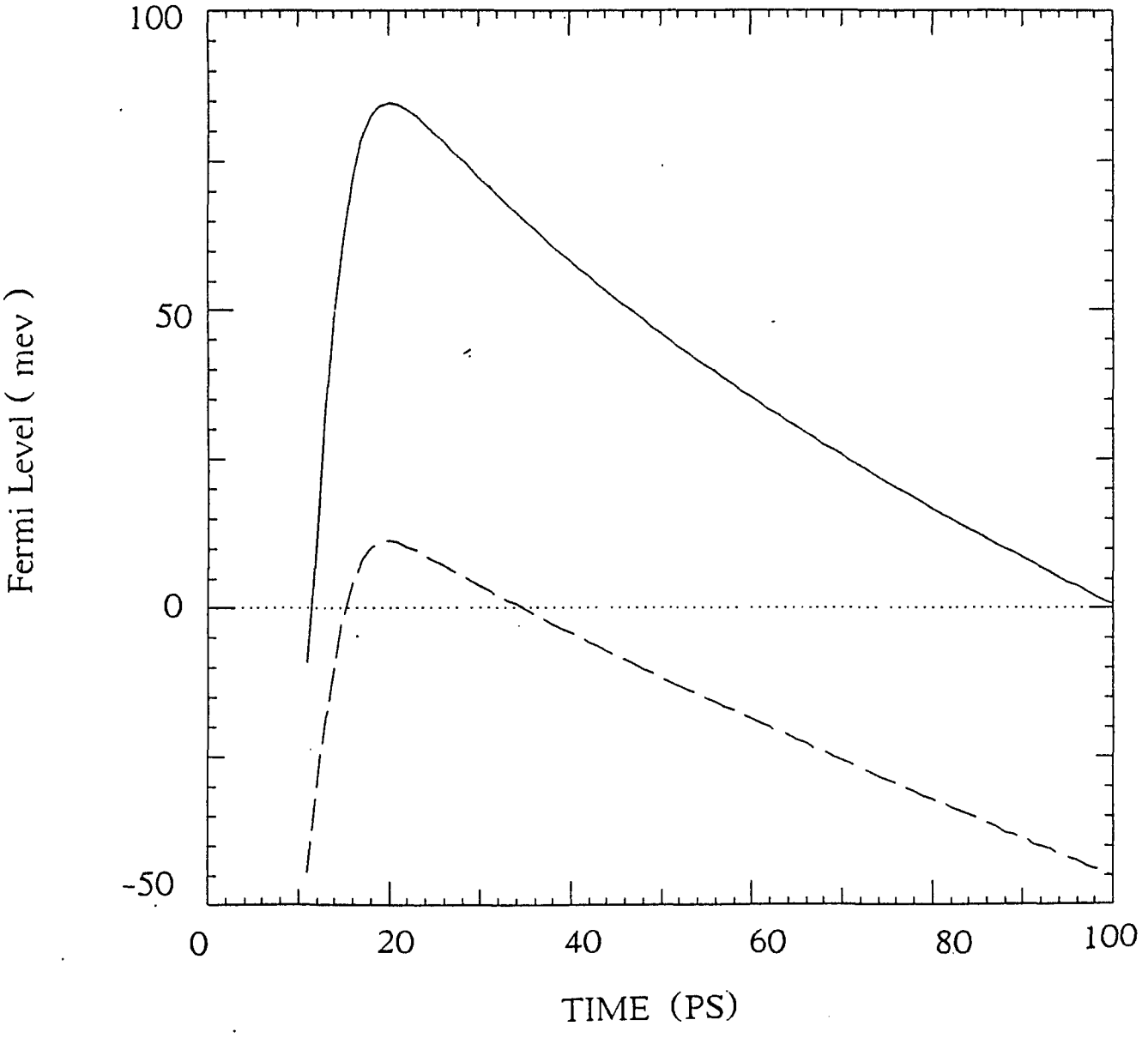

Fig. 3 . 3 . 27 The time dependence of Fermi level of electrons in Γ valley as a function of time for excitation power fluence of 10 and 50 MW / cm^2 .

The main physical process involved in the observation of the second peak at long wavelength is the downward motion of the Fermi levels due to cooling of carriers and depletion of the carriers due to spontaneous and stimulated emission. The Fermi levels are thus moved down rapidly, which by Eq. (3.3.41) converts the absorption coefficient ($\alpha > 0$, loss) to the gain coefficient ($\alpha < 0$, gain) .

Fig. 3.3.28 shows the Fermi level of electrons in Γ valley as a function of time for excitation power fluence of 10 and 50 MW/cm^2 . At low excitation power of $10MW/cm^2$, the Fermi level of electrons in Γ valley is mostly below the conduction band and only between $t = 15$ and $t = 35\ ps$ the Fermi level is above the conduction band and its maximum value is around 10 mev . So in this case there is no gain which means α is always positive for all the wavelengths . However , at excitation power of $50MW/cm^2$ the Fermi level is moved up into the conduction band for most of the time . In this case the behavior of α at different wavelengths is described by Eq. 3.3.47 and Eq. 3.3.48 .

The phenomena observed here , especially the dynamics of the carriers could play a role in the performance design and fabrication of semiconductor lasers .

In conclusion we have used picosecond time resolved spectroscopy technique to observe some novel picosecond laser dynamics in high quality MBE grown GaInP semiconductor we also have shown that a model which includes the broad band stimulated emission and intervalley scattering accounts for the most of the observed features of our experiment .

References

1 A. G . Sigai, C. J. Nuese, R.E. Enstrom, T. J. Zamerowski Electrochem. Soc.120, 947 (1973).

2 Campbell, J. Cryst. Growth. 27, 154 (1974).

3 P. Blood, J.S. Roberts, J.P. Stagg, J. Appl. Phys. 53, 3145 (1982).

4 F. H . Pollak, G.W. Higgibotham, M. Cardona, J. Phys. Soc. Japan, Suppl. 21, 20 (1966).

5 J . A. Van Vechten, Phys. Rev. 187, 1007 (1969).

6 M .R . Lorenz, W. Reuter, W . P . Dumke, R . J . Chicotka, G . D . Petit, J . M . Woodall, Appl. Letters, 13, 42 (1968).

7 H . Rodot, J . Horak, G . Rouy, J . Bourneix, Compt. Rend. 269, 381 (1969).

8 E. W . Williams, A . M . White, A . Achford, C . Hilsum, J . Phys. D3, 1322 (1970).

9 B . W . Hakki, A . Jayaraman, C . K . Kim, J . Appl. Phys. 41, 5291 (1970).

10 A . Onton, R . J . Chicotka, Phys. Rev. B4, 1847 (1971).

11 C . Alibert, G . Borduri, A . Laugier, J . Chevallier, Phys. Rev. B6, 1301 (1972).

12 R . J . Nelson, N . Holonyak Jr. , J . Phys. Chem. Solids, 37, 629 (1976).

13 B . W . Halkki, J . Appl. Phys. 42, 4981 (1971).

14 Semiconductor Statistics , J . S . Blakemore , Pergamon Press , NewYork (1962).

15 W . B . Joyce , R . W . Dixon , Appl. Phys. Lett. 31 , 354 (1977) .

16 E . M . Conwll , High Field Transport in Semiconductors , Supp. 9 in solid state physics series , Academic Press , (1967) .

17 G . Schmidt , Physics of high Temperature Plasmas , Second Edition , Academic press , NewYork , (1979) .

18 G . Bauer , H . Kahlert , Phys. Rev. B7 , 1508 (1973) .

19 G . Mahan , Polarons in Ionic Crystals and Polar Semiconductors , Edited by J . Devreese , North Holand , Amsterdam (1972) .

20 M . Pugnet , J . Collet , A . Cornel , Solid State Comm. 38 , 531 (1981) .

21 T . L . Koch , L . C . Chiu , C . Harder , A . Yarive , Appl. Phys. Lett. 41 , 6 (1982) .

22 T . L . Koch , Ph.D. dissertation , California Institute of Technology , (1982) .

23 J . F . Young , H . M . van Driel , Phys. Rev. B26 ,2147 (1982) .

24 J . Birman , M . Lax , R. Loundon , Phys. Rev. 145 , 620 (1966) .

25 T . S . Moss , G . J . Burrel ,B . Ellis , Semiconductor Opto-electronics , John Wiley and Sons , NEW York , (1973) .

26 D . von der Linde , R . Lambrich , Phys. Rev. Lett. 42 , 1090 (1979) .

CHAPTER 4

Time Resolved Photoluminescence Spectra of $Ga_x In_{(1-x)}P$ under Picosecond Laser Pulse Excitation measured by a streak camera

In this chapter , the experimental technique involved in the measurements of photoluminescence spectra in $Ga_x In_{(1-x)}P\,(x=.56)$ with 10 ps time resolution using a streak at various times following the exciting picosecond laser pulse will be presented . From the theoretical fitting of photoluminescence spectra we have determined the time evolution of the carrier density and carrier temperature . We measured that the carrier energy loss rate to be slower than predicted from a simple model assuming a Maxwell Boltzmann distribution function . This is attributed to the screening of the hot carrier energy relaxation under high carrier densities . Integro-differential equations describing the time dependence of carrier temperature in the case of Maxwell Boltzman distribution , Fermi Dirac distribution and in the presence of screening have been solved and the results are compared with the experimental data .

4.1 INTRODUCTION

Information about the dynamics of hot carrier energy relaxation in highly excited semiconductor is important and fundamental in the design and fabrication of high speed devices . Time resolved absorption and luminescence spectroscopy of semiconductors provides direct information about the evolution of the carrier density as well as the distribution function[1]. To study the ultrafast processes in semiconductor there are a variety of direct and indirect techniques such as pump and probe[2],optical Kerr gate[3], upconversion gate[4], and streak camera[5]. Energy relaxation of low density carriers in GaAs has been studied by Ulbrich by measuring the photoluminescence spectra under nanosecond laser pulse excitation[6]. From the results of picosecond reflection measurements Shank at el.[7] concluded that in GaAs , carriers with initial energy .6 ev lose their energy and thermalize with the lattice in about 2 ps . In most of the experiments done to date , the semiconductor samples were excited at low temperatures . There has not been that much information available in the literature about carrier energy relaxation at room temperature even though most of the electronic and optical devices fabricated from semiconductors are used at room temperature .

Steady state photoluminescence spectra of $Ga_x In_{1-x} P$ alloy system has been reported by many groups at different temperatures . The main objective of these measurements was to characterize the band structure of $Ga_x In_{1-x} P$ and to determine the cross over composition . Kressel et al.[8] studied the photoluminescence spectra of $Ga_{.5}In_{.5}P$ grown by VPE between 4.2 and 300 K at various doping levels . At very low temperature , four major emission bands were identified , involving intrinsic recombination , donor-to valence band transition , conduction band to acceptor transitions and donor to acceptor transition . The intrinsic recombination dominated when $T > 150$ K . The value of shallow donor ionization energy was determined to be 7 ± 1 mev , the same value as in InP . The spectral data of Cd doped samples (with p doping varying

from 1.8×10^{16} to $9.3\times10^{17}cm^{-3}$) suggested a consistent shift of acceptor ionization energy to lower values with increasing doping .

In steady state photoluminescence where usually the excitation source is the low power (10-100 mW) argon laser , the density of photogenerated carriers is less than impurity concentrations , therefore impurities play a major role in the photoluminescence spectra . When carriers are photogenerated above $10^{18}cm^{-3}$ by picosecond laser pulse , the emission spectra will be the result of radiative recombination of electron-hole plasma . In this chapter , we report on the measurements of the time resolved spectra of $Ga_x In_{(1-x)}P$ ($x=.56$) at room temperature using the streak camera as the detection system . The photoluminescence spectra at various times were fitted to the theoretical expression for direct transitions . From the fitting , the time evolution of the photogenerated carrier density and distribution function has been determined .

4 . 2 EXPERIMENTAL METHODS

The experimental setup used in this research has been described in detail in chapter 2 . A second harmonic (527 nm) of the Nd : glass laser pulse of 8 ps duration was used to excite the sample of $Ga_{(1-x)}In_x P(x=.56)$ on the front surface . The excitation area was measured to be approximately $8\times10^{-3}cm^2$. The sample was 1.5 μm thick , moderately pure ($10^{16}cm^{-3}$) and grown by VPE on a GaAs substrate . The composition of the sample was determined from the calibration of the band gap versus composition of [9] . The band gap of the sample was determined to be 1.903 ev at room temperature from the direct relationship $E_g = h\nu_p - \frac{1}{2}kT$ where $h\nu_p$ is the peak energy in the low power steady state photoluminescence spectra and $\frac{1}{2}$kT accounts for the direct transition of the carriers . The photoluminescence of the sample was collected by a combination of lenses and imaged into a 30 μm slit of a Hamamatsu streak camera . The output was detected by temporal analyzer and computer for data analysis .

The time resolution of the detection system was approximately 10 ps . Various narrow band filters centered at different energies were placed in front of the streak camera to select different spectral regions of the photoluminescence spectra corresponding to carriers with different energies .

4 . 3 EXPERIMENTAL RESULTS

Time resolved photoluminescence profiles at different energies are shown in Fig. 4 . 3 . 1 for an excitation pulse of 60 μJ . We used $N(E,t) = A [\exp(\frac{-t}{\tau_{d(E)}}) - \exp(\frac{-t}{\tau_{r(E)}})]$ to fit the experimental time resolved profiles of Fig . 4 . 3 . 1 to determine rise and decay times of the emission at different energies . In the above equation , N(E,t) is the number of photons detected at energy E where E is the central energy of the narrow band filter ,$\tau_d(E)$ and $\tau_{r(E)}$ are the decay and rise time of the time resolved profiles at energy E , A is the proportionality constant . The vertical scale of the time resolved profile at E=1.981 ev has been normalized to 1000 counts and the rest of the vertical scales are relative to E=1.981 ev for comparison . All the time resolved profiles shown in Fig. 4 . 3 . 1 are corrected for nonlinearity of the detection system , streak camera tube spectral response and the transmission of the narrow band filters . Each time resolved profile shown in Fig. 4 . 3 . 1 was repeated several times and deviation in the vertical scale was less than 5% . The salient features of the time resolved profiles shown in Fig. 4 . 3 . 1 are as follow : The rise time $\tau_r(E)$ of the emission increased moderately from 10 ps at E=2.107 ev (Fig. 4 . 3 . 1 - a) to 18 ps at E=1.919 ev (Fig. 4 . 3 . 1f) . The decay time of the emission $\tau_d(E)$ increased from 47 ps at E=2.107 (Fig. 4 . 3 . 1 - a) to 310 ps at E=1.919 ev near the band edge (Fig. 4 . 3 . - 1f) . Figure 4. 3 . 2 shows the plot of the rise time of the emission vs energy. The variation of the decay time with respect to energy is shown in Figure 4 . 3 . 3 . Since the number of photons detected N(E) dE at different energies decayed with different decay

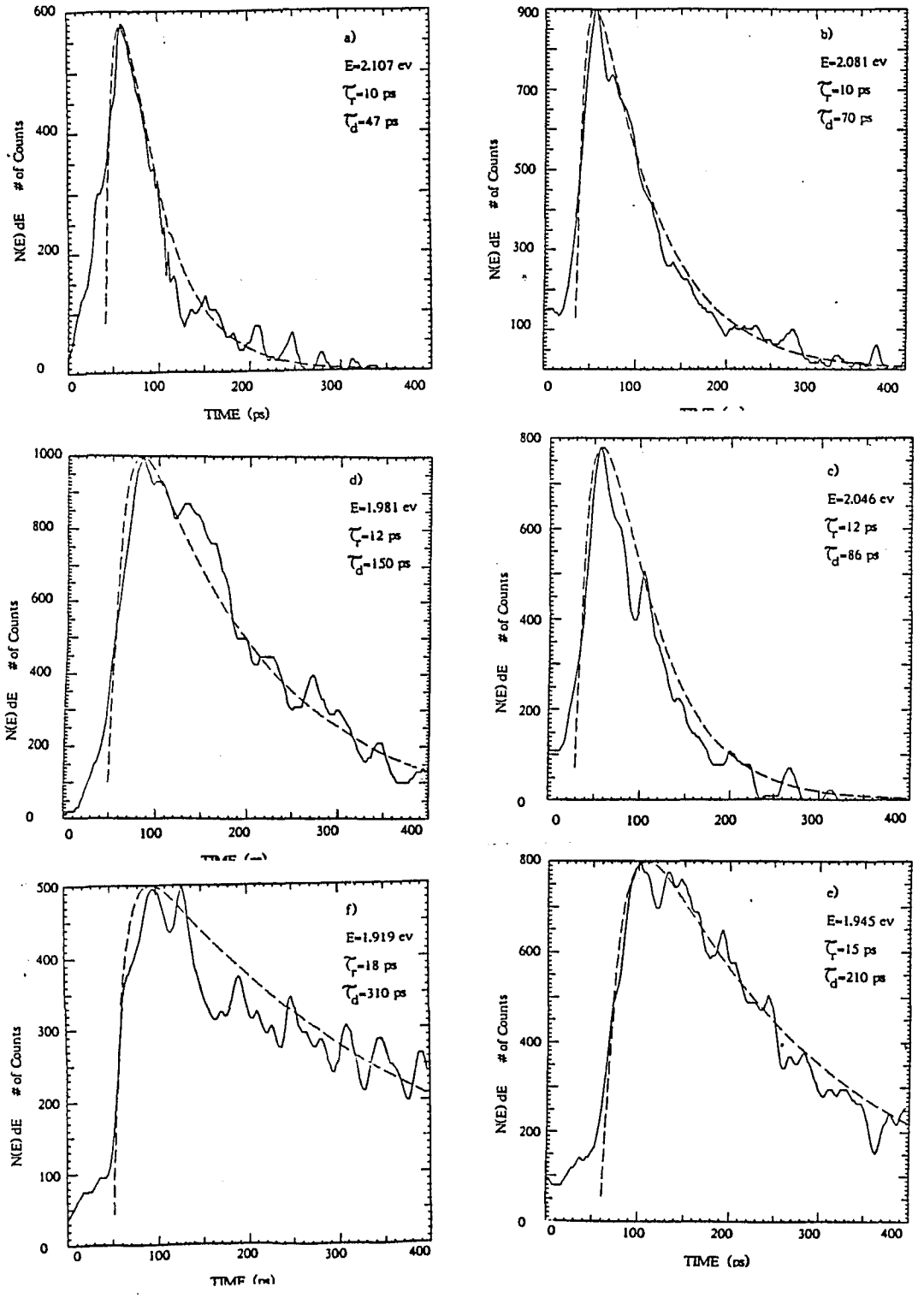

Fig. 4.3.1 (a)-(f) Time resolved photoluminescence profile of $Ga_{.56}In_{.44}P$ at energies of 2.107 , 2.081 , 2.046 , 1.981 ,1.945 and 1.919 ev , respectively .

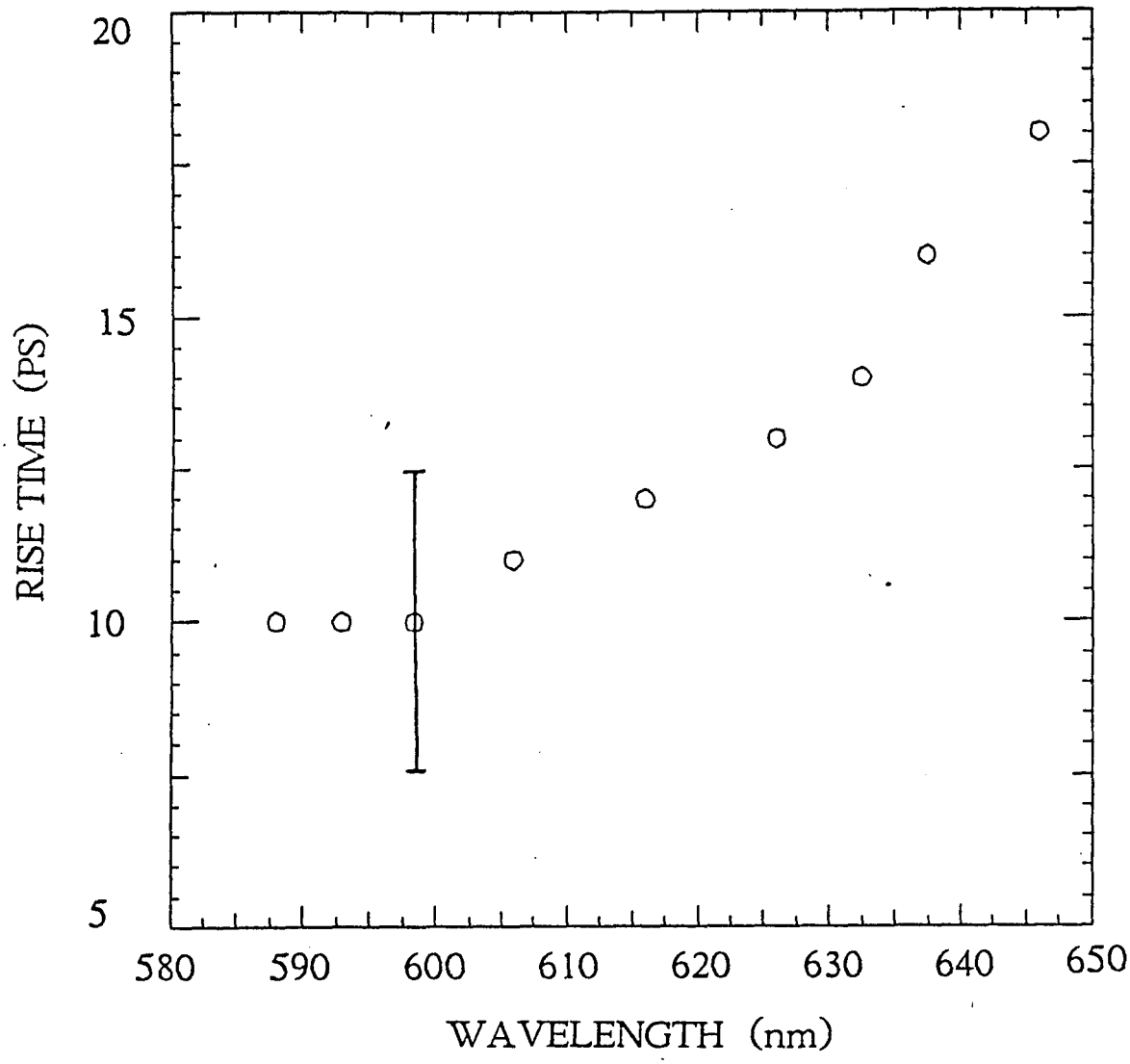

Fig. 4. 3 . 2 Plot of the rise time of the time resolved photoluminescence profiles as a function of the energy .

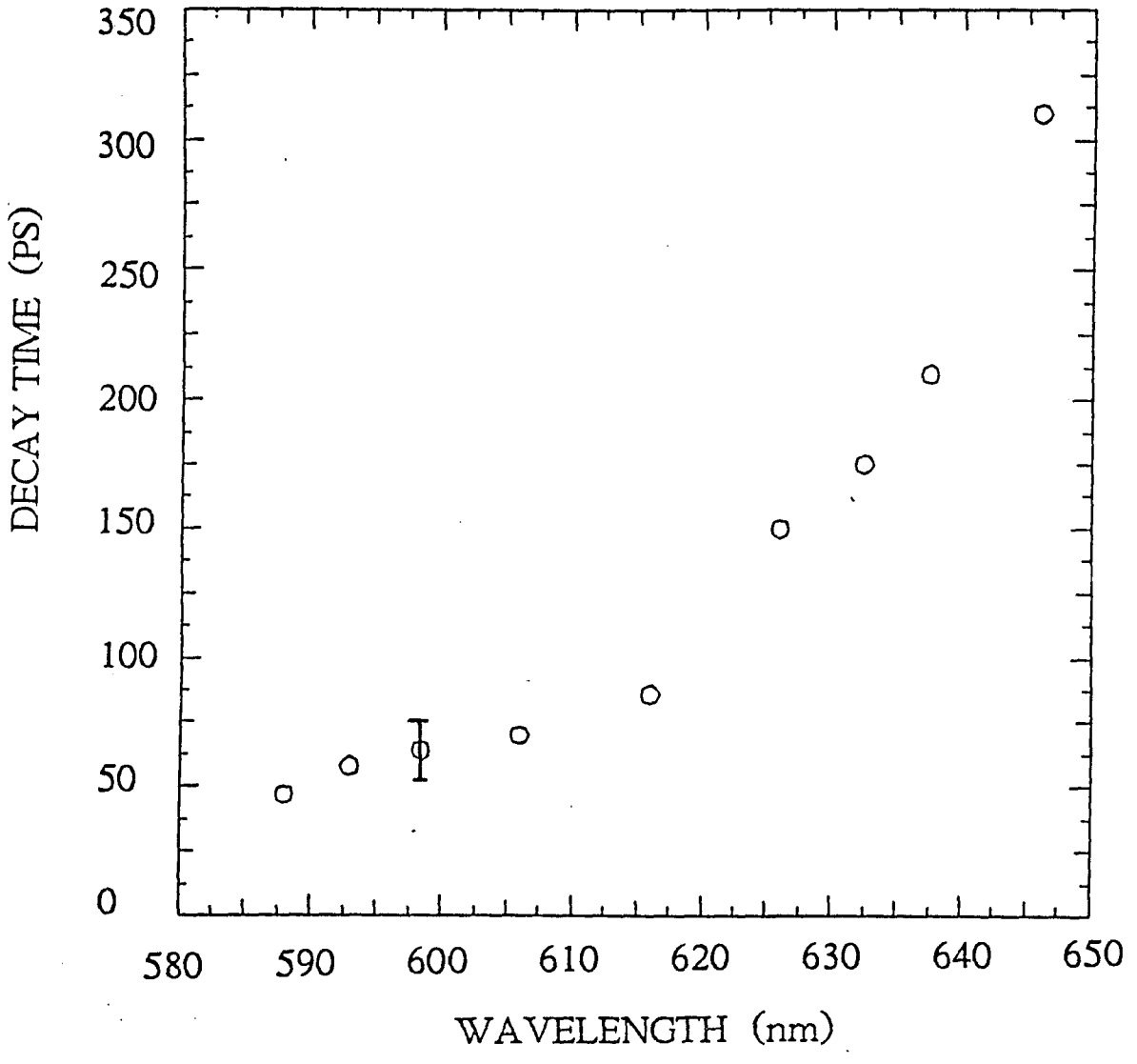

Fig. 4 . 3 . 3 Plot of the decay time of the time resolved photoluminescence profiles as a function of the energy .

time we have plotted N(E,t) versus E to obtain the photoluminescence spectra at different times . Figure 4 . 3 . 4 shows the photoluminescence spectra at t=0 , 25 , 50 , 100 , 150 , and 200 ps . The circles are the experimental results and the solid lines are the theoretical line shapes assuming direct transitions of the carriers with k conservation . Theoretical fitting will be discussed in the next section . The photoluminescence spectrum at t=0 ps (Fig. 4 . 3 . 4 - a) is very broad with FHWM of $\sim$ 200 mev . At longer times the spectra become narrower and the maximum shifts to lower energies . The slope of the high energy tail becomes steeper reflecting the cooling of the carriers . At t=200 ps (Fig. 4 . 3 . 4 f) the peak of the spectrum is around 635 nm with FHWM of $\sim$ 100 mev . The decrease in the FHWM of the spectra with time is due to the reduction of the photogenerated carrier density by recombination and possibly plasma expansion[10] . Comparing the spectra at t=0 ps and t=200 ps shows that the intensity of the photoluminescence around the band edge (645 nm) increased with time .

4 . 4 Recombination Models

In order to obtain information about the carrier density and carrier temperature a line shape analysis of the photoluminescence spectra is necessary . There are various recombination channels in a photoexcited semiconductor . At low temperatures one has to consider the possibility of recombination due to different sources like exciton recombination , intrinsic emission , donor to valence band (D-B) , conduction band to acceptor (B-A) and donor to acceptor (D-A) . Depend upon the experimental condition of temperature or excitation power fluence one can eliminate some of the above recombination models . For example , at room temperature where the thermal energy of carriers (kT = 25 mev) is larger than the exciton binding energy (typically 5-7 mev) , it is very unlikely to observe the photoluminescence due to excitons . Also at high carrier densities achievable by picosecond laser pulse , the exciton state becomes

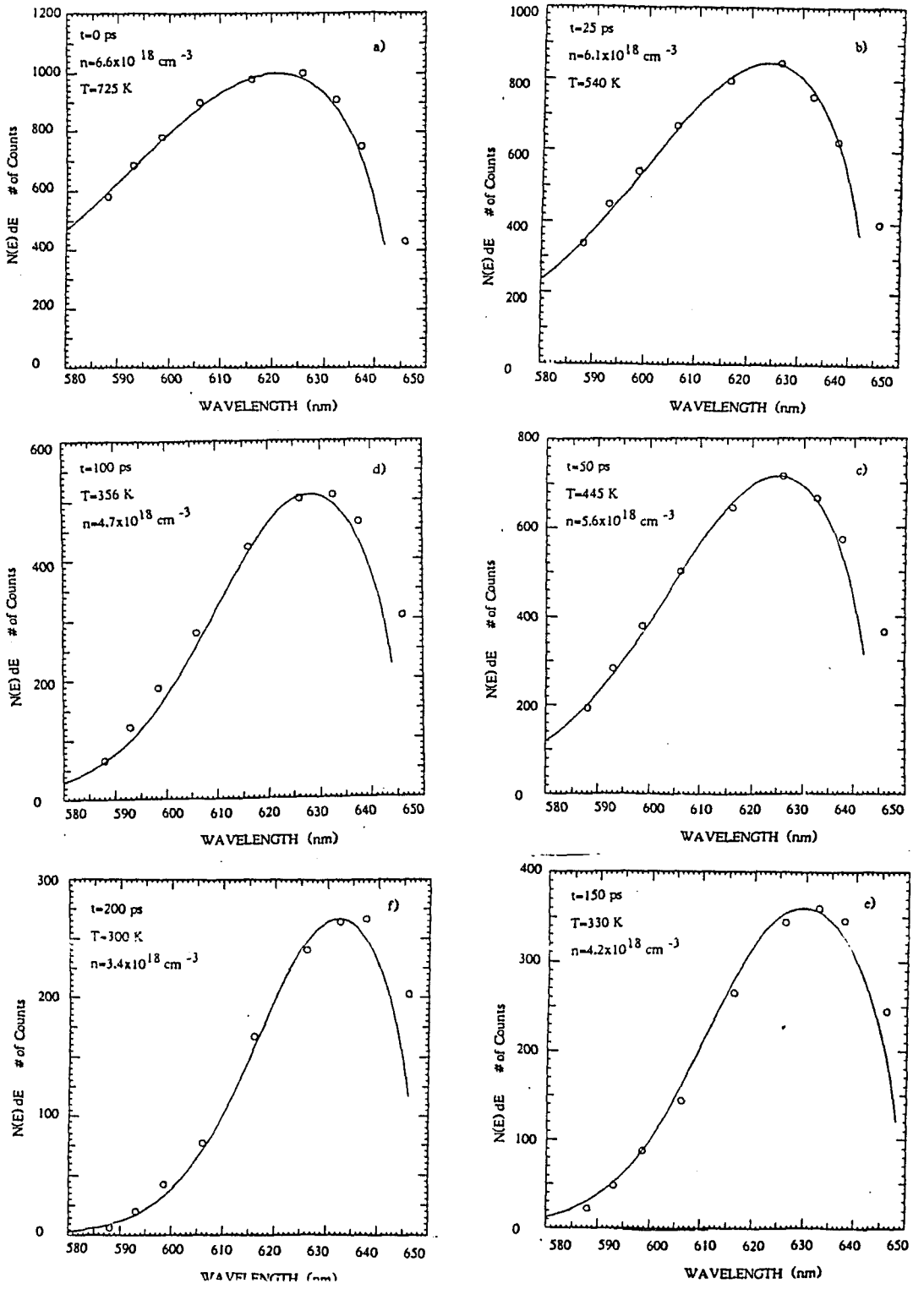

Fig . 4 . 3 . 4 The photoluminescence spectra of $Ga_{.56}In_{.44}P$ at t = 0 , 25 , 50 , 100 , 150 and 200 ps following the exciting laser pulse .

unstable due to the screening of the Coloumb interaction . Furthermore , the density of photogenerated carriers exceeds the impurity concentration , therefore the recombination is most likely arises from band to band recombination of e-h plasma . In this case , the electrons in conduction band can recombine with holes in the valence bands either by direct (k-selection) or indirect transition (non-k-selection) .

For a direct transition , the spontaneous emission intensity at photon energy $\hbar\omega$ can be written as

$$I(\hbar\omega) \sim \sum_{\vec{k}} \sum_{k\vec{}} |M(\vec{k_e}, k_{\vec{h}})|^2 f_e(\vec{k_e}) f_h(\vec{k_h}) \delta(\vec{k_e} - \vec{k_h}) \delta(\hbar\omega - E_g - E_e^{\vec{k_e}} - E_h^{\vec{k_h}}) \quad (4.4.1)$$

where $\hbar\vec{k_e}$ and $\hbar\vec{k_h}$ are the momenta of electrons and holes , $M(\vec{k_e}, k_{\vec{h}})$ is the transition matrix , $f_e(\vec{k_e})$ and $f_h(\vec{k_h})$ are the probability of occupation of electrons and holes , E_g is the band gap , $E_e^{\vec{k_e}}$ and $E_h^{\vec{k_h}}$ are the kinetic energy of electron and holes .

In order to obtain an analytical expression for the spontaneous emission intensity at photon energy $\hbar\omega$ the summation in Eq. 4 . 4 . 1 is converted to integral in k space and we have

$$I(\hbar\omega) \sim \int \frac{d^3k_e}{2\pi^3} \int \frac{d^3k_h}{2\pi^3} |M|^2 f_e(k_e) f_h(k_h) \delta(k_e - k_h) \delta(\hbar\omega - E_g - E_e^{k_e} - E_h^{k_h}) \quad (4.4.2)$$

where in direct transition we have $k_e = k_h$. After performing the first integral we obtain

$$I(\hbar\omega) \sim \int \frac{d^3k}{2\pi^3} |M|^2 f_e(\epsilon^{e_k}) f_h(\epsilon^{h_k}) \delta(k_e - k_h) \delta(\hbar\omega - E_g - \epsilon_k^e - \epsilon_k^h) \quad (4.4.3)$$

Further simplification of Eq. 4 . 4 . 3 can be obtained by considering $\epsilon_k^e = \frac{\hbar^2 k^2}{2m_e}$, $\epsilon_k^h = \frac{\hbar^2 k^2}{2m_h}$ and thier sum can be written as

$$\epsilon_k^e + \epsilon_k^h = \frac{\hbar^2 k^2}{2}\left(\frac{1}{m_e} + \frac{1}{m_h}\right) = \frac{\hbar^2 k^2}{2\mu} = \epsilon_k \quad (4.4.4)$$

where μ is the reduced mass of electron and holes . Therefore , Eq. 4 . 4 . 4 can be written as

$$I(\hbar\omega) \sim \int \frac{d^2k}{(2\pi)^2} \int \frac{d\Omega_s}{(2\pi)} \mid M \mid^2 f_e(\epsilon^{e_k}) f_h(\epsilon^{h_k}) \delta(k_e - k_h) \delta(\hbar\omega - E_g - \epsilon_k^e - \epsilon_k^h) \tag{4.4.5}$$

After substitution of $k^2 = (\frac{2\mu}{\hbar^2})\epsilon_k$ and $dk = (\frac{\mu}{2\hbar^2})^{\frac{1}{2}} \epsilon_k^{-\frac{1}{2}} d\epsilon_k$ in Eq. 4 . 4 . 5 and assuming the transition matrix is independent of energy we can write

$$I(\hbar\omega) \sim (\hbar\omega - E_g)^{\frac{1}{2}} f_e(\frac{m_h}{m_e + m_h}(\hbar\omega - E_g), F_e) f_h(\frac{m_e}{m_e + m_h}(\hbar\omega - E_g), F_h) \tag{4.4.6}$$

where $f(x, y)$ is the Fermi Dirac distribution function is given by

$$f(x, y) = \left\{ 1 + e^{\frac{x-y}{kT}} \right\}^{-1} \tag{4.4.7}$$

In the case of low carrier densities where Maxwell distribution applies , the Eq. 4 . 4 . 6 can be written as

$$I(\hbar\omega) \sim (\hbar\omega - E_g)^{\frac{1}{2}} \exp\left\{ -\frac{\hbar\omega - E_g}{kT} \right\} \tag{4.4.8}$$

The peak energy of photoluminescence described by Eq. 4 . 4 . 8 is at $\hbar\omega_{max} = E_g + \frac{1}{2}kT$ and its FHWM is about 1.8 kT . At low carrier densities , the carrier temperature can be extracted from the shape of high energy tail of the photoluminescence spectra . This is done by plotting the intensity of photoluminescence vs. photon energy on a semilog paper . The result is a straight line and the slope of this line would be $-\frac{1}{kT}$. This method has been used by Shah at el.[11] to study the effect of pumping intensity on the carrier temperature .

For an indirect band to band transition (non-k-selection) one can go through similar derivation and after some algebra , the spontaneous emission intensity at

photon energy $\hbar\omega$ in a semiconductor with band gap E_g for non-k-selection rule can be written as[12]

$$I(\hbar\omega) \sim \int_0^{\hbar\omega - E_g} E'^{\frac{1}{2}} (\hbar\omega - E_g - E')^{\frac{1}{2}} \left\{1 + e^{\frac{E' - F_e}{kT}}\right\}^{-1} \left\{1 + e^{\frac{\hbar\omega - E_g - E'}{kT}}\right\}^{-1} \qquad (4.4.8)$$

Again in the limit of low excitation power where Maxwell Boltzmann statistics can be applied , Eq. 4 . 4 . 8 simplifies to

$$I(\hbar\omega) \sim (\hbar\omega - E_g)^2 \; e^{\frac{-(\hbar\omega - E_g)}{kT}} \qquad (4.4.9)$$

The peak of the photoluminescence spectra described by Eq. 4 . 4 . 9 is at $\hbar\omega_{max} = E_g + 2kT$ and its FHWM is 3.4 KT .

In order to see the difference between the shapes of the photoluminescence spectra of direct and indirect transitions , the theoretically calculated spectra in $Ga_{.5}In_{.5}P$ at room temperature for $n = 1\times10^{18}$ and $5\times10^{18}\ cm^{-3}$ is shown in Fig. 4 . 4 . 1 and Fig. 4 . 4 . 2 , respectively .

4 . 5 THEORETICAL FITTING

In order to determine the carrier temperature and photogenerated carrier density at different times the photoluminescence spectra of Fig. 4 . 3 . 2 were fitted to the theoretical expression of line shape assuming direct transitions . The photoluminescence spectra neglecting the effect of the reabsorption of the emitted photons through the epilayer can be described by [13]

$$N(E)dE \sim E^2 (E - \hat{E}_g)^{\frac{1}{2}} f_e \left\{\frac{m_e}{m_e + m_h}(E - \hat{E}_g), \mu_e\right\} f_h \left\{\frac{m_h}{m_h + m_e}(E - \hat{E}_g), \mu_h\right\} dE \qquad (4.5.1)$$

where $N(E)dE$ is the number of photons detected within energy dE of energy E , $\hat{E}_g$ is the reduced band gap , f_e and f_h are the electron and hole occupation probabilities which is given by

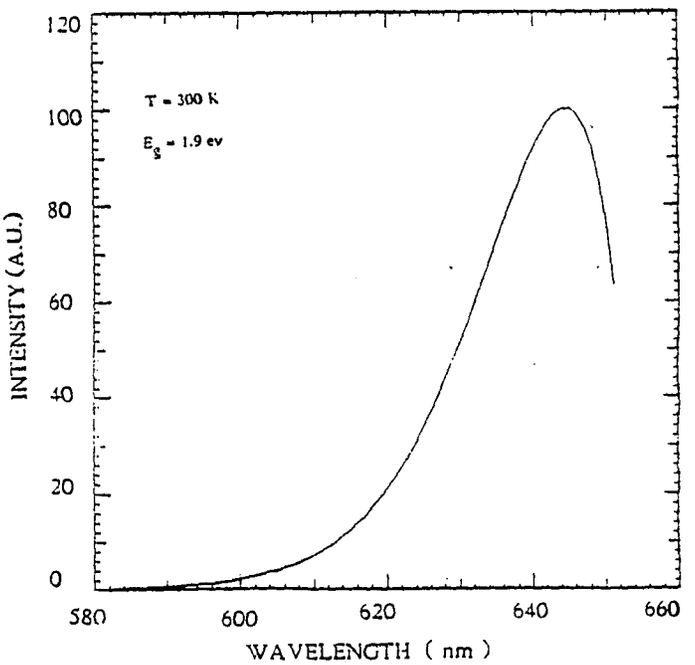

Fig. 4 . 4 . 1 (a) - The calculated photoluminescence spectra in $Ga_{.56}In_{.44}P$ at RT for carrier density of 1×10^{18} for the case of direct transition (k-selection rule) .

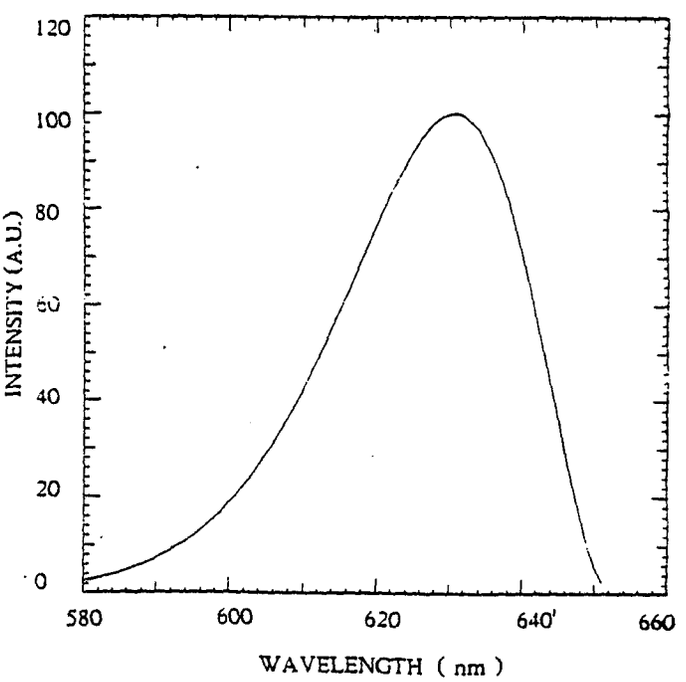

(b) - The calculated photoluminescence spectra in $Ga_{.56}In_{.44}P$ at RT for carrier density of $1\times10^{18}cm^{-3}$ for the case of indirect transition (non-k-selection rule) .

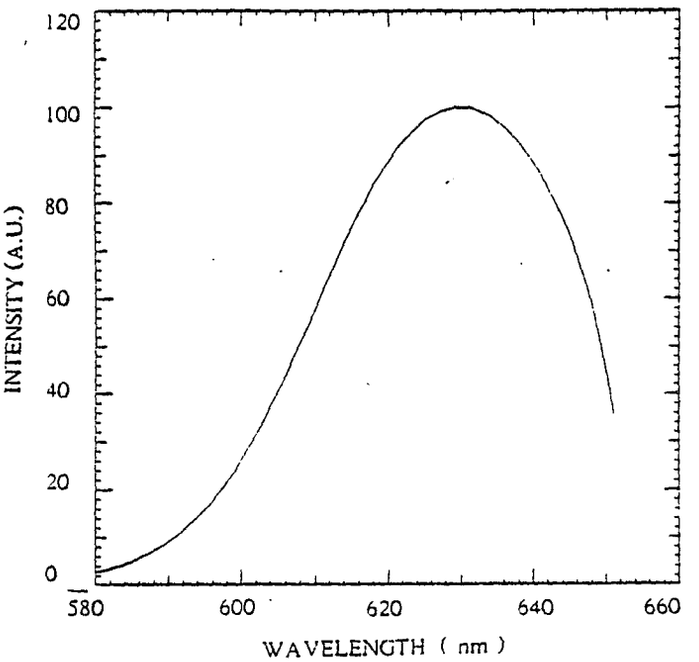

Fig. 4 . 4 . 2 (a) - The calculated photoluminescence spectra in $Ga_{.56}In_{.5}P$ at RT for carrier density of $5\times10^{18}cm^{-3}$ for the case of direct transition (k selection rule).

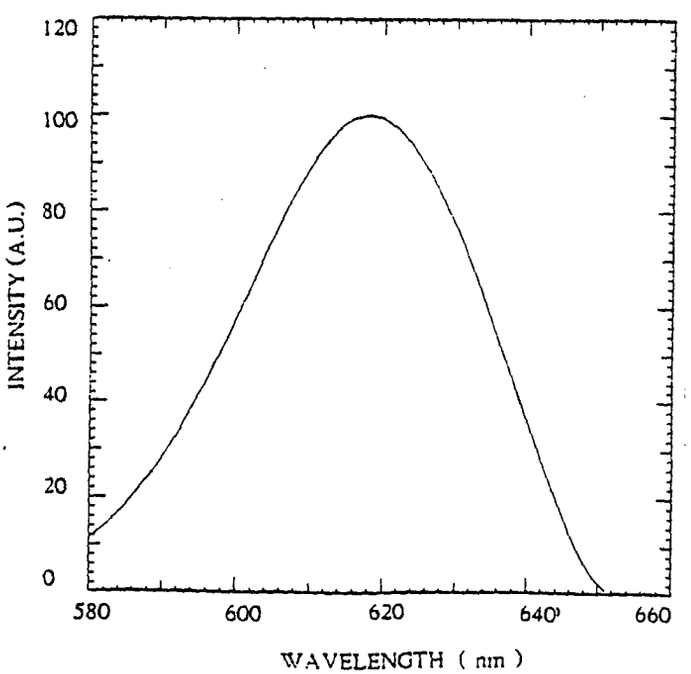

(b) - The calculated photoluminescence spectra in $Ga_{.56}In_{.44}P$ at RT for carrier density of $5\times10^{18}cm^{-3}$ in the case of indirect transition (non-k-selection rule).

$$f_i(\epsilon\ ,\ \mu_i)=\left\{1+\frac{(\epsilon-\mu_i)}{kT_i}\right\}^{-1} \qquad \text{for } i=e\ ,h \tag{4.5.2}$$

where T_i is the carrier temperature . In Eq. (4 . 5 . 1) the recombination matrix element is assumed to be independent of the carrier energy .

The carrier density for a degenerate distribution is given by

$$n=N_c F_{1/2}(\eta_i) \qquad \text{for } i=e\ ,h \tag{4.5.3}$$

where $N_c=2(\frac{2\pi m_i^* kT_i}{h^2})^{\frac{3}{2}}$ and $\eta_i=\frac{\mu_i}{kT_i}$. The $F_{1/2}(\eta_i)$ is the Fermi integral and is given by [14]

$$F_j(\eta_i)=\frac{1}{\Gamma(j+1)}\int_0^\infty \frac{x^j}{1+\exp(x-\eta_i)}\,dx \qquad . \tag{4.5.4}$$

Since μ_e and μ_h are related to carrier temperature by equation (3) through the Fermi integral we used the approximate analytical expression for η given by [15]

$$\eta=\ln(\frac{n}{N_c})+.353(\frac{n}{N_c})-4.95\times10^{-3}(\frac{n}{N_c})^2+1.48\times10^{-4}(\frac{n}{N_c})^3-4.42\times10^{-6}(\frac{n}{N_c})^4+\ldots\ldots \tag{4.5.5}$$

for simplifying the fitting procedure . The equation (4 . 5 . 5) is accurate at low carrier densities $(\frac{n}{N_c})\leqslant 1$ and at high carrier densities $(\frac{n}{N_c})\sim 15$ there is less than 5 % error in calculation of Fermi levels . To determine the carrier density (n) , reduced band gap $\hat{E}_g$ and carrier temperature (T_c) we have fitted the time resolved photoluminescence spectra to Eq. (4 . 5 . 1) assuming electrons and holes have the same temperature . At t= 200 ps (Fig. 4 . 3 . 1f) the carrier temperature was assumed to be the same as room temperature namely , T_c= 300 K and $\hat{E}_g$ and n were treated as parameters to obtain the best fit between the experimental photoluminescence spectrum and the theoretical line shape given by equation (4 . 5 . 1) . The best fit was obtained when E_g=1.913 ev and n = $3.4\times10^{18}\ cm^{-3}$. The reduced band gap obtained from the fitting of the spec-

trum at t= 200 ps is lower than the band gap by ~ 10 mev as a result of band gap renormalization at high carrier densities[16,17]. The fact that we assumed that the carriers are in thermal equilibrium with the lattice at t=200 ps is justified by the fact that the carrier temperature drops at the rate of ~ 1000 K/ps assuming a Maxwell Boltzmann distribution function[18]. For the rest of the photoluminescence spectra we used the value of $\hat{E}$=1.913 ev as a fixed parameter and carrier temperature (T_c) and carrier density (n) as dynamical variables . The best fit of the experimental data of Fig.4.3.4 to Eq. 4.5.1 was when n=6.6×10$^{18}cm^{-3}$, T_c = 725 K for t= 0 ps spectra (Fig. 4 . 3 . 4 a) ; n=6.1×10$^{18}cm^{-3}$, T_c=540 K for t= 25 ps (Fig. 4 . 3 . 4 b) ; n =5.6×10$^{18}cm^{-3}$, T_c =445 K for t= 50 ps spectra (Fig. 4 . 3 . 4 c) ; n =4.7×10$^{18}cm^{-3}$, T_c=325 K for t=100 ps spectra (Fig. 4 . 3 . 4 d) ; n =4.2×10$^{18}cm^{-3}$, T_c=310 K for t= 150 ps spectra (Fig. 4 . 3 . 4 e) and n =3.4×10$^{18}cm^{-3}$ and T_c= 300 K for t=200 ps spectra (Fig. 4 . 3 . 4 f) . The theoretical fits are shown by solid line in Fig. 4.3.2 . The main objective of the fitting was to obtain the best fit on the high energy side of the photoluminescence spectra where the effect of the band gap renormalization and band filling is not important . The time dependence of the photogenerated carrier density as determined from the fitting is plotted in Fig. 4 . 5 . 1 . The experimental points of Fig. 4 . 5 . 1 were fitted to the equation

$$n(t) = n(0) \exp(-\frac{t}{\tau}) \qquad (4.3.6)$$

where τ is the time were the carrier density drops to $\frac{1}{e}$ of its initial value . The best fit was obtained when τ=290±10 ps . Note that this value is very close to the decay time of the time resolved profile near the band edge (see Fig. 4 . 3 . 1f) . The carrier temperature obtained from the fitting of the time resolved photoluminescence spetra is plotted in Fig. 4 . 5 . 2 as a function of time by circles . The dot-dot curve is the theoretically calculated curve assuming M . B . distribution , the dot-dash curve is calculated for F . D . distribution function and solid line is calculated when the effects of

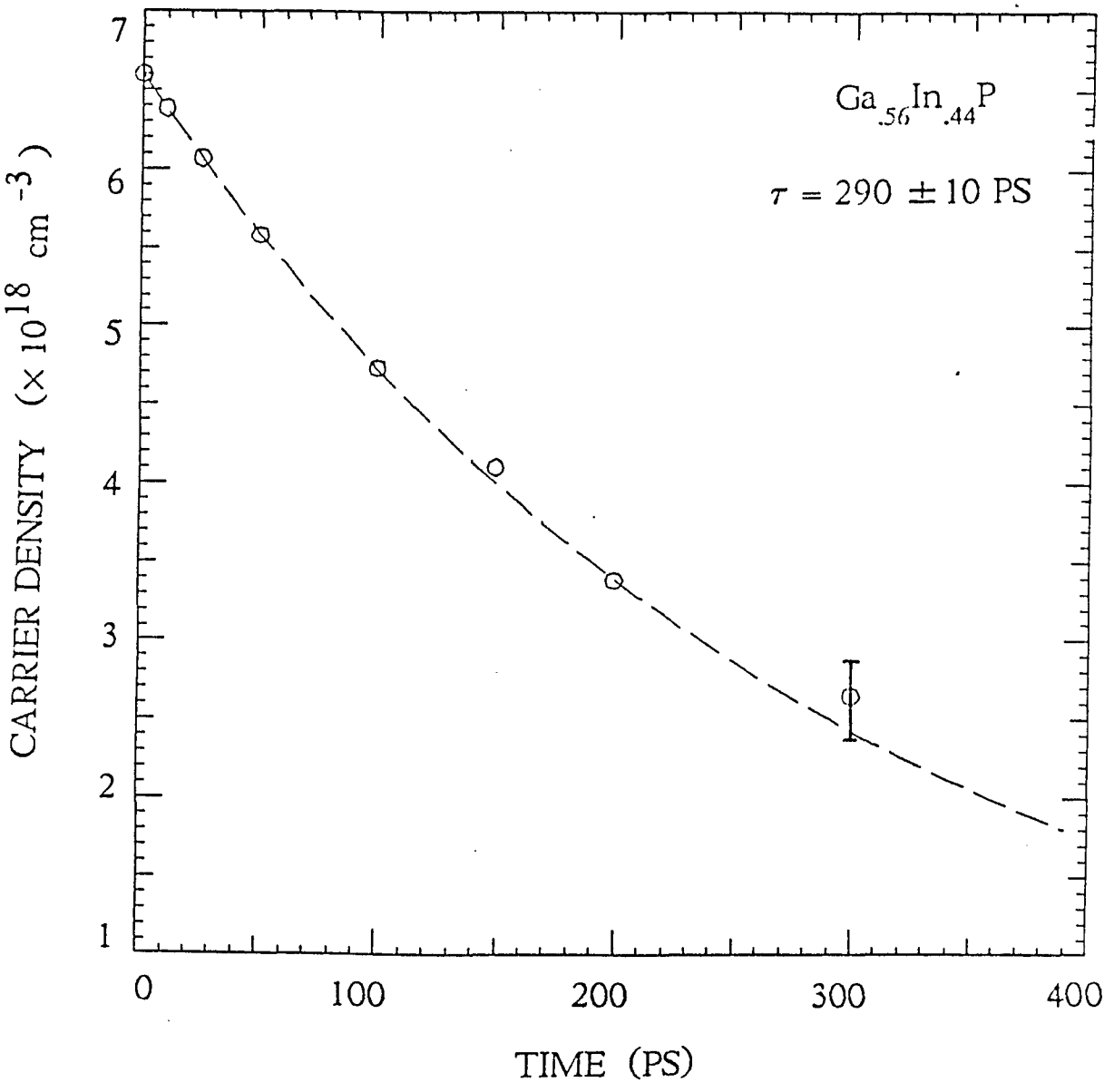

Fig. 4 .5 . 1 The plot of the photogenerated carrier density vs. time . The circles are the experimental points and dashed line is a fit assuming exponential decay .

screening of hot carriers has been taken into account . The calculation of these curves will be discussed in the next section .

4 . 6 . DISCUSSION

Excitation of $Ga_{.56}In_{.44}P$ (E_g =1.903 ev) by a 527 nm (2.34 ev) picosecond laser pulse creates electrons with initial energy of $\frac{m_h}{m_e+m_h}(h\nu_L - E_g)$=.35 ev in the conduction band and holes with excess energy of $\frac{m_e}{m_e+m_h}(h\nu_L - E_g)$=.09 ev in the valence band . The photogenerated carriers lose their energy by interaction with LO phonons as long as their temperature is above 40 K . The average rate of energy loss due to carrier LO phonon interaction for a Maxwell Boltzmann distribution is given by[18]

$$<\frac{d\epsilon}{dt}>=-P_0\left[\frac{e^{x_0-x_c}-1}{e^{x_0}-1}\right]\left[\frac{(\frac{x_c}{2})^{\frac{1}{2}}e^{\frac{x_c}{2}}K_0(\frac{x_c}{2})}{\sqrt{\pi/2}}\right] \qquad (4.6.1)$$

where P_0 is a parameter independent of carrier temperature and is given by

$$P_0 = 3.54\times10^{11}\left[\hbar\omega_{LO}(mev)\right]^{\frac{3}{2}}(\frac{m_e^*}{m})^{\frac{1}{2}}\left[\frac{1}{\epsilon_\infty}-\frac{1}{\epsilon_s}\right] \quad \frac{ev}{sec} \qquad (4.6.2)$$

In equation (4 . 6 . 1) $x_0=\frac{\hbar\omega_{LO}}{kT_L}$, $x_c=\frac{\hbar\omega_{LO}}{kT_c}$ and $K_0(x)$ is the modified Bessel function of zero order and the rest of the parameters have their usual meanings . Since electrons in conduction bands are Fermi gas , the average energy $<\epsilon>$ of electrons is $\frac{3}{2}kT_c$ assuming the electrons can be described by M . B . distribution function . Therefore the left hand side of equation (4 . 6 . 1) may be replaced with $\frac{3}{2}k\frac{dT_c}{dt}$ to obtain the differential equation describing the time evolution of carrier temperature . For $Ga_{.56}In_{.44}P$ this equation simplifies to

$$\frac{dT_c}{dt} = -8\times10^3 \left[\frac{e^{x_0-x_c}-1}{e^{x_0}-1} \right] \left[\frac{(\frac{x_c}{2})^{\frac{1}{2}} e^{\frac{x_c}{2}} K_0(\frac{x_c}{2})}{\sqrt{\pi/2}} \right] \frac{K}{ps} \qquad (4.6.3)$$

To determine T_c vs t from Eq. (4 . 6 . 3) we used the value of m_c=.094 for electron effective mass [19] , ϵ_∞=11.6 ,ϵ_s=9.1 and 48 mev for the LO phonon energy[20]. The Eq. (4 . 6 . 3) has been solved numerically by computer to obtain the time dependence of the carrier temperature . This is shown in Fig. 4 . 5 . 2 by a dot-dash curve and it shows that in the case of a Maxwell Boltzmann distribution ($\eta < 0$) the carriers are thermalized with the lattice temperature in less than 1 ps for the initial temperature of 725 K . In $Ga_{.56}In_{.44}P$ the distribution of electrons is degenerate when $n > 3.5\times10^{17} cm^{-3}$ and one has to consider the Fermi Dirac distribution function . The cooling rate in the case of F . D . distribution is calculated by Bauer and Kahlert and is given by[21]

$$\langle \frac{d\epsilon}{dt} \rangle = -P_0 x_c^{\frac{1}{2}} (\frac{2}{\sqrt{\pi}}) \frac{1}{F_{1/2}(\eta)} \left\{ N_q \int_0^\infty f(\epsilon) \left| 1-f(\epsilon+x_c) \right| \sinh^{-1}(\frac{\epsilon}{x_c})^{\frac{1}{2}} d\epsilon \right.$$

$$\left. - (N_q+1) \int_0^\infty f(\epsilon+x_c) \left| 1-f(\epsilon) \right| \sinh^{-1}(\frac{\epsilon}{x_c})^{\frac{1}{2}} d\epsilon \right\} \qquad (4.6.4)$$

where $N_q = \frac{1}{e^{\frac{\hbar\omega_{LO}}{kT}}-1}$ is the occupation probability of phonons . In the case of F . D . distribution the changes in carrier temperature is given by[22]

$$\frac{d\epsilon}{dt} = \frac{3}{2}k \left[\frac{\frac{5}{2}F_{\frac{3}{2}}(\eta)}{F_{\frac{1}{2}}(\eta)} - \frac{\frac{3}{2}F_{\frac{1}{2}}(\eta)}{F_{-\frac{1}{2}}(\eta)} \right] \frac{dT_c}{dt} \qquad (4.6.5)$$

where F_j is the Fermi integral of order j and $\eta = \frac{\mu_i}{kT}$. When ($\eta < 2$) the bracket in Eq. (11) is close to unity . The Eqs. (4 . 3 . 6) , (4 . 6 . 4) and (4 . 6 . 5) together give a complete description of the time evolution of carrier temperature in the case of a F . D

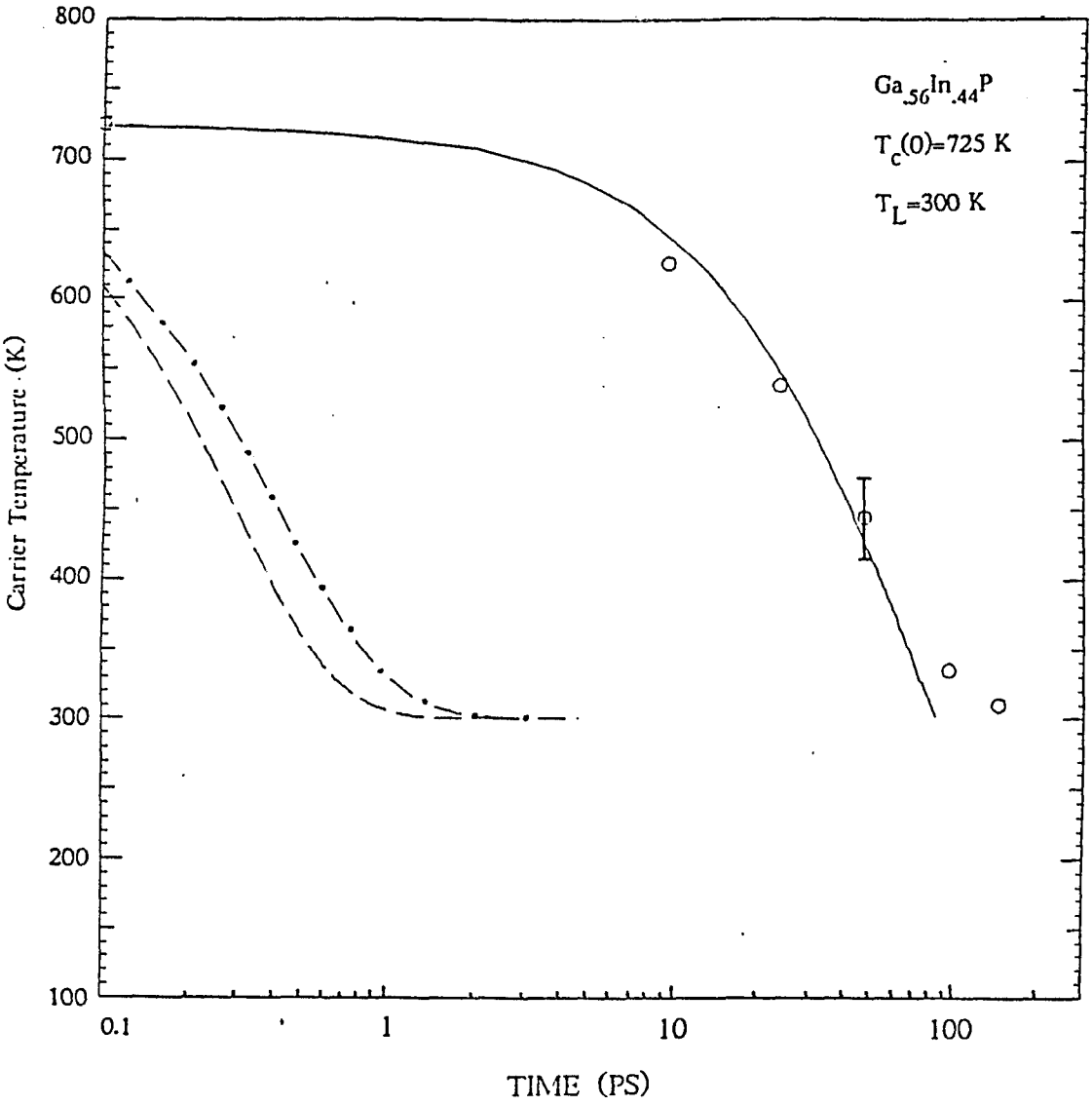

Fig. 4 . 5. 2 The time evolution of electron temperature in $Ga_{.56}In_{.44}P$. The circles are the experimental data , dash-dot curve is calculated for M.B. distribution function , broken curve is calculated for F.D. distribution and the solid curve is calculated in the presence of screening .

. distribution They have to be solved together to yield the time dependence of the carrier temperature . Note that carrier temperature and carrier density are both dynamical variables and change with time . The time evolution of carrier temperature in the case of the F . D . distribution is given by Eq. 4.6.5 and has been solved numerically assuming the initial carrier temperature to be 725 K . The result is shown in Fig. 4 . 5 . 2 by a broken line and it shows even in the case of a F . D . distribution the carriers are thermalized in less than 3 ps . The temperature of carriers determined from the fitting even at t= 50 ps is around 450 K and shows that the carriers are not thermalized with the lattice.

In order to calculate the changes in carrier temperature at high carrier densities one has to take into account the effect of the screening of the carriers . This topic has been discussed in detail in chapter 2 and here we only write the rate at which carriers lose thier energy .

The equation describing the rate of energy loss of carriers in the presence of screening is given by [23]

$$\frac{d\epsilon}{dt} = \frac{-m_e^* e^2(\omega_{LO})^2}{2\pi^2\bar{\epsilon}} \left[N_{LO}(T_c) - N_{LO}(T_L)\right] \int_0^\infty kdk \left| f\left(\frac{\epsilon_k}{kT_c}\right) - f\left(\frac{\epsilon_k + \hbar\omega_{LO}}{kT_c}\right) \right|$$

$$\left\{ \ln \left| \frac{\left(k + \sqrt{k^2 + 2m_e\omega_{LO}/\hbar}\right)^2 + Q^2}{\left(k - \sqrt{k^2 + 2m_e\omega_{LO}/\hbar}\right)^2 + Q^2} \right| - \frac{Q^2}{\left(k - \sqrt{k^2 + 2m_e\omega_{LO}/\hbar}\right)^2 + Q^2} \right.$$

$$\left. + \frac{Q^2}{\left(k + \sqrt{k^2 + 2m_e\omega_{LO}/\hbar}\right)^2 + Q^2} \right\} \qquad (4.6.6)$$

where $N(T_c) - N(T_L)$ is the difference in phonon occupation at the carrier temperature and lattice temperature and is equal to

$$N(T_c)-N(T_L)=\frac{1}{e^{\frac{\hbar\omega_{LO}}{kT_c}}-1}-\frac{1}{e^{\frac{\hbar\omega_{LO}}{kT_L}}-1} \tag{4.6.7}$$

where Q is the screening length and is given by[24]

$$Q=\left(\frac{32\pi e^2 n_e}{\epsilon_0 k_B T_c}\right)^{\frac{1}{2}} \tag{4.6.8}$$

In Eq. 4.6.4 , the value of $\bar{\epsilon}$ is given by

$$\frac{1}{\bar{\epsilon}}=\frac{1}{\epsilon_\infty}-\frac{1}{\epsilon_s} \tag{4.6.9}$$

where ϵ_∞ and ϵ_s are the optical and static dielectric constants and the rest of the parameters have been defined previously . The values of thses parameters are the same as the one we used in the case of F . D . distribution . At low carrier densities where screening is not important $Q \rightarrow 0$ and in addition the Maxwell Boltzmann statistics can apply the the electron distribution becomes

$$f\left(\frac{\epsilon_k}{kT_c}\right)=\exp\left(\eta_e-\frac{\epsilon_k}{kT_c}\right)=\frac{n_e}{2}\left(\frac{h^2}{2\pi m_e kT_c}\right)^{\frac{3}{2}}\exp\left(\frac{-\hbar^2k^2}{2m_e kT_c}\right) \tag{4.6.8}$$

Under these conditions , the integral in Eq. (4 . 6 . 6) can be worked out analytically to give the equation

$$\frac{d\epsilon}{dt}=n_e\left\langle\frac{d\epsilon}{dt}\right\rangle_{M.B.} \tag{4.6.9}$$

where $\left\langle\frac{d\epsilon}{dt}\right\rangle_{MB}$ is given by Eq. (4 . 6 . 1) . To obtain the time evolution of carrier temperature in the presence of screening we solved the Eq. (4 . 6 . 6) numerically considering the fact that carrier density is a dynamical variable and its time dependence is given by Eq. (4 . 3 . 6) . The result is shown in Fig. 4. 5 . 2 by solid line . The cooling curve fits the experimental data well for (t $<$ 50 ps) and at longer times there is some deviation . This curve shows that carriers with initial temperature of 725 $\pm$ 25 K lose their energy and reach the temperature of 325 $\pm$ 25 K in about 100 ps . One of the

reasons that the theoretically calculated cooling curve from theory is slightly off from the experimental data is the fact that one has to consider other factors such as energy loss to coupled plasmon phonon modes[25] , the population of nonequilibrium phonons[26] and plasma expansion due to Fermi pressure[27] .

4 . 7 CONCLUSION

In conclusion we have measured time resolved spectra of $Ga_{.56}In_{.44}P$ with 10 ps resolution . From the theoretical fitting of the photoluminescence spectra we have obtained the time dependence of the carrier temperature . The theoretical time dependence of carrier temperature in the presence of screening has been determined and compared with experimental data . It is found that the electron phonon interaction has been reduced as a result of the screening of the carriers. The rate at which carriers lose their energy has been reduced from 100 K / ps (in the case of F . D . distribution) to 4 K / ps (in the presence of screening) .

References

1- Semiconductors probed by Ultrafast Laser Spectroscopy , R . R . Alfano , Academic press , (1984) .

2- C . V . Shank , R . L . Fork , R . Yen , J . Shah , A . C . Gossard and C . Wiesbuch , Solid state Comm. , 47 , 981 , (1983) .

3- M . A . Duguay , J .W . Hansen , Appl. Phy. Lett. , 15 ,192 , (1969) .

4- H . Mahr , M . D . Hirsch , Opt. Comm. , 13 ,96 , (1975) .

5- R . J . Seymour , M . R . Junnarkar and R . R . Alfano ,Solid state Comm. , 41 , 657 , (1982) .

6- R . G . Ulbrich , Solid State Electron. , 21 , 51 , (1975) .

7- C . V . Shank , D . H . Auston ,E . P . Ippen and O . Teschke , Solid State Comm. , 26 , 567 , (1978) .

8- R . J . Nelson , N . Holonyak Jr. , J. Phy. Chem. Solids , 37 ,629 , (1976) .

9- P .Y . Lu , Z . X . Yu ,R .R . Alfano and J . I . Gersten ,Phy. Rev A26 ,3610 , (1982) .

10- S . Modesti , L . G . Quagliano and A . Frova ,J.Luminesc. , 24 ,581 , (1981) .

11- R . F . Leheny , J . Shah , R . L . Fork , C . V . Shank , A . Migus , Solid state Comm. 31 , 809 (1979) .

12 T . K . Lo , Solid State Comm. 15 , 1231 (1974) .

13- Van Driel , A . Elci , J . S . Bessey and M . O . Scully ,Solid State Comm. , 20 , 837 , (1976) .

14- Semiconductor Statistics , J . S . Blakemore , Pergamon Press , (1962) .

15- W . B . Joyce , R . W . Dixon , Appl. Phy. Lett. , 31 , 354 , (1977) .

16- W . F . Brinkman , T . M . Rice , Phy. Rev. B7 , 1508 , (1973) .

17- P .Vashista , R . K . Kalia ,Phy. Rev. , B25, 6492 , (1980) .

18- E . M . Conwell , High Field Transport in semiconductors , Academic Press , NewYork , (1967).

19- C .Alibert , G . Bordure , A . Laugier , J . Chevallier ,Phy. Rev. B6, 1301 ,(1972) .

20- S . Sugai , J . H . Harris , A . V . Nurmikko , Solid State Comm. , 43, 913 , (1982) .

21- G . Bauer , H .Kahlert , Phy. Rev. B7, 1508 , (1973) .

22- D .Von Der Linde , R . Lambrich , Phy. Rev. Lett., 42, 1090 , (1979) .

23- T . L . Koch , Ph.D. Thesis , California Institute of Technology , (1982) .

24- J . F . Young , H . M . van Driel ,Phys. Rev. B26 , 2147 (1982) .

25- K . Kash , J . Shah , App. Phy. Lett. 45, 401 , (1984) .

26- H M . Van Driel , Phy. Rev. B19, 5928 , (1979) .

27- E . M . Romanek , H . Nather , J . Fisher ,E . O . Gobel J. of Luminesc. , 24, 585 , (1981) .

CHAPTER 5

Time Resolved Kinetics of e - h plasma in GaAsP under Intense Picosecond Laser Pulse Excitation

5 . 1 Introduction

Information about carrier recombination rates are essential in the design and implementation of semiconductor lasers , light emitting diodes and electro-optical switches[1] . Over the past three decades a great deal of effort has been devoted to the understanding of radiative and nonradiative processes in semiconductors[2] . The reliability of photonic devices has to be tested under extreme operational conditions , and any deviation from linearity may limit their applications . Most of the problems encountered regarding nonlinearity has been attributed to loss mechanisms associated with the nonradiative Auger process . Therefore , it is important to determine the radiative and nonradiative recombination rates in semiconductors under high excitation power . There are a variety of direct and indirect techniques to measure or estimate recombination rates in semiconductors under current injection or laser pulse excitation . Conventional techniques such as turn on delay , phase shift and photons counting are limited to the nanosecond time scale[3,4] . In most of the experiments to date , semiconductors were excited under quasi stationary conditions where the exciting laser pulse duration was longer or comparable to the carrier lifetime . Since direct band gap semiconductors have inherently short radiative lifetime , radiative and nonradiative processes have to be studied by picosecond techniques such as pump and probe[5] , optical Kerr gate[6] , upconversion gate[7] and streak camera[8] .

In this chapter , the radiative and nonradiative processes involved in a photoexcited semiconductor particularly $GaAs_{1-x}P_x$ (x= .38) is investigated . Time resolved photoluminescence kinetics of $GaAs_{1-x}P_x$ were measured by streak camera in order to determine the radiative and nonradiative recombination rates . The photoluminescence decay profiles was found to be intensity dependent . When excitation power fluence increased to $6\times10^{8}W/cm^{2}$, the decay profile of emission deviated from an exponential form . This is attributed to bimolecular and Auger processes . The bimolecular and auger rates were determined to be $B_R=9\times10^{-10}cm3/s$ and $C_{NR}=(5\pm2)\times10^{-29}cm^{6}/s$ by fitting the time resolved photoluminescence decay profiles to the solution of rate equation which describes the dynamical behavior of the photogenerated carriers . Before embarking on the technical aspects of the experiment , the band structure of $GaAs_{1-x}P_x$ is discussed to give some background about the sample .

5 . 2 Band Structure of $GaAs_{1-x}P_x$

Because of its technological importance , GaAs is the most widely studied semiconductor . The band structure of this semiconductor has been thoroughly investigated by many groups and the band structure parameters have been determined both experimentally and theoretically[9,10] . The observation of stimulated emission in GaAs has led to the intense interest in the fabrication of junction lasers . Because of small band gap , the emission of GaAs lasers is in IR (.8 μm) region of spectrum . Limited tunability can be achieved in GaAs lasers by operating it at different temperature . In order to increase the tunability and makig visible junction lasers and light emitting diodes , $GaAs_{1-x}P_x$ alloy system can be fabricated from GaAs and GaP . In 1962 , Holonyak at el.[11] announced the first p-n junction laser in the visible part of the spectrum and after that a considerable amount of work was devoted by many groups to study the physical properties of this material . Following the work of Ehrenreich[12] , it is accepted that band structure of $GaAs_{1-x}P_x$ consists of a high

mobility , low effective mass conduction band at Γ point [000] in the Brillouin zone and six equivalent low mobility high effective mass conduction bands at X point [100] . Fig. 5.2.1 shows the schematic diagram of the band structure of $GaAs_{1-x}P_x$ [13] . As GaP is added to the system , the GaAs band edges (solid lines) sweep continuously through shaded area and approaches the GaP band edges (dashed lines) . The variation of the direct band gap with composition has been studied by many groups . Thompson at el.[14] used the Electro-reflectance technique to study the compositional dependence of direct band gap in $GaAs_{1-x}P_x$. He concluded that the variation of direct band gap with composition x can be written as

$$E_g(ev) = 1.424 + 1.150\,x + .176\,x^2 \qquad (5.2.1)$$

Fig. 5 . 2 . 2 shows the variation of the direct Γ and indirect X band gap with composition . The effective mass of electrons in Γ valley increases linearly with composition and roughly can be written as

$$m_e^* = .072\,(1 + x)\,m^*{}_0 \qquad (5.2.2)$$

Since this chapter deals with the dynamics of carriers at high excitation power ($\sim 3\times10^9 W/cm^2$) , we will discuss the process which is important at high carrier density , namely the Auger process . The Auger process is a third order reaction kinetics . In an Auger process , the energy released by the recombination of an electron-hole pair is transferred to a second electron or to a second hole , which the second carrier will be energetically lifted within the thier band or into another band . The Auger carriers dissipate this energy by emission of phonons . During the energy relaxation , a radiative recombination of these carriers with the thermalized carriers in the opposite band is possible . This leads to an extremely weak luminescence spectrum above the band gap . This has been observed in GaSb experimentally by Benz and Conradt[16] .

The Auger processes can be divided into conduction band or valence band

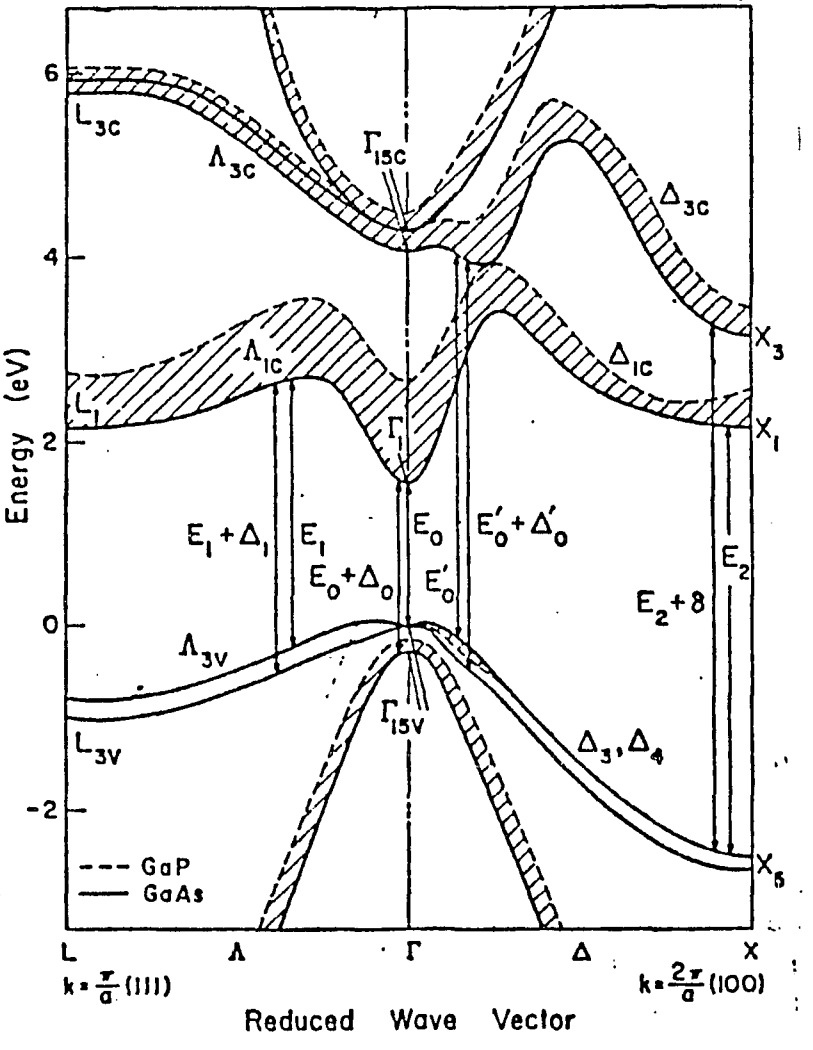

Fig. 5 . 2 . 1 Schematic diagram for the band structure of $GaAs_{1-x}P_x$ (Ref. 13) .

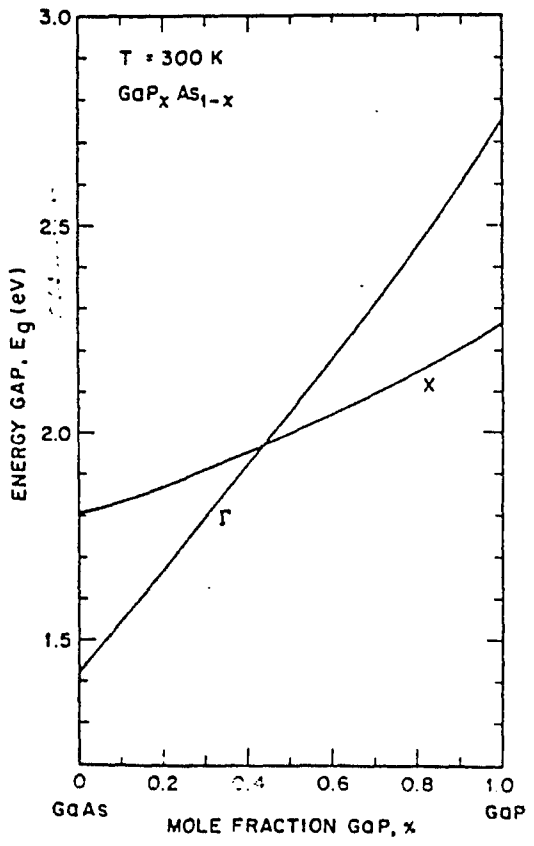

Fig. 5 . 2 . 2 The variation of the direct and indirect band gap in $GaAs_{1-x}P$ with composition (Ref. 14) .

processes . Fig. 5.2.3 shows schematic diagram for these processes .

In the CHCC Auger process , an electron and a hole recombine and the released energy is given to another electron in the conduction band which is then lifted to higher states . In the CHSH Auger process , the energy released by recombination of an electron-hole pair is given to a hole in the split off valence band which then will be lifted to the heavy valence band . Similarly , in the CHLH Auger process , the releaed energy resulting from the recombination of an electron-hole pair will lift a hole from the light hole valence band to the heavy valence band . In a semiconductor with the band gap E_g , and split off valence band separation of Δ , if $E_g \gg \Delta$, then the CHSH is dominante Auger process . For semiconductors where $E_g < \Delta$, the CHLH would be the dominant Auger process[17] .

5 . 3 Experimental Methods

The experimental set up used in this research has been described in detail elsewhere in chapter 2 . A 527 nm pulse of 8 pa duration was used to excite the sample of $GaAs_{1-x}P_x$ (x=.38) on the front surface. The sample was 30 μm thick, n type, Te doped ($\sim 2\times10^{17} cm^{-3}$) and grown by VPE on a GaAs substrate. The composition of sample was calculated by calibration of band gap vs composition [14]. The band gap of the sample was determined to be 1.892 ev at room temperature from the direct transition relationship $E_g = h\nu_p + E_d - 1/\ 2kT$ where $h\nu_p$ is the energy of the peak in the low power steady state photoluminescence spectra,E_d is the donor ionization energy ($\sim 5\ mev$) and 1/2 kT term accounts for the direct transition of the carrier. The photoluminescence was collected by a combination of lenses and imaged into a 30 μm slit of a Hamamatsu Streak Camera. The output was detected by a temporal analyzer and computer for data analysis. The time resolution of the detection system was approximately 10 ps . The excitation area was measured to be approximately $8\times10^{-3} cm^{-3}$ and excitation power fluence was varied by placing neutral

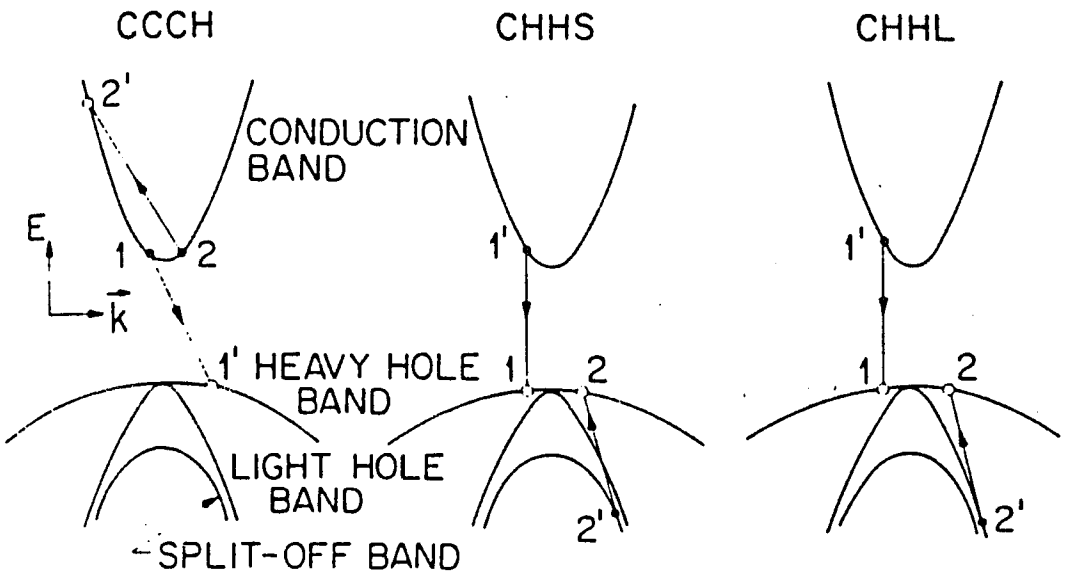

Fig. 5 . 2 . 3 The schematic diagram for three possible Auger precesses in semiconductors (Ref. 17) .

density filters in the path of the laser pulse.

5 . 4 Experimental Results

The time resolved photoluminescence profiles of $GaAs_{1-x}P_x$ (x=.38) at room temperature for different excitation power fluences are displayed in Fig. 5 . 4 . 1 . The solid curves are experimental data , the dashed lines are theoretical fit assuming a simple exponential decay and the circles are the theoretical fit to the model which includes the bimolecular and Auger rates . The salient features of the experimental curves shown in Fig. 5. 4 . 1 are the following . The rise time of photoluminescence did not change appreciably with excitation power fluence and was between 10 to 15 ps . The decay time of the emission decreased from 207 ps to 44 ps when excitation power fluence increased from3×10^{18} to $3\times10^{9}\ W/\ cm^2$. When excitation power fluence was below $6\times10^{8}\ W/\ cm^2$ the decay profile was exponential (see Fig. 5 . 4 . 1 a and 5 . 4 . 1 b) . As the excitation power fluence increased above $6\times10^{8}\ W/\ cm^2$the decay profile of the photoluminescence deviated from an exponential form . This was most apparent at the highest excitation power fluence of $3\times10\ ^{9}W/\ cm^2$ (see Fig 5 . 4 . 1 d) . An effective decay time $\tau_{eff}(n)$ defined as the time which photoluminescence intensity dropped to 1/e of its maximum value , were determined form the experimental time resolved profiles . The $\tau_{eff}(n)$ are plotted versus the excitation power fluence in Fig. 5 . 4 . 2. Each experimental point is the average of 3 to 4 shots . The scattering of data points around a given excitation power fluence was due to changes in the duration of the laser pulse and could not be controlled . Fig. 5 . 4 . 3 shows the maximum intensity of the time resolved photoluminescence profiles as a function of excitation power fluence . The instantaneous intensity of photoluminescence shown in Fig. 5 . 4 . 3 grew with excitation power fluence as $I_F\ \alpha\ P_L^{1\pm.05}$ when excitation power fluence was below $1.510^{9}\ W/\ cm^2$. When excitation power fluence increased beyond $1.6\times10^{9}W/\ cm^2$ there was some deviation from linearity . The

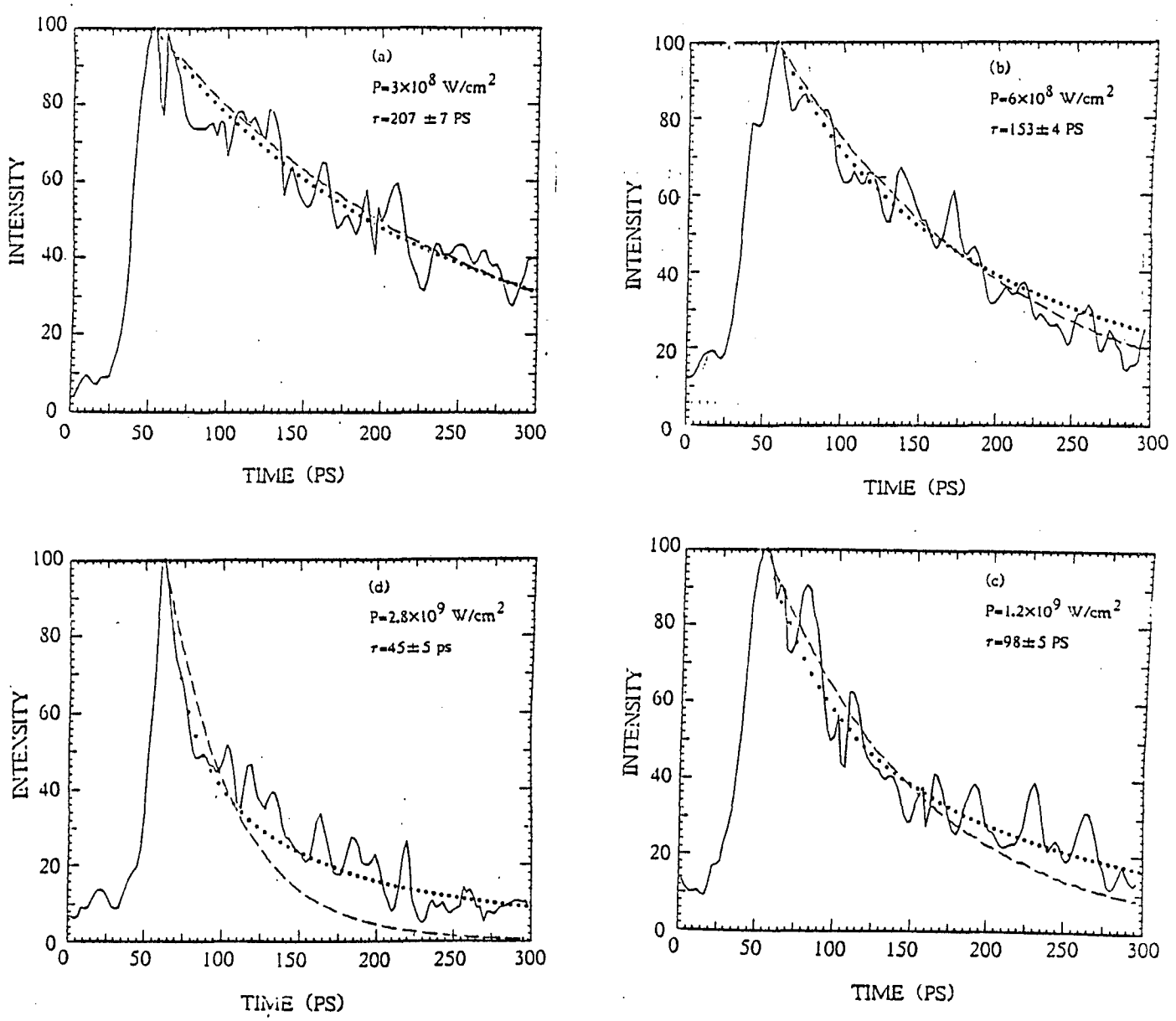

Fig. 5.4.1 (a)-(d) The time resolved photoluminescence profile of $GaAs_{1-x}P_x$ at room temperature for excitation power fluence of 3×10^8 , 6×10^8 , 1.2×10^9 and 2.8×10^9 W/cm^2.

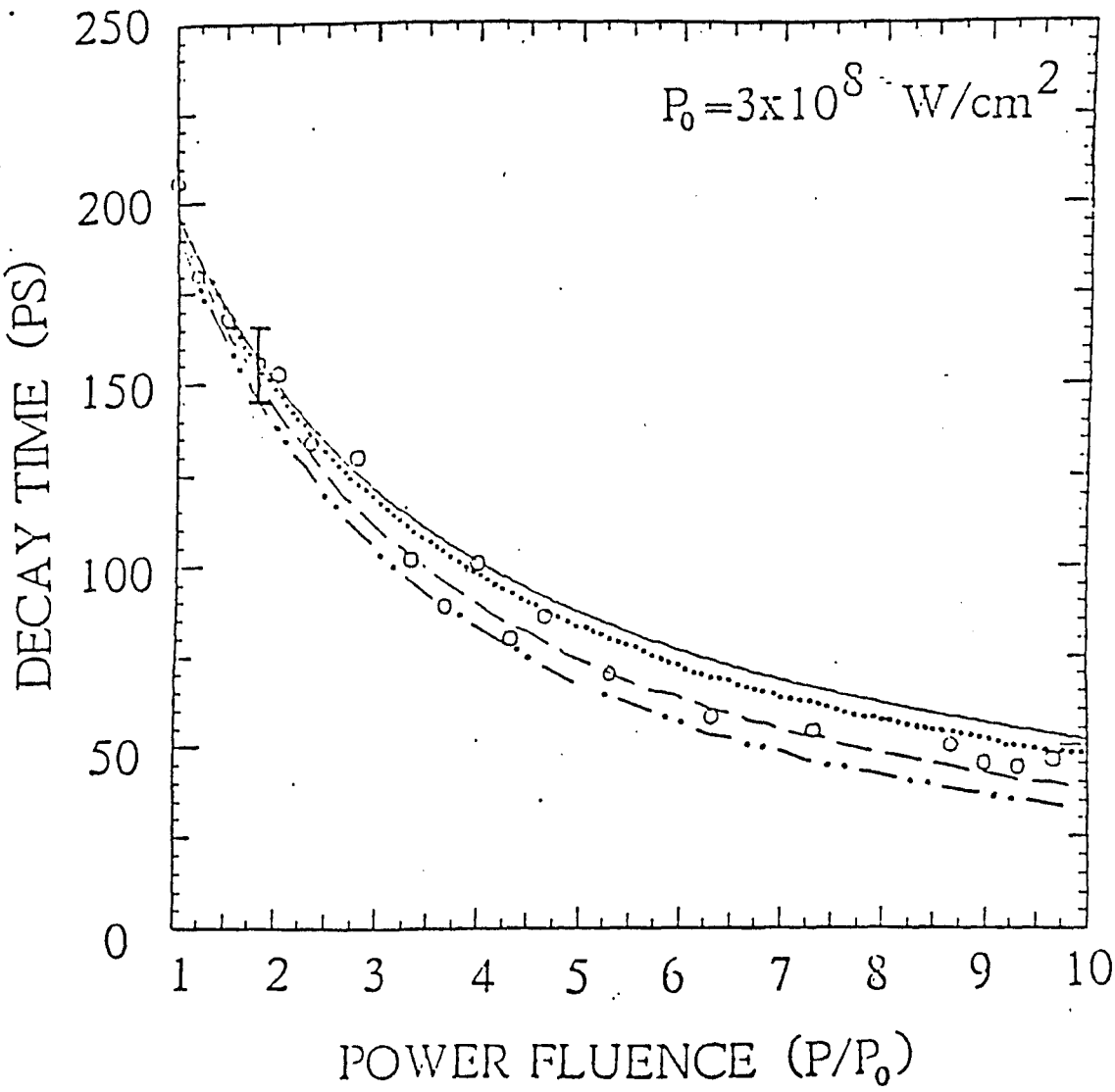

Fig. 5 . 4 . 2 The effective decay time $\tau_{eff}(n)$ vs. excitation power fluence . The circles are the experimental points , solid line is calculated from model (1) for $A=3.4\times10^9/s$, $B_R=9\times10^{-10}cm^3/s$ and dots , dashs , dot-dashs curves are calculated from model (2) for $C_{NR}=1.3.5\times10^{-29}cm^6/s$, respectively .

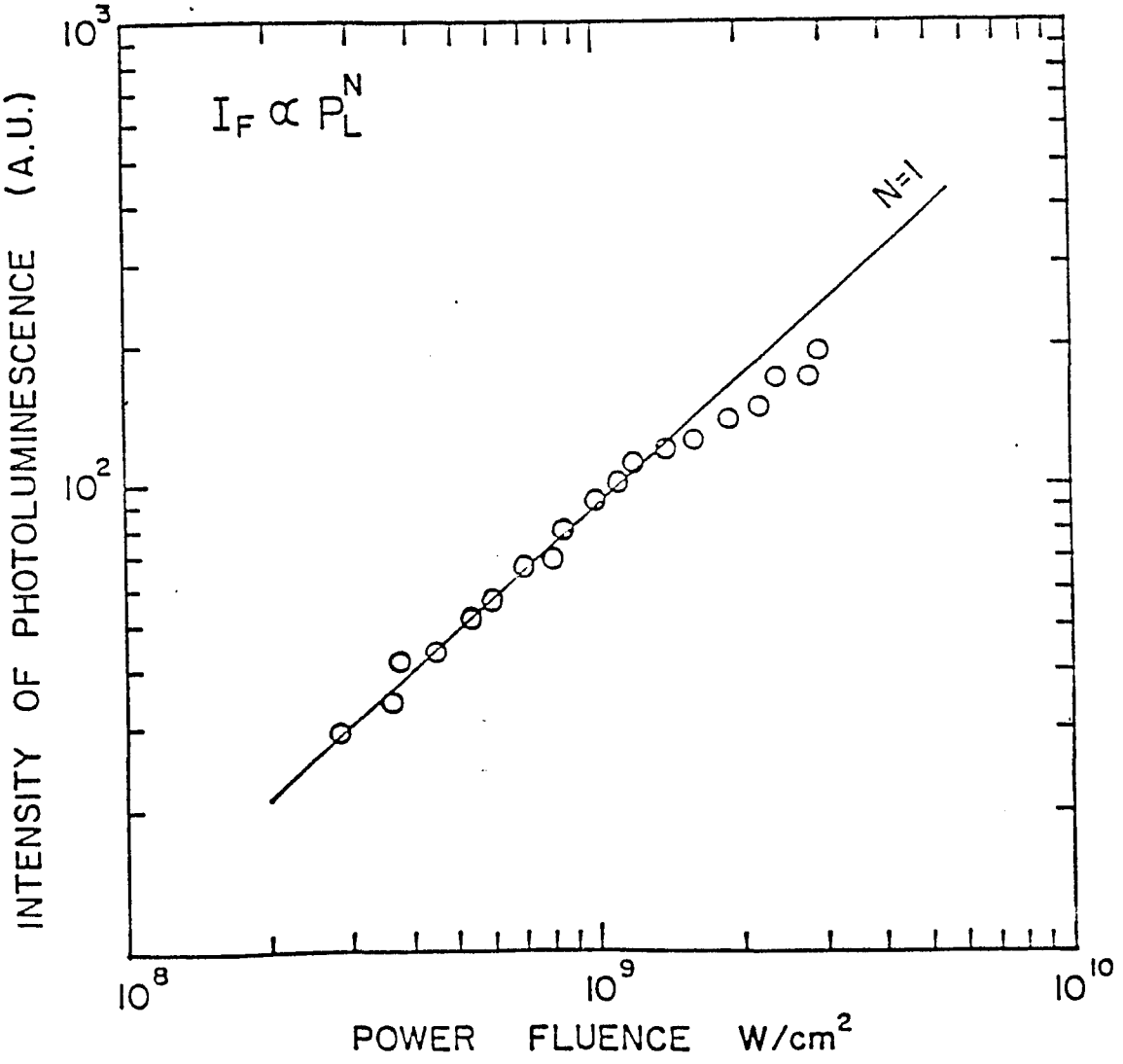

Fig. 5 . 4 . 3 The peak intensity of the time resolved photoluminescence profile in $GaAs_{.62}P_{.38}$ versus the excitation power fluence .

observed sublinearity of photoluminescence intensity may be attributed to loss mechanisms at high carrier densities most likely arising from nonradiative Auger process .

5 . 5 Recombination Models

To analyze and explain the changes observed in the decay profile of the time resolved photoluminescence of GaAsP at room temperature under different excitation power fluence the following two models for rate equations have been developed . In model 1, the rate equation describing the time dependence of photogenerated carriers is given by

$$\frac{dn}{dt} = g(t) - A_R\, n - A_{NR}\, n - B_R n^2 \qquad (5.4.1)$$

where g(t) is the generation term which depends on the actual pulse shape of the exciting laser, A_{NR} , A_R and B_R are nonradiative, radiative and bimolecular recombination coefficients independent of carrier density. The rate equation for the second model includes the Auger nonradiative rate is given by

$$\frac{dn}{dt} = g(t) - A_{NR}\, n - A_R\, n - B_R\, n^2 - C_{NR}\, n^3 \qquad (5.4.2)$$

where C_{NR} is the nonradiative Auger rate . At low excitation power fluence where the density of photogenerated carrier is low and ($A_R\, n + A_{NR}\, n + B_R\, n^2 \gg C_{NR}\, n^3$) the two models will approach each other in calculation of the decay time. The absence of any term representing the population of excitons is justified by the fact that at high carrier densities ($n > 5\times10^{17} cm^{-3}$) the exciton state becomes unstable due to the screening of Coloumb interaction [18]. The Mott transition in $GaAs_{1-x}P_x$ (x=.38) at room temperature from exciton state to plasma state occurs at carrier density of $3\times10^{17} cm^{-3}$. The photogenerated[19] carrier densities here are in the range of 3×10^{18} to $3\times10^{19} cm^{-3}$

Since we are concerned with the changes in the decay profile of the time resolved photoluminescence, we set g(t)=o for $t > t_r$ where t_r is the rise time of time resolved profiles. solution of model (1) becomes [19]

$$n(t) = \frac{A}{B_R} \frac{n(0)}{\left[\frac{A}{B_R} + n(0)\right] \exp(At) - n(0)} \tag{5.4.3}$$

where $A = A_R + A_{NR}$. The time for which the carrier density drops to 1/e of its initial value $\tau_{eff}(n)$ for the model (1) is given by

$$\tau_{eff} = \frac{1}{A} \ln \left[\frac{2.718 + B_R n(0)}{1 + \frac{B_R n(0)}{A}} \right] \tag{5.4.4}$$

In order to determine A and B_R the experimental data of Fig 5 . 4 . 2 were fitted to the equation (5 . 4 . 4) for excitation power fluence below $8\times10^8\ W/cm^2$. The best fit was obtained for $A = 3.4\times10^9 s^{-1}$ and $B_R = 9\times10^{-10} cm^3/s$. Modesti estimated the bimolecular recombination rate $GaAs_{1-x}P_x$ (x= .38) to be $3.6\times10^{-8} cm^3/s$ in terms of hydrodynamic expansion model [21]. This rate is 40 times larger than the rate we have determined. A simple calculation assuming only bimolecular recombination yields an estimate for lifetime ie, $\tau = \frac{1}{Bn}$. If we use the $B_R = 3.6\times10^{-8} cm^3/s$ and the lifetime of 98 ps measured by streak camera at $1.2\times10^9\ W/cm^{-2}$ we see that carrier density should be around $3\times10^{17} cm^{-3}$. This value is about 40 times smaller than the estimated carrier density of $1.3\times10^{19} cm^{-3}$ at P = $1.2\times10^9 W/cm^2$. Also the value of $B_R = 9\times10^{-10} cm^3/s$ determined by us is within an order of magnitude of the values reported for GaAlAs [22] and GaInAsP [23].

The radiative and nonradiative rates at low excitation power are related to the internal efficiency of a semiconductor by the relationship

$$\eta_{in} = \frac{\tau_{NR}}{\tau_{NR} + \tau_R} \tag{5.4.5}$$

assuming the internal efficiency is independent of the density of photogenerated carriers. The external efficiency of this sample was measured to be 2×10^{-4} by comparing the area under low power steady state photoluminescence spectra with GaInP [24]. Taking into account the geometry of the emission, a value of 7×10^{-2} was estimated for the internal efficiency of this sample [25]. Note the decay times measured by the streak camera are the photoluminescence lifetime and the relation between photoluminescence lifetime (τ), radiative (τ_R) and nonradiative time (τ_{NR}) is given by

$$\frac{1}{\tau} = \frac{1}{\tau_R} + \frac{1}{\tau_{NR}} \qquad (5.4.6)$$

Because equation (5 . 4 . 5) is true only at low excitation power and we have measured the external efficiency of our sample at low carrier density ($\sim 2\times10^{17} cm^{-3}$) we have estimated the τ for $n = 2\times10^{17} cm^{-3}$. Using the Eq. (5 . 4 . 4) and the values of A and B_R obtained by fitting, a value of 285 ps has been calculated for τ at low carrier density . Since the photoluminescence lifetime was calculated to be 285 ps at low carrier density , a simple calculation using the equations (5 .4 . 5) and (5 . 4 . 6) yields a value of 2.5×10^{8} an $3.25\times10^{9} s^{-1}$ for the radiative ($A_R = \frac{1}{\tau_R}$) and nonradiative ($A_{NR} = \frac{1}{\tau_{NR}}$) rates , respectively .

So far, we have determined all the recombination rates involved in model (1) , therefore $\tau_{eff}(n)$ for this model has been calculated from equation (5 . 4 . 4) and is shown in Fig. 5 . 4 . 2. by a solid line . This curve as expected fits the experimental points at low power fluence but does not fit the experimental points at higher excitation power fluence ($> 2\times10^{9}\ W/cm^2$). This is due to the fact that at high carrier densities the Auger effect can not be ignored . Clearly the model (2) is a more complete model to describe the changes observed in the decay profile of photoluminescence in GaAsP (x=.38) at room temperature particularly at high carrier densities.

Since C_{NR} has not been determined experimentally, it was treated as the only

adjustable parameter to obtain the best fit between the experimental measured decay time and the theoretical value calculated numerically by computer based on model (2) at different excitation power fluences. The $\tau_{eff}(n)$ for model (2) versus the excitation power fluence is shown in Fig. 5 . 4 . 2 by a dashed line for $C_{NR}=3\times10^{-29}cm^6/s$ and it fits the experimental data well. The Auger rate of $3\times10^{-29}cm^6/s$ is larger than the rate in GaAs [26] by a factor of 2 and is 3 times smaller than the rate estimated for InGaAsP[23]. In order to determine the uncertainty in the value of C_{NR} , $\tau_{eff}(n)$ from model (2) has been calculated as a function of excitation power fluence for $C_{NR}=(5\pm2)\times10^{-29}cm^6/s$. These curves are shown by dots and dot-dash in Fig. 5 . 4 . 2 . In further support of the second model, each decay profile were calculated using the recombination rates obtained from fitting. The circles in the time resolved photoluminescence profiles of Fig. 5 . 4 . 1 are the numerical solution of model (2) for $A_R=2.5\times10^8/s$, $A_{NR}=3.25\times10^9/s$, $B_R=9\times10^{-10}cm^3/s$ and $C_{NR}=3\times10^{-29}cm^6/s$. The theoretical curves fit all the time resolved photoluminescence profiles well at different excitation power. The significance of model (2) was apparent at highest excitation power (see Fig. 5 . 4 . 1 -d) where there was significant deviation from an exponential form . As to the question of which type of Auger processes involved in this research , one can eliminate the CHCC Auger process because this is very improbable in large band gap semiconductors [26] . So it is very likely that the CHSH Auger process is dominant process in $GaAs_{.62}P_{.38}$.

In conclusion, the transient behavior of photogenerated carriers by picosecond laser pulses in GaAsP (x=.38) at room temperature can be described in terms of recombination model where nonradiative Auger term played an important role . Auger process is included in order to explain the changes observed in the decay profile of time resolved photoluminescence kinetics .

References

1 A . Bergh , J . A . Copeland , R . W . Dixon , Proc. IEEE 68 , 1240 (1980) .

2 Semiconductors probed by Ultrafast Laser Spectroscopy by R . R . Alfano , Academic Press , NewYork , (1984) .

3 R . W . Dixon , W . B . Joyce , J. Appl. Phys. 50 , 4591 (1979) .

4 R . J . Nelson ,R . G . Sobers , J . Appl. Phys. 49 , 6103 (1979) .

5 R . R . Alfano , S . L . Shapiro , Phys. Rev. Lett. 26 , 147 (1971) .

6 M . A . Duguay , J . W . Hansen , Appl. Phys. Lett. 15 , 192 (1969) .

7 H . Mahr , M . D . Hirsch ,Opt. Comm. 13 , 96 (1975) .

8 R . J . Seymour ,M . R . Junarkar ,R . R . Alfano , Solid state Comm. 41 , 657 (1982) .

9 F . H . Pollak , M . Cardona , J. Phys. Chem. solids 27 , 423 (1966) .

10 G . W . Gobeli , F . F . Allen , Phys. Rev. A137 , 245 (1965) .

11 N . Holonyak Jr. , S . F . Bevaqua , Appl. Phys. Lett. 1 , 82 (1962) .

12 H . Ehrenreich , Phys. Rev. 120 , 1951 (1960) .

13 M . G . Craford , G . E . Stillman , J . A . Rossi , H . Holonyak Jr. , Phys. Rev. 168 , 867 (1968) .

14 A . G . Thompson , M . Cardona , K . L . Shaklee , J . C . Wooly , Phys. Rev. 146 , 601 (1966) .

15 D . E . Hill , Bull. Am. Phys. Soc. 11 , 205 (196) .

16 G . Benz , R . Conradt , Phys. Rev. B 16 , 843 (1977) .

17 N . K . Dutta , R . J . Nelson , J. Appl. Phys. 53 , 74 (1982) .

18 O . Hilbrand , E . G . Goeble , K . M . Romaneck , H . Weber , G . Mahler , Phys. Rev. B17 , 4775 (1978) .

19 The carrier density was determined by fitting the experimental photoluminescence spectra of e-h plasma to the theoretical expression of direct band to band transition , see for example E . Goeble , O . Hilbrand , K . Lochnert , IEEE J. Quantum Elec. 13 , 848 (1977) .

20 B . A . Wilson , J . Hegarty , W . M . Yen , Phys. Rev. Lett. 24 , 268 (1978) .

21 S . Modesti , L . G . Quagliano , A . Frova , J . L . Staehli , M . Guzzi , J. Lumm. 24 , 581 (1981) .

22 C . B . Su , R . Olshansky , Appl. Phys. Lett. 41 , 833 (1982) .

23 C . B . Su , J . Schlafer , J . Manning , R . Olshansky , Electr. Lett. 18 , 595 (1982) .

24 The external efficiency of GaInP was measured to be 1.8×10^{-5} (see Ref. 25) . We also have compared the external efficiency of our sample against a dye (erythrosin) with .02 quantum efficiency . The results of these two independent measurements were within 10 percent of each other .

25 J . S . Roberts , G . B . Scott . , J . P . Gowers , J. Appl. Phys. 52 , 4018 (1981).

26 A . Haug , J. Phys. C : Solid State Physics 16 , 4159 (1983) .

TABLE 1

$Ga_{.5}In_{.5}P$ Parameters

Parameter	Definition	Value	Reference
E_g	Direct band gap	1.9 ev	12
E_X	Indirect band gap	2.25 ev	12
m_e	Electron effective mass	.094	12
m_{hh}	Heavy hole effective mass	.51	11
m_{lh}	Light hole effective mass	.16	11
m_{sh}	Split off hole effective mass	.1	11
ϵ_∞	Optical dielectric constant	11.6	12
ϵ_s	Static dielectric constant	9.1	12
ρ	Mass density	4.455 gr / cm^3	13
$h\omega_{LO}$	LO phonon energy	48 mev	13
$h\omega_{LA}$	LA phonon energy	29 mev	13
$D_{\Gamma X}$	Deformation Potential	5×10^8 ev/cm	13

TABLE 2

$GaAs_{.62}P_{.38}$ Parameters

Parameter	Definition	Value	Reference
E_g	Direct band gap	1.892 ev	14
m_e	Electron effective mass	.099	14
m_h	Hole effective mass	.53	Interpolation
ϵ	Dielctric constant	11.86	Interpolation

Feb 8 13:28 1985 ehf.F Page 1

```
C       THIS PROGRAM CACULATES THE FERMI INTEGRAL EQ. 3.3.5
        EXTERNAL FX
        DIMENSION AF(1400)
        REAL XL,XU,ETA
        INTEGER N
        COMMON ETA,XL,XU,N
        XL=0
        XU=50
        N=10000
        DO 50 I=1,1000
        ETA=-4.02+(I*.02)
        APRO=TRAP(XL,XU,N,FX)
50      AF(I)=2*APRO/1.7725385
        OPEN(17,FILE='FERMI.ZAP')
        WRITE(17,300)(AF(I),I=1,1000)
300     FORMAT(5(F10.5,3X))
        STOP
        END
        FUNCTION FX(X)
        COMMON ETA,XL,XU,N
        FX=SQRT(X)/(1.+EXP(X-ETA))
        RETURN
        END
```

Feb 8 13:26 1985 frm.F Page 1

```
c       THIS SUBROUTINE CALCULATES EQ. 3.3.8
        SUBROUTINE FRM(AM,T,AN,eta)
        ANC=2.51E19*((AM*T/300.)**1.5)
        C=AN/ANC
        ATE=ALOG(C)+.3335*C- 90495*(C**2)+1.48E-4*(C**3)
        eta=ATE-4.43E-6*(C**4)
        RETURN
        END
```

Feb 8 13:38 1985 dscr2.F Page 1

```
C       THIS PROGRAM WAS USED FOR CALCULATIONS OF FIG. 3.3.5 , 3.36.
        CHARACTER*10 FILE1
        EXTERNAL FX
        COMMON /ZAP/ETA,AN,T,Q,TC
        ATL=300.0
        WRITE(6,45)
45      FORMAT(1X,'TYPE PHONON ENERGY IN MEV  , CARRIER DENSITY ')
        READ(5,46)PH,AN
46      FORMAT(2G10.4)
        T=300.0
        AKT=(ATL/300.)*25
444     AKTC=(T/300.)*25
        A=0
        B=1.E7
        N=1000
        TC=(T/300.0)*25
        TCE=TC/1000.0
        Q2=1.491E-6*AN/TCE
        Q=SQRT(Q2)
        CALL FRM(.094,T,AN,ETA)
        CALL TRAP(A,B,N,FX,RES)
        Y=8.87E4*RES/(AN*1.6E-12)
        YEC=Y*1.E-12*1000.0
        WRITE(6,*)T,YEC
        WRITE(17,*)T,YEC
        T=T+100.0
        IF(T.LT.2200)GO TO 444
        STOP
        END
        FUNCTION FX(X)
        COMMON /ZAP/ETA,AN,T,Q,TC
        PH=40.0
        AKH=2.988E6
        AKP=AKH*AKH
        AK=X
        AE=4.03E-12*(X*X)
        A1=AE/TC
        F1=1./(1.+EXP(A1-ETA))
        A2=(AE+PH)
        F2=1./(1.+EXP(A2-ETA))
        F3=F1-F2
        C1N=((AK+SQRT((AK*AK)+AKP))**2)+(Q*Q)
        C1D=((AK-SQRT((AK*AK)+AKP))**2)+(Q*Q)
        C=LOG(C1N/C1D)
        D=Q*Q/(((AK-SQRT((AK*AK)+AKP))**2)+(Q*Q))
        G=Q*Q/(((AK+SQRT((AK*AK)+AKP))**2)+(Q*Q))
        FAC=AK*F3*(C-D+G)
        FX=FAC
        RETURN
        END
```

```
Feb  8 13:31 1985  dtmb.F Page 1

C       THIS PROGRAM CALCULTES TEMPERATURE EVOLUTION FOR M.B. DISTRIBUTION
        EXTERNAL EQNS,PRINT
        DIMENSION ERRPAR(2)
        REAL X(2),DT,TSTART
        DIMENSION AY(300)
        COMMON/DATA/ERRPAR,DT,X,TSTART
        COMMON /ZAP/NP,D,ATL,PH,JK,AY(300)
        CHARACTER*10 FILE1
        WRITE(6,83)
83      FORMAT('TYPE LATTICE TEMP,CARRIER TEMP AT T=0,PH IN MEV  FORMAT 3G10.4')
        READ(5,87)ATL,X(1),PH
87      FORMAT(3G10.4)
        TSTART=0.
        ERRPAR(1)=1.E-5
        ERRPAR(2)=1.E-6
        DT=1.E-8
        WRITE(6,50)
50      FORMAT('TYPE THE NAME OF FILE')
        READ(5,51)FILE1
51      FORMAT(A10)
        OPEN(17,FILE=FILE1)
        TSTOP=1.E-1
        JK=1
        WRITE(6,996)TSTART,X(1)
        WRITE(17,996)TSTART,X(1)
77      CALL ODES(EQNS,X,1,TSTART,TSTOP,DT,ERRPAR,PRINT)
        TSTART=TSTOP
        TSTOP=TSTOP+1.E-1
        JK=JK+1
        X(1)=AY(JK-1)
        IF(JK.LT.101)GO TO 77
        DO 99 I=1,100
        TM=I*1.E-1
99      WRITE(17,996)TM,AY(I)
996     FORMAT(G10.4,1X,G10.4)
        STOP
        END
        SUBROUTINE EQNS(T,X,N,DX)
        EXTERNAL ZBES
        REAL T,X(1),DX(1)
        COMMON /ZAP/NP,D,ATL,PH,JK,AY(300)
        AKT=(ATL/300.)*25
        AKTC=(X(1)/300.)*25
        YC=PH/AKTC
        Y0=PH/AKT
        R1N=EXP(Y0-YC)-1.
        R1D=EXP(Y0)-1.
        R1=R1N/R1D
        R2N=SQRT(YC/2.)*EXP(YC/2.)*.798
        Y=YC/2.
        CALL ZBES(Y,AKB)
        R3N=R2N*AKB
        R4=R1*R3N
        DX(1)=-23.37*(PH**1.5)*R4
        RETURN
        END
        SUBROUTINE PRINT(T0,X0,T1,X1,N,DT,TSTOP,E)
        COMMON /ZAP/NP,D,ATL,PH,JK,AY(300)
        REAL T0,X0(N),T1,X1(N),DT,TSTOP
        REAL E(N)
        IF(T1.NE.TSTOP)RETURN
        WRITE(6,391)T1,X1(1)
391     FORMAT(G10.4,1X,G10.4)
        AY(JK)=X1(1)
        RETURN
        END
```

```
Feb  8 13:33 1985  dtext F Page 1

C       THIS PROGRAM CALCULTAES EQ. 3.3.22
        EXTERNAL EQNS,PRINT
        COMMON/DATA/ERRPAR,DT,X,TSTART
        COMMON /ZAP/AME,TC,ATL,PH,AN,JK,TAU,AY(300)
        COMMON /ZAP2/ETA,AXC,ANQ
        COMMON /ZAP3/BF,RES1,RES2,CT1,CT2,DE,DE2,DE3
        DIMENSION ERRPAR(2)
        REAL X(2),DT,TSTART
        CHARACTER*10 FILE1
        WRITE(6,83)
33      FORMAT('TYPE ME,TC,ATL,PH(EV),N,TAU     5G10.4$ ')
        READ(5,87)AME,X(1),ATL,PH,X(2),TAU
87      FORMAT(6G10.4)
        WRITE(6,515)
515     FORMAT('TYPE DT,TSTOP      2G10.4')
        READ(5,516)BDT,BST
516     FORMAT(2G10.4)
        KK=(BST/BDT)+1
        TSTART=0.
        ERRPAR(1)=1.E-5
        ERRPAR(2)=1.E-6
        DT=1.E-8
        WRITE(6,50)
50      FORMAT('TYPE THE NAME OF FILE')
        READ(5,51)FILE1
51      FORMAT(A10)
        OPEN(17,FILE=FILE1)
        TSTOP=BDT
        JK=1
        WRITE(6,996)TSTART,X(1)
        WRITE(17,996)TSTART,X(1)
77      CALL ODES(EQNS,X,2,TSTART,TSTOP,DT,ERRPAR,PRINT)
        WRITE(6,995)X(2),X(1),ANQ,ETA,BF,CT1,CT2
        TSTART=TSTOP
995     FORMAT(6(G10.4,1X))
        TSTOP=TSTOP+BDT
        JK=JK+1
        X(1)=AY(JK-1)
        IF(JK.LT.KK)GO TO 77
        DO 99 JJ=1,KK
        TM=JJ*BDT
        TML=LOG(TM)
99      WRITE(17,996)TML,AY(JJ)
996     FORMAT(G10.4,1X,G10.4)
        STOP
        END
        SUBROUTINE EQNS(T,X,N,DX)
        EXTERNAL FX,GX
        REAL T,X(2),DX(2)
        COMMON /ZAP/AME,TC,ATL,PH,AN,JK,TAU,AY(300)
        COMMON /ZAP2/ETA,AXC,ANQ
        COMMON /ZAP3/BF,RES1,RES2,CT1,CT2,DE,DE2,DE3
        AKTC=X(1)*.025/300.
        AKT=ATL*.025/300.
        ANC=1.2039E19*(AME*X(1)/300.)**1.5
        ANC=ANC*2
700     BF=X(2)/ANC
        CALL FRM(AME,X(1),X(2),ETA)
        ANQ=1./(EXP(PH/AKT)-1.)
        AXC=PH/AKTC
        XL=0.
        XU=ETA*10
        M=200
        CALL ZARA(XL,XU,M,FX,RES1)
        CALL ZARA(XL,XU,M,GX,RES2)
        CT1=ANQ*RES1
        CT2=(1.+ANQ)*RES2
        DE=5.56E11*SQRT(AXC)/BF
        DE2=DE*(CT1-CT2)
        DE3=DE2*(1.E-12)*300./.025
        DX(1)=DE3/1.5
        DX(2)=-X(2)/TAU
        RETURN
        END
        SUBROUTINE PRINT(T0,X0,T1,X1,N,DT,TSTOP,E)
        COMMON /ZAP/AME,TC,ATL,PH,AN,JK,TAU,AY(300)
        COMMON /ZAP2/ETA,AXC,ANQ
        COMMON /ZAP3/BF,RES1,RES2,CT1,CT2,DE,DE2,DE3
        REAL T0,X0(N),T1,X1(N),DT,TSTOP
```

Feb 8 13:33 1985 dtex1.F Page 2

```
      REAL E(N)
      IF(T1.NE.TSTOP)RETURN
      WRITE(6,391)T1,X1(1)
391   FORMAT(G10.4,1X,G10.4)
      AY(JK)=X1(1)
      RETURN
      END
      FUNCTION FX(X)
      COMMON /ZAP2/ETA,AXC,ANQ
      C1=1./(1.+EXP(X-ETA))
      C2=1./(1.+EXP(X+AXC-ETA))
      C3=X/AXC
      C4=SQRT(1.+(C3*C3))
      C5=LOG(C3+C4)
      FX=C1*(1.-C2)*C5
      RETURN
      END
      FUNCTION GX(X)
      COMMON /ZAP2/ETA,AXC,ANQ
      D1=1./(1.+EXP(X+AXC-ETA))
      D2=1./(1.+EXP(X-ETA))
      D3=X/AXC
      D4=SQRT(1.+(D3*D3))
      D5=LOG(D3+D4)
      GX=D1*(1.-D2)*D5
      RETURN
      END
```

Feb 8 13:52 1985 temscr.F Page 1

```
C       THIS PROGRAM CALCULATES TIME DEPENDENCE OF TEMPERAURE IN THE
        PRESENCE OF SCREENING
        EXTERNAL EQNS,PRINT
        DIMENSION ERRPAR(2)
        REAL X(2),DT,TSTART
        DIMENSION AY(300)
        COMMON/DATA/ERRPAR,DT,X,TSTART
        COMMON /ZAP/NP,EB,TAU,ATL,PH,JK,AY(300)
        CHARACTER*10 FILE1
        WRITE(6,83)
83      FORMAT('TYPE ALT,ACT,PH(MEV),N(AT T=0),TAU(PS),EPSBAR- 5G10.4')
        READ(5,88)ATL,X(1),PH,X(2),TAU,EB
88      FORMAT(6G10.4)
        WRITE(6,125)
125     FORMAT('TYPE DT,TSTOP    2G10.4')
        READ(5,126)BDT,BTS
126     FORMAT(2G10.4)
        TSTART=0.
        ERRPAR(1)=1.E-5
        ERRPAR(2)=1.E-6
        MM=(BTS/BDT)+1
        DT=1.E-8
        WRITE(6,50)
50      FORMAT('TYPE THE NAME OF FILE')
        READ(5,51)FILE1
51      FORMAT(A10)
        OPEN(17,FILE=FILE1)
        TSTOP=BDT
        JK=1
        WRITE(6,996)TSTART,X(1)
77      CALL ODES(EQNS,X,2,TSTART,TSTOP,DT,ERRPAR,PRINT)
        TSTART=TSTOP
        TSTOP=TSTOP+BDT
        JK=JK+1
        X(1)=AY(JK-1)
        IF(AY(JK-1).LT.300.0)GO TO 990
        IF(JK.LT.MM)GO TO 77
990     DO 553 I=JK-1,MM
553     AY(I)=300.0
        DO 99 I=1,MM
        TM=I*BDT
        TLG=LOG(TM)
99      WRITE(17,996)TLG,AY(I)
996     FORMAT(G10.4,1X,G10.4)
        STOP
        END
        SUBROUTINE EQNS(T,X,N,DX)
        REAL T,X(1),DX(1)
        COMMON /ZAP/NP,EB,TAU,ATL,PH,JK,AY(300)
        CALL SC2(X(1),X(2),RHN)
        RH1=(2.696E5/EB)*(RHN/X(2))
        RH2=RH1/1.6E-12
        RH3=RH2*1.0E-12
        RH4=(RH3/.025)*(300/1.5)
        DX(1)=-RH4
        DX(2)=-X(2)/TAU
        RETURN
        END
        SUBROUTINE PRINT(T0,X0,T1,X1,N,DT,TSTOP,E)
        COMMON /ZAP/NP,EB,TAU,ATL,PH,JK,AY(300)
        REAL T0,X0(N),T1,X1(N),DT,TSTOP
        REAL E(N)
        IF(T1.NE.TSTOP)RETURN
        WRITE(6,391)T1,X1(1)
391     FORMAT(G10.4,1X,G10.4)
        AY(JK)=X1(1)
        RETURN
        END
```

Feb 8 13:53 1985 sc2.F Page 1

```
      SUBROUTINE SC2(CC,DD,RH)
      EXTERNAL FX
      COMMON /ZAQ/ETA,AN,BT,Q,TC
      BT=CC
      AN=DD
      A=0
      B=1.3E7
      N=200
      TC=(BT/300.0)*25
      TCE=TC/1000.0
      ANM=AN*EXP(-1.0/300.)
      DELN=AN-ANM
      CALL FRM(.094,BT,AN,H1)
      CALL FRM(.094,BT,ANM,H2)
      DF=(H1-H2)*TCE
      DNDM=DELN/(DF*1.6E-12)
      Q2=4*3.14*(4.8E-10**2)*DNDM/10.0
      Q=SQRT(Q2)
      CALL FRM(.094,BT,AN,ETA)
      CALL TRAP(A,B,N,FX,RES)
      RH=RES
      RETURN
      END
      FUNCTION FX(X)
      COMMON /ZAQ/ETA,AN,BT,Q,TC
      PH=40.0
      AKH=2.988E6
      AKP=AKH*AKH
      AK=X
      AE=4.03E-12*(X*X)
      A1=AE/TC
      F1=1./(1.+EXP(A1-ETA))
      A2=(AE+PH)
      F2=1./(1.+EXP(A2-ETA))
      F3=F1-F2
      C1N=((AK+SQRT((AK*AK)+AKP))**2)+(Q*Q)
      C1D=((AK-SQRT((AK*AK)+AKP))**2)+(Q*Q)
      C=LOG(C1N/C1D)
      D=Q*Q/(((AK-SQRT((AK*AK)+AKP))**2)+(Q*Q))
      G=Q*Q/(((AK+SQRT((AK*AK)+AKP))**2)+(Q*Q))
      FAC=AK*F3*(C-D+G)
      FX=FAC
      RETURN
      END
```

Feb 8 13.40 1985 dngxo F Page 1

```
C       THIS PROGRAM CALCULATES EQ. 3.3.40
        SUBROUTINE DNGXO(BT,BN,RES)
        EXTERNAL FX
        COMMON /ZAP/ATX,XI,ETAX
        CALL FRM(.094,BT,BN,ETA1)
        AKT=BT*.025/300.
        FE=ETA1*AKT
        XI=.029/AKT
        ATX=AKT/.04
        ETAX=FE/.04
        CALL TRAP(8.1,30.,100,FX,SUM1)
        H5=1.121E20*SUM1
        RES=H5
        RETURN
        END
        FUNCTION FX(X)
        COMMON /ZAP/ATX,XI,ETAX
        A1=SQRT(X)
        A2=1./(1.+EXP((X-ETAX)/ATX))
        A3=1./(EXP(XI)-1.0)
        A4=SQRT(X+.6-8.1)
        A5=EXP(XI)*SQRT(X-7.5-.6)
        A6=A1*A2*A3*A4*A5
        FX=A6
        RETURN
        END
```

Feb 8 13:41 1985 dnxgo.F Page 1

```
C       THIS PROGRAM CALCULATE EQ. 3.3.40
        SUBROUTINE DNXGO(CT,CN,RES)
        EXTERNAL F2X
        COMMON /ZAP/ATX,XI,ETAX
        CALL FRM(1.2,CT,CN,ETA1)
        AKT=CT*.025/300.
        FE=ETA1*AKT
        XI=.029/AKT
        ATX=AKT/.04
        ETAX=FE/.04
        CALL TRAP(.6,30.,100,F2X,SUM1)
        RES=7.62E18*SUM1
        RETURN
        END
        FUNCTION F2X(X)
        COMMON /ZAP/ATX,XI,ETAX
        A1=SQRT(X)
        A2=1./(1.+EXP((X-ETAX)/ATX))
        A3=1./(EXP(XI)-1.0)
        A4=SQRT(X+.6)
        A5=EXP(XI)*SQRT(X-.6)
        A6=A1*A2*A3*A4*A5
        F2X=A6
        RETURN
        END
```

Feb 8 13:43 1985 dtt3.F Page 1

```
C       THIS PROGRAM CALCULATES EQ. 3.3.57 AND 3.3.58
        EXTERNAL EQNS,PRINT
        DIMENSION ERRPAR(2)
        REAL X(3),DT,TSTART
        COMMON /DATA/ERRPAR,DT,X,TSTART
        COMMON /ZAP1/JK,AY(200),BY(200),CY(200),AMX,TAU,AFN,FAC
        WRITE(6,11)
11      FORMAT(1X,'TYPE NG(0),NX(0),AMX,TAU,AFN,DFAC,NO. OF PTS 6G10.4,I4')
        READ(5,12)X(1),X(2),AMX,TAU,AFN,FAC,NN
12      FORMAT(6G10.4,I4)
        TSTART=0.
        ERRPAR(1)=1.E-2
        ERRPAR(2)=1.E-2
        TSTOP=1.E0
        DT=1.E-2
        X(3)=300.
        PH=.048
        JK=1
        WRITE(6,111)TSTART,X(1),X(2),X(3)
        WRITE(17,*)TSTART,X(1)
        WRITE(18,*)TSTART,X(2)
        WRITE(19,*)TSTART,X(3)
77      CALL ODES(EQNS,X,3,TSTART,TSTOP,DT,ERRPAR,PRINT)
        TSTART=TSTOP
        TSTOP=TSTOP+1.E0
        JK=JK+1
        X(1)=AY(JK-1)
        X(2)=BY(JK-1)
        X(3)=CY(JK-1)
        WRITE(6,111)TSTART,X(1),X(2),X(3)
111     FORMAT(1X,4(G10.4,2X))
        IF(JK.LT.NN-1)GO TO 77
        DO 1015 I=1,NN-1
        WRITE(17,*)I,AY(I)
        WRITE(18,*)I,BY(I)
        STT=CY(I)
        IF(STT.LT.300)STT=300
1015    WRITE(19,*)I,STT
        STOP
        END
        SUBROUTINE EQNS(T,X,N,DX)
        REAL T,X(3),DX(3)
        COMMON /ZAP1/JK,AY(200),BY(200),CY(200),AMX,TAU,AFN,FAC
        CGX=750.0
        IF(X(3).GE.1000)CGX=.01
        IF(X(3).GE.900)CGX=.1
        IF(X(3).GE.700)CGX=.5
        IF(X(3).GE.600)CGX=1.0
        IF(X(3).GT.400)CGX=5.0
        IF(X(3).GT.425)CGX=30.
        IF(X(3).GE.350)CGX=100.0
        IF(X(3).GE.330)CGX=230.0
        IF(X(3).GE.310)CGX=500.0
        IF(X(3).GE.305)CGX=600.0
        CGX=CGX/FAC
        A1=(T-10.0)/4.0
        A2=A1*A1*.693
        A3=AMX*EXP(-A2)/8.5
        DX(1)=A3-(X(1)/TAU)-(X(1)/CGX)+(X(2)/(20./FAC))
        DX(2)=(X(1)/CGX)-(X(2)/(20./FAC))
        AKT=.025
        AKTC=(X(3)/300.)*.025
        PH=.04
        YC=PH/AKTC
        Y0=PH/AKT
        R1N=EXP(Y0-YC)-1.
        R1D=EXP(Y0)-1.
        R1=R1N/R1D
        R2N=SQRT(YC/2.)*EXP(YC/2.)*.798
        Y=YC/2.
        CALL ZBES(Y,AKB)
        R3N=R2N*AKB
        R4=R1*R3N
        Z5=23.37*(40.0**1.5)*R4
        BFN=1+(AFN*X(1)/X(3))
        Z6=Z5/BFN
        S1=(.4/.025)*300.*(1.0/CGX)
        CALL TRS(T,S2)
        DX(3)=S2-S1-Z6
```

Feb 8 13:43 1985 dtt3 F Page 2

```
771       RETURN
          END
          SUBROUTINE PRINT(T0,X0,T1,X1,N,DT,TSTOP,E)
          COMMON /ZAP1/JK,AY(200),BY(200),CY(200),AMX,TAU,AFN,FAC
          REAL T0,X0(N),T1,X1(N),DT,TSTOP
          REAL E(N)
          IF(T1.NE.TSTOP)RETURN
          AY(JK)=X1(1)
          BY(JK)=X1(2)
          CY(JK)=X1(3)
          RETURN
          END
```

```
Feb  8 13:44 1985  dtt3mg.F Page 1

C       THIS PROGRAM CALCULATES EQ. 3.3.60
        EXTERNAL EQNS,PRINT
        DIMENSION ERRPAR(2)
        DIMENSION AT(200),AN(200)
        DIMENSION XR(50),YR(50)
        REAL X(4),DT,TSTART
        COMMON/DATA/ERRPAR,DT,X,TSTART
        COMMON /ZP/AFN,TAU,ATL,PH,JK,A(300),B(300),C(300),D(300),GA1,GA2
        CHARACTER*10 FL1,FL2,FL3
        WRITE(6,421)
421     FORMAT(1X,'TYPE N FILE . T FILE ')
        READ(5,422)FL1,FL2
422     FORMAT(A10)
        WRITE(6,845)
845     FORMAT(1X,'TYPE THE FINAL TIME IN PS ')
        READ(5,846)NN
846     FORMAT(I4)
        OPEN(17,FILE=FL1)
        READ(17,*)(DM,AN(I),I=1,NN)
        CLOSE(17)
        OPEN(17,FILE=FL2)
        READ(17,*)(DM,AT(I),I=1,NN)
        CLOSE(17)
        X(1)=100.0
        X(2)=100.0
        WRITE(6,125)
125     FORMAT('TYPE DT,TSTOP ,CONF  FAC ,EG, AL1,AL2       5G12.4')
        READ(5,126)BDT,BTS,CF,EG,AL1,AL2
126     FORMAT(6G10.4)
        TSTART=0.
        TSTOP=BDT
        DT=1.E-3
        ERRPAR(1)=1.E-2
        ERRPAR(2)=1.E-2
        MM=(BTS/BDT)+1
        BFN1=CF
        BFN2=CF
        WRITE(,,50)
50      FORMAT('TYPE THE NAME OF FILE')
        READ(5,51)FL3
51      FORMAT(A10)
        OPEN(19,FILE=FL3)
        JK=1
        HN1=12400./AL1
        HN2=12400./AL2
77      BKT=(AT(JK)/300.0)*.025
        CALL FRM(.094,AT(JK),AN(JK),ETA1)
        FE=BKT*ETA1
        CALL FRM(.5,AT(JK),AN(JK),ETA2)
        FH=BKT*ETA2
        PH1=1./(1.+EXP((.16*(HN1-EG)-FH)/BKT))
        PH2=1./(1.+EXP((.16*(HN2-EG)-FH)/BKT))
        PE1=1./(1.+EXP((.84*(HN1-EG)-FE)/BKT))
        PE2=1./(1.+EXP((.84*(HN2-EG)-FE)/BKT))
        DD1=PE1+PH1-1.0
        DD2=PE2+PH2-1.0
        G1=2.E4*SQRT(HN1-EG)*DD1
        GA=.6*(3.E10/3.4)*G1
        GA1=GA/BFN1
        DD2=PE2+PH2-1.0
        G2=2.E4*SQRT(HN2-EG)*DD2
        GB=.6*(3.E10/3.4)*G2
        GA2=GB/BFN2
        WRITE(19,367)AT(JK),AN(JK),X(1),X(2),GA,GA1,GB,GA2
367     FORMAT(8G10.4)
        CALL ODES(EQNS,X,2,TSTART,TSTOP,DT,ERRPAR,PRINT)
        TSTART=TSTOP
        TSTOP=TSTOP+BDT
        JK=JK+1
        X(1)=A(JK-1)
        X(2)=B(JK-1)
        IF(JK.LT.MM)GO TO 77
        DO 185 I=1,20
        YR(I)=B(1)*EXP(-FLOAT(I)/5.0)
        XR(I)=A(1)*EXP(-FLOAT(I)/5.0)
        XR(I)=XR(I)*100./A(1)
185     YR(I)=YR(I)*100./B(1)
        DO 186 I=1,20
        WRITE(18,187)I,YR(21-I)
```

Feb 8 13:44 1985 dtt3mg.F Page 2

```
186     WRITE(17,187)I,XR(21-I)
187     FORMAT(I4,4X,G10.4)
        DO 99 I=1,MM-1
        JH=I+20
        A(I)=A(I)*100./A(1)
        B(I)=B(I)*100./B(1)
        WRITE(17,187)JH,A(I)
99      WRITE(18,187)JH,B(I)
        STOP
        END
        SUBROUTINE EQNS(T,X,N,DX)
        REAL T,X(2),DX(2)
        COMMON /ZP/AFN,TAU,ATL,PH,JK,A(300),B(300),C(300),D(300),GA1,GA2
        DX(1)=GA1*1.E-12*X(1)
        DX(2)=GA2*1.E-12*X(2)
        RETURN
        END
        SUBROUTINE PRINT(T0,X0,T1,X1,N,DT,TSTOP,E)
        COMMON /ZP/AFN,TAU,ATL,PH,JK,A(300),B(300),C(300),D(300),GA1,GA2
        REAL T0,X0(N),T1,X1(N),DT,TSTOP
        REAL E(N)
        IF(T1.NE.TSTOP)RETURN
        A(JK)=X1(1)
        B(JK)=X1(2)
        RETURN
        END
```

```
Feb  8 13:46 1985  smres.F Page 1

C       THIS PROGRAM CALCULTAES EQ. 4.4.6
        DIMENSION AF(1000),X(1000),SX(1000),Z(1000),IRB(50),IZ(1000)
        CHARACTER*10 FILE1
        OPEN(17,FILE='FERMI.ZAP')
        READ(17,300)(AF(I),I=1,1000)
300     FORMAT(5(F10.5,3X))
        CLOSE(17)
3000    XM=0.
        ZM=0.
        DO 555 I=1,500
        X(I)=X(I)*0.
        SX(I)=SX(I)*0.
        Z(I)=Z(I)*0.
555     IZ(I)=IZ(I)*0.
        WRITE(6,1)
1       FORMAT('TYPE ME,MH,AT,N       FORMAT(4G10.4)')
        READ(5,2)EM,HM,AT,BN
2       FORMAT(4G10.4)
        BT=AT*.025/300.
        ANC=1.2039E19*(EM*AT/300.)**1.5
        ANC=ANC*2
        ANV1=ANC*((HM/EM)**1.5)
700     BF=BN/ANC
        DO 6 I=1,1000
        IF(BF.LT.AF(I))GO TO 11
6       CONTINUE
11      ETE=-4.02+(I*.02)
        EF=ETE*BT
        CF=BN/ANV1
        DO 8 I=1,1000
        IF(CF.LT.AF(I))GO TO 12
8       CONTINUE
12      H1=-4.02+(I*.02)
        EH=H1*BT
        WRITE(6,66)EF,EH
66      FORMAT(1X,'FE=',F10.4,'FH=',F10.4)
        WRITE(6,77)
77      FORMAT(1X,'TYPE L1,DL,EG,BLANDA FORMAT   4G10.4')
        READ(5,78)AL1,DL,AEG,BL
78      FORMAT(4G10.4)
        AM1=HM/(HM+EM)
        AM2=1.-AM1
        N=((12400./AEG)-AL1)/DL
        DO 10 I=1,N
        G=AL1+(I-1)*DL
        HN=12400./G
        A=(AM1*(HN-AEG))-EF
        B=A/BT
        C=1./(1.+EXP(B))
        AA=(AM2*(HN-AEG))-EH
        BB=AA/BT
        CC=1./(1.+EXP(BB))
10      X(I)=(HN**2)*(SQRT(HN-AEG))*C*CC
        XM=X1
        DO 20 I=1,N
20      IF(X(I).GT.XM)XM=X(I)
        WRITE(6,734)XM
734     FORMAT('INTESITY=',G10.4)
        DO 401 I=1,N
        IF(X(I).EQ.XM)GO TO 402
401     CONTINUE
402     LM=AL1+(I*DL)
        WRITE(6,403)LM
403     FORMAT(1X,'LANDA MAX=',I4)
        DO 610 J=1,16
        IRB(J)=BL+(J-1)*50
        DO 620 I=1,50
        ALL=IRB(J)-25
        G=ALL+(I-1)
        H=12400./G
        A=(AM1*(H-AEG))-EF
        B=A/BT
        C=1./(1.+EXP(B))
        AA=(AM2*(H-AEG))-EH
        BB=AA/BT
        CC=1./(1.+EXP(BB))
620     Z(J)=Z(J)+(H**2)*(SQRT(H-AEG))*C*CC
610     CONTINUE
        ZM=Z(1)
```

```
      DO 630 I=1,16
630   IF(Z(I).GT.ZM)ZM=Z(I)
      DO 640 I=1,16
640   IZ(I)=(Z(I)/ZM)*100.
      WRITE(6,650)(IRB(I),IZ(I),I=1,16)
650   FORMAT(8('(',I4,')=',I4))
      WRITE(6,660)
660   FORMAT(1X,'TYPE 1 TO REPEAT,2 TO WRITE')
      READ(5,670)IR
670   FORMAT(I4)
      IF(IR.EQ.1)GO TO 3000
      DO 680 I=1,N
680   SX(I)=(X(I)/XM)*100.
      WRITE(6,681)
681   FORMAT(1X,'TYPE THE OFILE NAME')
      READ(5,682)FILE1
682   FORMAT(A10)
      OPEN(17,FILE=FILE1)
      DO 683 I=1,N
      JL=AL1+(I-1)*DL
683   WRITE(17,687)JL,SX(I)
687   FORMAT(1X,I4,1X,F10.1)
      STOP
      END
```

Feb 8 13:47 1985 indr.F Page 1

```
C       THIS PROGRAM CALCULATES EQ. 4.4.8
        DIMENSION X(500),Y(500)
        COMMON /ZAP/FE,FH,BB,AKT
        EXTERNAL FX
        WRITE(6,1)
1       FORMAT(1X,'TYPE EG,N,T,AL1,DL')
        READ(5,2)AEG,AN,AT,AL1,DL
2       FORMAT(5G10.4)
        CALL FRM(.094,AT,AN,ETA1)
        CALL FRM(.5,AT,AN,ETA2)
        AKT=(AT/300.0)*.025
        FE=ETA1*AKT
        FH=ATA2*AKT
        N=((12400./AEG)-AL1)/DL
        DO 10 I=1,N
        AL=AL1+(I-1)*DL
        HN=12400./AL
        BB=HN-AEG
        CALL TRAP(0.,BB,200,FX,RES1)
10      X(I)=RES1
        XM=X(1)
        DO 20 I=1,N
20      IF(X(I).GT.XM)XM=X(I)
        DO 30 I=1,N
30      Y(1)=(X(1)/XM)*100.0
        DO 40 I=1,N
        IL=AL1+(I-1)*DL
40      WRITE(17,*)IL,Y(I)
        STOP
        END
        FUNCTION FX(X)
        COMMON /ZAP/FE,FH,BB,AKT
        A1=SQRT(X)
        A2=SQRT(BB-X)
        A3=1./(1.+EXP((X-FE)/AKT))
        A4=1./(1.+EXP((BB-X)/AKT))
        FX=A1*A2*A3*A4
        RETURN
        END
```

Feb 8 13:56 1985 taueff.F Page 1

```
C       THIS PROGRAM CALCULATES THE EFFECTIVE DECAY TIME IN CHAPTER 5
        EXTERNAL EQNS,PRINT
        CHARACTER*10 F1
        COMMON/DATA/ERRPAR,DT,X,TSTART
        COMMON A,B,C,JK,AMAX,Y(300)
        REAL X(2),DX,DT,TSTART
        REAL AY(300),Y(300)
        DIMENSION IT(100)
        CHARACTER*10 F1
        REAL ERRPAR(2)
        WRITE(6,115)
115     FORMAT('TYPE A,B,C,ANZ,AMAX')
        READ(5,116)A,B,C,ANZ,AMAX
116     FORMAT(5G10.4)
        WRITE(6,116)A,B,C,ANZ,AMAX
303     X(1)=ANZ
        TSTART=0.
        ERRPAR(1)=1.E-4
        ERRPAR(2)=1.E-4
        DT=1.E-16
        TSTOP=1.E-12
        DO 55 JK=1,300
        CALL ODES(EQNS,X,1,TSTART,TSTOP,DT,ERRPAR,PRINT)
        TSTART=TSTOP
55      TSTOP=TSTOP+1.E-12
        YE=Y(1)*EXP(-1.)
        DO 61 J=20,281
        IF(Y(J).LT.YE)GO TO 71
61      CONTINUE
71      ITM=J
        WRITE(6,88)
88      FORMAT('TYPE THE NAME OF FILE')
        READ(5,89)F1
89      FORMAT(10A)
        OPEN(17,FILE=F1)
        DO 665 I=1,200
665     WRITE(17,612)I,Y(I)
612     FORMAT(I4,1X,G10.4)
        BR=1./ITM
991     FORMAT(10(F5.1,1X))
        WRITE(6,887)ITM,BR
887     FORMAT(1X,'DECAY TIME=',I4,10X,'RATE=',G10.3)
        STOP
        END
        SUBROUTINE EQNS(T,X,N,DX)
        REAL T,X(1),DX(1)
        COMMON A,B,C,JK,AMAX,Y(300)
        AA=(T-1.E-11)/4.E-12
        BB=.693*AA*AA
        CC=AMAX*EXP(-BB)
        DX(1)=CC-A*X(1)-(B*X(1)*X(1))-((C*X(1))*X(1)*X(1))
        RETURN
        END
        SUBROUTINE PRINT(T0,X0,T1,X1,N,DT,TSTOP,E)
        REAL T0,X0(N),T1,X1(N),DT,TSTOP
        COMMON A,B,C,JK,AMAX,Y(300)
        REAL E(N)
        IF(T1.NE.TSTOP)RETURN
        Y(JK)=X1(1)
        RETURN
        END
```

The energy of a system of carriers with carrier density n_e and carrier temperature of T_c can be written as

$$E\ (\ n_e\ .\ T_c\ ) = N_c\, kT_c\, F_{\frac{3}{2}}(\eta) \tag{1}$$

where $N_c = (\frac{2\pi m_e kT}{h^2})^{\frac{3}{2}}$ and m_e is the effective mass .

$$\frac{dE}{dt} = \frac{dE}{dT_c}\,\frac{dT_c}{dt} \tag{2}$$

$$\frac{dE}{dT_c} = \frac{5}{2}(\frac{2\pi m_e}{h^2})^{\frac{3}{2}}\ (kT_c)^{\frac{3}{2}}(\ k\ )F_{\frac{3}{2}}(\eta) + (\frac{2\pi m_e}{h^2})^{\frac{3}{2}}(kT_c)^{\frac{5}{2}}\ \frac{dF_{\frac{3}{2}}(\eta)}{dT_c} \tag{3}$$

To obtain $\frac{dF_{\frac{3}{2}}}{dT_c}$ we can use the chain rule and the result becomes

$$\frac{dF_{\frac{3}{2}}(\eta)}{dT} = \frac{dF_{\frac{3}{2}}(\eta)}{d\eta}\,\frac{d\eta}{dT_c} \tag{4}$$

where $\frac{d\eta}{dT_c}$ has been calculated by Blackemore (Ref.14,ch 3,page 86) and is given by

$$\frac{d\eta}{dT_c} = \frac{-3}{2T_c}\,\frac{F_{\frac{1}{2}}(\eta)}{F_{\frac{-1}{2}}(\eta)} \tag{5}$$

and considering the fact $\frac{dF_{\frac{3}{2}}(\eta)}{d\eta} = F_{\frac{1}{2}}(\eta)$ we can write

$$\frac{dE}{dt} = \frac{5}{2}(\frac{2\pi m_e}{h^2})^{\frac{3}{2}}(\ k\ )\,F_{\frac{3}{2}}(\eta)\ - (\frac{2\pi m_e}{h^2})^{\frac{3}{2}}kT_c\ F_{\frac{1}{2}}(\eta)\,(\frac{3}{2T_c})\frac{F_{\frac{1}{2}}(\eta)}{F_{\frac{-1}{2}}(\eta)} \tag{6}$$

IF we divide both sides of the Eq. 6 by carrier density which is equal to $n_e = N_c\ F_{\frac{1}{2}}(\eta)$ and after some algebra we obtain the change of energy with respect to

time per carrier which is given by

$$\frac{dU}{dt} = \frac{3}{2}k\left[\frac{F_{\frac{3}{2}}(\eta)}{F_{\frac{1}{2}}(\eta)} - \frac{F_{\frac{1}{2}}(\eta)}{F_{\frac{-1}{2}}(\eta)}\right] \tag{7}$$